10-1-1977

A Water Quality Model of the Pagan River

Arlene Rosenbaum
Virginia Institute of Marine Science

A. Y. Kuo
Virginia Institute of Marine Science

Bruce J. Neilson
Virginia Institute of Marine Science

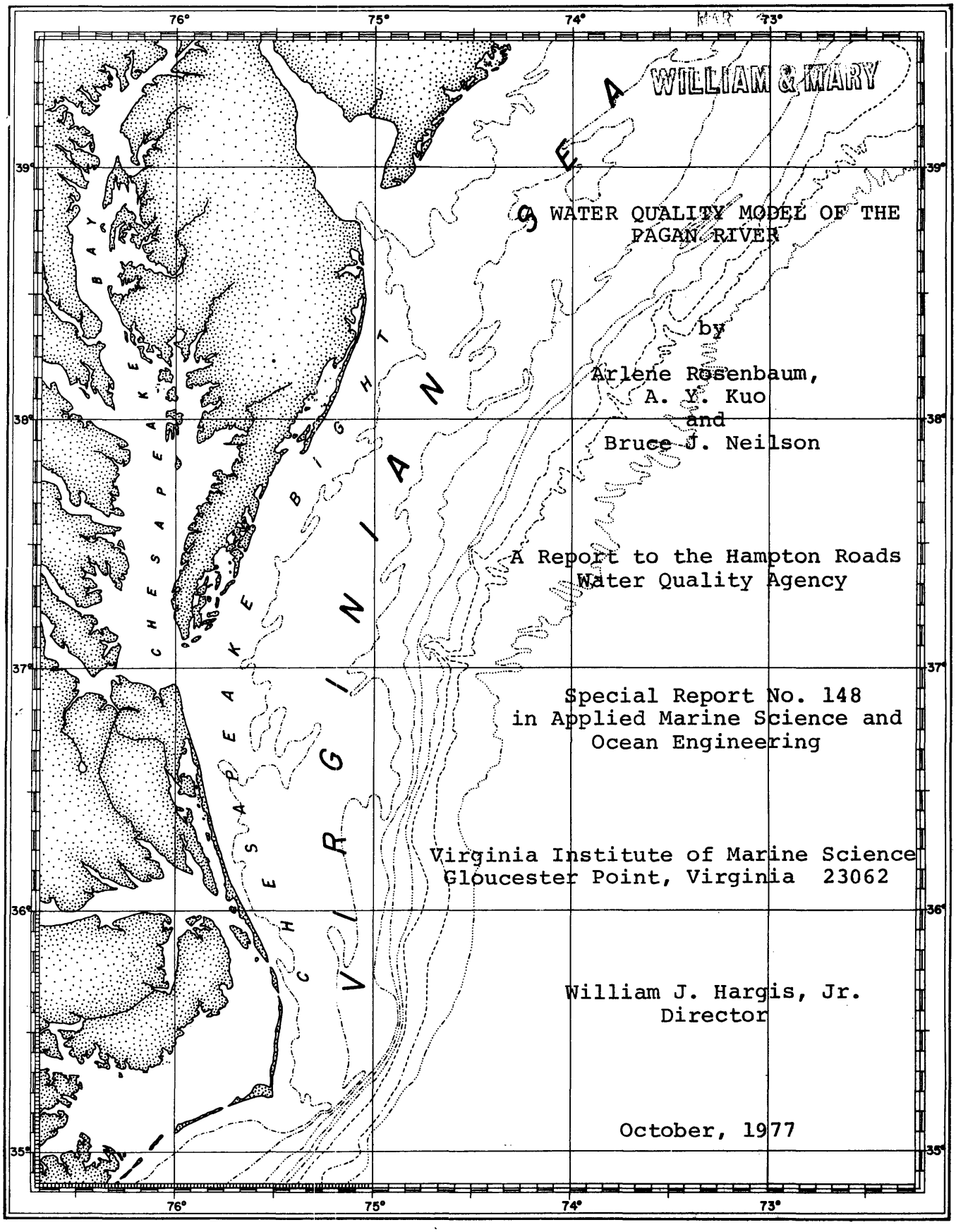

A WATER QUALITY MODEL OF THE PAGAN RIVER

by

Arlene Rosenbaum,
A. Y. Kuo
and
Bruce J. Neilson

A Report to the Hampton Roads Water Quality Agency

Special Report No. 148
in Applied Marine Science and
Ocean Engineering

Virginia Institute of Marine Science
Gloucester Point, Virginia 23062

William J. Hargis, Jr.
Director

October, 1977

A WATER QUALITY MODEL OF THE PAGAN RIVER

by

Arlene Rosenbaum,
A. Y. Kuo
and
Bruce J. Neilson

A Report to the Hampton Roads Water Quality Agency

Special Report No. 148
in Applied Marine Science and
Ocean Engineering

The preparation of this report was financed through a grant from the U. S. Environmental Protection Agency under Section 208 of the Federal Water Pollution Control Act Amendments of 1972.

Virginia Institute of Marine Science
Gloucester Point, Virginia 23062

William J. Hargis, Jr.
Director

October, 1977

TABLE OF CONTENTS

LIST OF FIGURES

List of Figures (cont'd)

List of Figures (cont'd)

LIST OF TABLES

ACKNOWLEDGEMENTS

We would like to thank the entire field staff of VIMS Department of Physical Oceanography, supervised by William Matthews, and the laboratory staff supervised by Ronald Herzick, for their conscientious efforts, often under adverse circumstances. Special thanks are extended to Ms. J. C. Altemus for the extensive data compilation and editing, Ms. Linda Kilch for the preparation of the graphical data summaries, Ms. Patricia Svarney for drafting of the numerous figures, and Ms. Cathy Garrett for her noteworthy typing and report preparation.

We would also like to express our appreciation to Dr. P. V. Hyer for his design and supervision of the benthic oxygen demand survey and his helpful advice and consultation regarding the ecosystem model application, and Dr. C. S. Fang for directing the field program.

The Cooperative State Agencies Program between the State Water Control Board and the Virginia Institute of Marine Science has assisted the 208 modelling studies in many ways. In particular, the original generalized model was developed under this program and a considerable portion of the data base was collected for earlier CSA model studies. These contributions are gratefully acknowledged.

I. INTRODUCTION

Section 208 of the Federal Water Pollution Control Act Amendments of 1972 provides for the development and implementation of areawide waste treatment management plans. In addition to industrial and municipal waste water treatment facilities, the plans are to account for nonpoint sources of pollution, such as urban runoff, runoff from agriculture and silviculture, pollution due to construction activities and so on. The basic tool used in developing a management plan is a mathematical model of water quality for the estuary which receives the waste streams and land runoff. Once an appropriate model has been calibrated and verified for the water body under consideration, it can be used to simulate the response of the receiving waters to various combinations of point and nonpoint loadings. In this manner, it is possible to assess the impact of future loadings, proposed changes in treatment levels and other management alternatives.

The Hampton Roads 208 study area, shown in Figure 1, consists of the Peninsula and Southeastern Virginia Planning Districts. The Pagan River is located on the southern shore of the James River approximately 25 kilometers (15 miles) upriver of Old Point Comfort. The Pagan River basin lies primarily in Isle of Wight County. More than half the basin is forested and slightly over a third is used for agriculture. The major center of commerce and population is the town of Smithfield, as can be seen in Figure 2. During the summer of

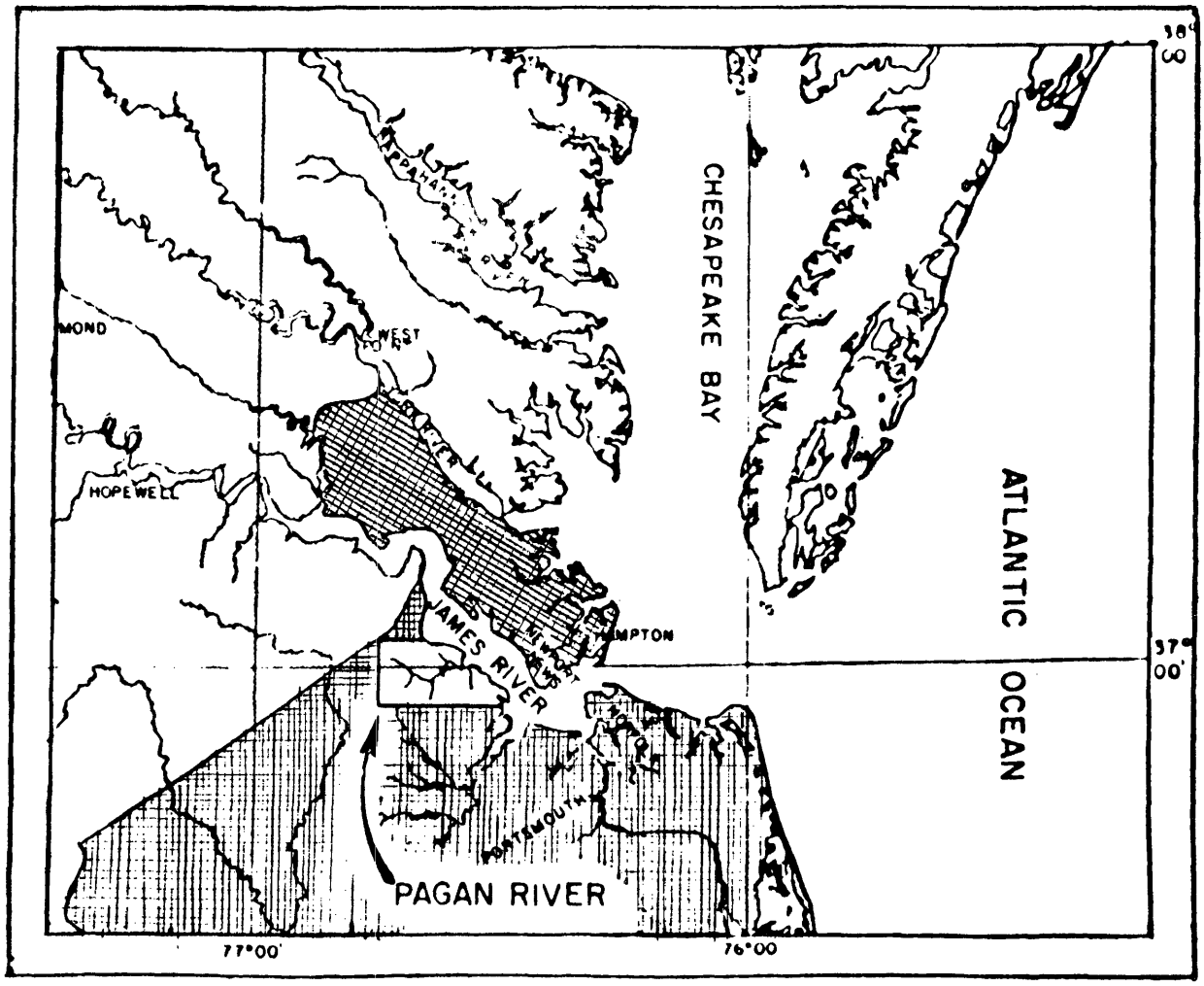

Figure 1. Location of the Hampton Roads 208 Study Area and the Pagan River.

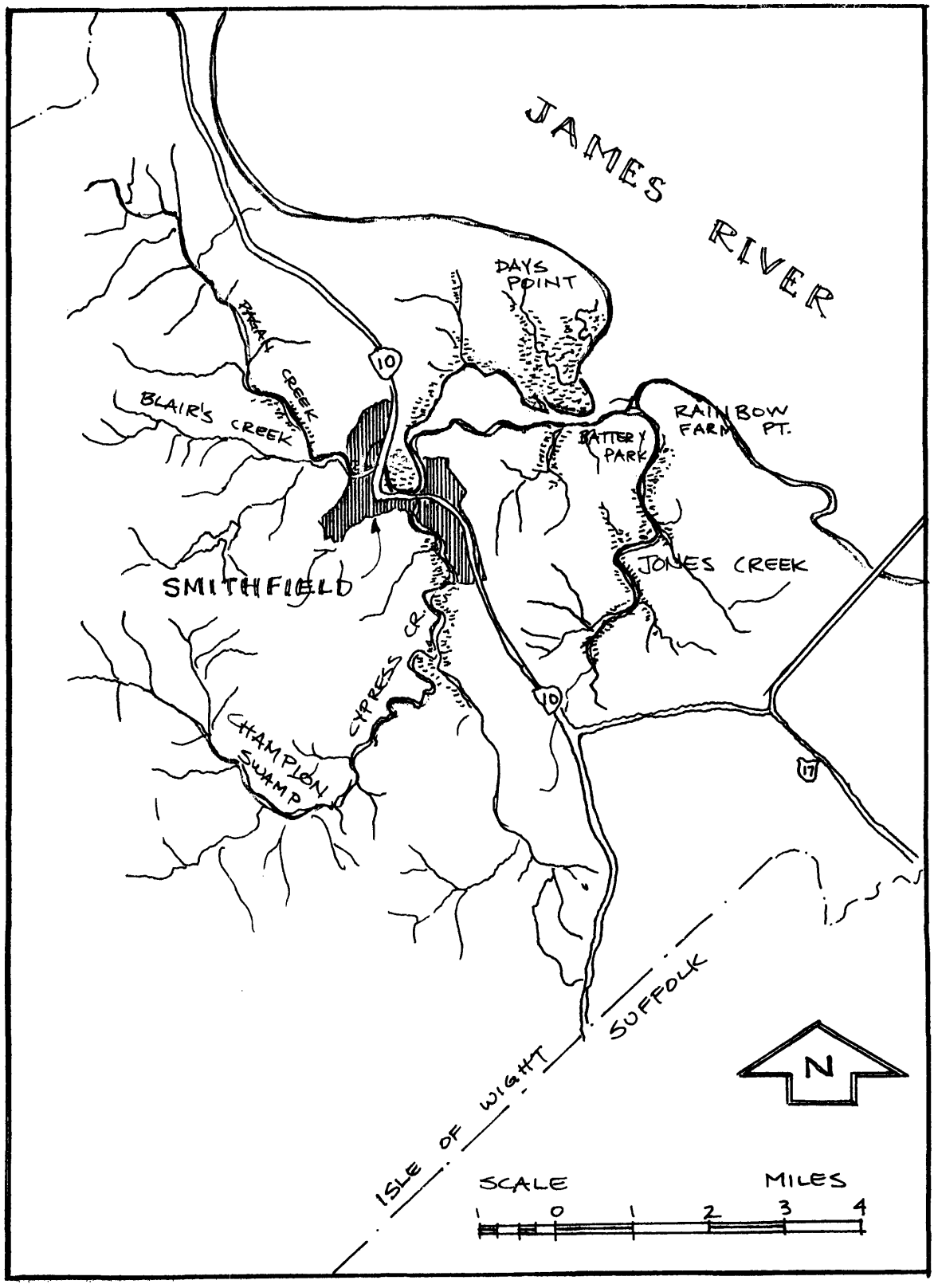

Figure 2. Pagan River drainage basin.

1976 field surveys were conducted in the river to determine present water quality conditions and to collect the data necessary to calibrate a mathematical model of water quality in these water bodies. The field program and an analysis of water quality conditions have been presented in a separate report to the Hampton Roads Water Quality Agency.

The purpose of this report is to describe the model which was applied to the Pagan River and to document its calibration and verification. A detailed description of the model, its many components, internal interactions and the various assumptions employed is given in Chapter 2. This discussion is of a rather technical nature, since it is intended to provide a definitive presentation of the model and its inner workings. A more general presentation of the model and how it works will be given in future reports on the results of the modelling studies. In Chapter 3, the various data sets required for the model are presented, and the calibration and verification results are included in Chapter 4. The final chapter is a discussion of several aspects of water quality which were observed during the model studies.

II. DESCRIPTION OF THE MODEL

The model used in this study is a one-dimensional, intra-tidal ecosystem model which simulates the longitudinal distribution of cross-sectional average concentrations of water quality parameters, including the temporal variation of these concentration fields in response to tidal oscillation. The model includes the following water quality variables: dissolved oxygen, carbonaceous oxygen demand, organic nitrogen, ammonia nitrogen, nitrite-nitrate nitrogen, organic phosphorus, inorganic phosphorus, phytoplankton represented by chlorophyll "a", coliform bacteria and salinity. Temperature, turbidity, and light intensity are important parameters for the biochemical interactions taking place, but they are not modeled directly. Rather they are assumed constant during model simulations and, therefore, are included in the input data set.

A. Basic Equations

The models are based on the one-dimensional equation describing the mass-balance of a dissolved or suspended substance in a water body.

$$\frac{\partial}{\partial t}(AC) + \frac{\partial}{\partial x}(QC) = \frac{\partial}{\partial x}\left(EA\frac{\partial C}{\partial x}\right) + A \cdot Se + A \cdot Si \qquad (1)$$

where

t is time,

x is the distance along the axis of the estuary,

A is the cross-sectional area

Q is discharge,

C is the concentration of dissolved or suspended substance,

E is the dispersion coefficient

Se is the time rate of external addition (or withdrawal) of mass across the boundaries, i.e. free surface, bottom, and lateral boundary;

Si is the time rate of increase or decrease of mass of a particular substance by biochemical reaction processes.

The advective transport term, the second term on the left hand side of the equation, represents advection of mass by water movement; the dispersive transport term, the first term on the right hand side, represents dispersion of mass by turbulence and shearing flow. These two terms represent the physical transport processes in the flow field and, are identical for all dissolved and suspended substances in the water. The last two terms of the equation represent the external additions and internal biochemical reactions which will differ for different substances.

B. Finite Difference Approximation

To facilitate the numerical computation, equation (1) was transfered into finite difference form. This was done by dividing the river into a number of volume elements, called reaches, with a series of lateral transects perpendicular to its axis and by integrating equation (1) with respect to the x-distance parameter, over each of the reaches. Considering the mth reach of the river bounded by the mth and (m+1)th transects as shown in the sketch below:

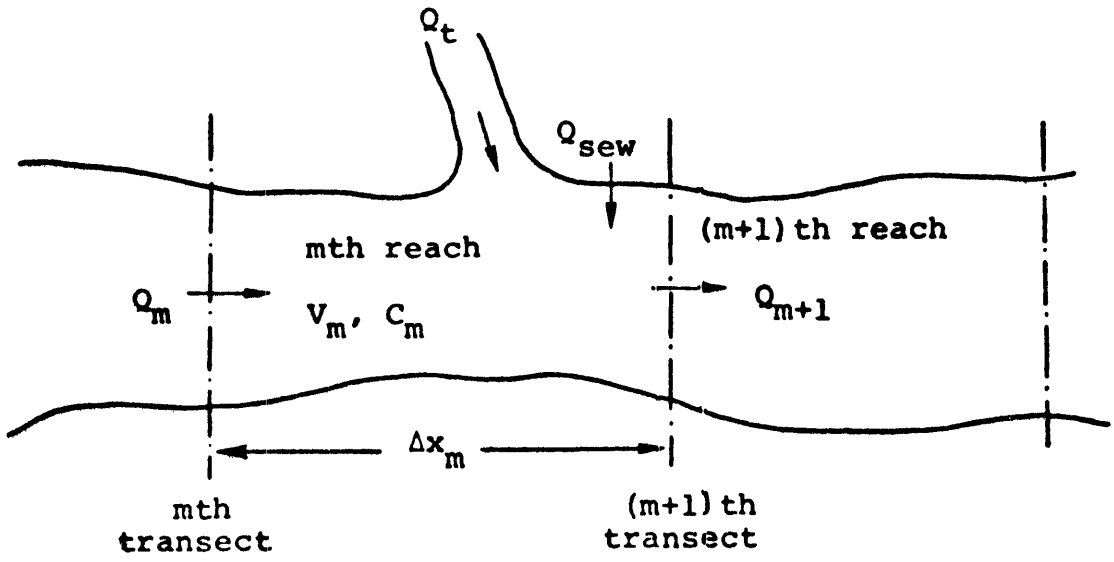

Equation (1) may be integrated with respect to x over the distance Δx_m to arrive at the equation

$$\frac{\partial}{\partial t}(C_m V_m) = Q_m C_m^* - Q_{m+1} C_{m+1}^* + \left(EA\frac{\partial C}{\partial x}\right)_{m+1} - \left(EA\frac{\partial C}{\partial x}\right)_m + Se_m \cdot V_m + Si_m \cdot V_m \quad (2)$$

where

C_m is the volume average concentration of the mth reach,

V_m is the volume of water in the mth reach,

Q_m is the discharge through the mth transect,

C_m^* is the concentration of the water, flowing through the mth transect,

$\left(EA\frac{\partial C}{\partial x}\right)_m$ is the dispersive flux through the mth transect.

The time rate of change of water volume may be expressed as

$$\frac{\partial V_m}{\partial t} = Q_m - Q_{m+1} + Q_\ell \quad (3)$$

where Q_ℓ is lateral inflow, including natural runoff, Q_t, and sewage flow, Q_{sew}.

Substituting equation (3) into equation (2) and dividing the resulting equation by V_m, it is obtained that

$$\frac{\partial C_m}{\partial t} = \frac{Q_m}{V_m}(C_m^* - C_m) - \frac{Q_{m+1}}{V_m}(C_{m+1}^* - C_m)$$

$$+ \frac{1}{V_m}\left(EA\frac{\partial C}{\partial x}\right)_{m+1} - \frac{1}{V_m}\left(EA\frac{\partial C}{\partial x}\right)_m$$

$$+ Se_m + Si_m - \frac{1}{V_m} \cdot Q_\ell \cdot C_m \qquad (4)$$

With proper initial and boundary conditions, equation (4) may be integrated with respect to time to obtain the temporal variations of concentration within each reach of the water body. To solve the equation with a digital computer, it is integrated numerically over successive finite time intervals. At each integration step over a time increment, the various parameters, such as flow rates, dispersion coefficients, etc., should assume representative values during this particular time interval. An implicit scheme is used to formulate the finite difference equation, i.e., the concentration at the end of the time step as well as that at the beginning of the time step is used to express the right hand side of equation (4).

Equation (4) is approximated by the following finite difference form,

$$\frac{C'_m - C_m}{\Delta t} = \frac{1}{2}\left\{\frac{Q'_m}{V'_m}(C^{*\prime}_m - C'_m) + \frac{Q_m}{V_m}(C^*_m - C_m)\right\}$$

$$- \frac{1}{2}\left\{\frac{Q'_{m+1}}{V'_m}(C^{*\prime}_{m+1} - C'_m) + \frac{Q_{m+1}}{V_m}(C^*_{m+1} - C_m)\right\}$$

$$+ \frac{E'_{m+1}A'_{m+1}}{V'_m}\frac{C'_{m+1} - C'_m}{\Delta x_m + \Delta x_{m+1}} + \frac{E_{m+1}A_{m+1}}{V_m}\frac{C_{m+1} - C_m}{\Delta x_m + \Delta x_{m+1}}$$

$$- \left(\frac{E'_m A'_m}{V'_m}\frac{C'_m - C'_{m-1}}{\Delta x_m + \Delta x_{m-1}} + \frac{E_m A_m}{V_m}\frac{C_m - C_{m-1}}{\Delta x_m + \Delta x_{m-1}}\right)$$

$$+ Se_m + Si_m - \frac{1}{V_m} Q_\ell C_m \qquad (5)$$

where Δt is the time increment. The primed and unprimed variables designate the parameters evaluated at the end and beginning of time interval respectively, and the over bar represents the average value over the time interval.

The concentration, C^*_m, of the water flowing through the mth transect is calculated as a weighted average of the concentrations in the adjacent reaches, C_{m-1} and C_m. Thus

$$C^*_m = \alpha C_{m-1} + (1 - \alpha) C_m \qquad (6)$$

$$C^{*\prime}_m = \alpha' C'_{m-1} + (1 - \alpha') C'_m \qquad (7)$$

where the weighting factors α and α' depend on the direction of flow through the transect,

$0.5 \leq \alpha \leq 1$ if $Q_m \geq 0$

$0 \leq \alpha \leq 0.5$ if $Q_m < 0$

and

$0.5 \leq \alpha' \leq 1$ if $Q'_m \geq 0$

$0 \leq \alpha' \leq 0.5$ if $Q'_m < 0$

Similarly,

$$C^{*}_{m+1} = \alpha_2 C_{m+1} + (1 - \alpha_2)\, C_m \tag{8}$$

$$C^{*'}_{m+1} = \alpha'_2 C'_{m+1} + (1 - \alpha'_2)\, C'_m \tag{9}$$

and

$$0.5 \leq \alpha_2 \leq 1 \qquad \text{if } Q_{m+1} < 0$$

$$0 \leq \alpha_2 \leq 0.5 \qquad \text{if } Q_{m+1} \geq 0$$

$$0.5 \leq \alpha'_2 \leq 1 \qquad \text{if } Q'_{m+1} < 0$$

$$0 \leq \alpha'_2 \leq 0.5 \qquad \text{if } Q'_{m+1} \geq 0$$

Substituting equations (6), (7), (8) and (9) into equation (5), it is obtained that

$$\begin{aligned} C'_m - C_m = {} & \frac{\Delta t}{2}\left\{\frac{Q'_m}{V'_m}\,\alpha'(C'_{m-1} - C'_m) + \frac{Q_m}{V_m}\,\alpha(C_{m-1} - C_m)\right\} \\ & - \frac{\Delta t}{2}\left\{\frac{Q'_{m+1}}{V'_m}\,\alpha'_2(C'_{m+1} - C'_m) + \frac{Q_{m+1}}{V_m}\,\alpha_2(C_{m+1} - C_m)\right\} \\ & + \frac{E'_{m+1}A'_{m+1}}{V'_m}\,\frac{\Delta t}{\Delta x_m + \Delta x_{m+1}}\,(C'_{m+1} - C'_m) \\ & + \frac{E_{m+1}\cdot A_{m+1}}{V_m}\cdot\frac{\Delta t}{\Delta x_m + \Delta x_{m+1}}\,(C_{m+1} - C_m) \\ & + \frac{E'_m \cdot A'_m}{V'_m}\cdot\frac{\Delta t}{\Delta x_m + \Delta x_{m-1}}\,(C'_m - C'_{m-1}) \\ & + \frac{E_m \cdot A_m}{V_m}\cdot\frac{\Delta t}{\Delta x_m + \Delta x_{m-1}}\,(C_m - C_{m-1}) \\ & + \Delta t\,(Se_m + Si_m) - \frac{\Delta t}{V_m}\,Q_\ell C_m \end{aligned} \tag{10}$$

Defining

$$ADV_m = \frac{\Delta t}{2} \cdot \frac{AC_m}{V_m}$$

$$ADV2_m = \frac{\Delta t}{2} \frac{AC_{m+1}}{V_m}$$

$$DIF_m = \frac{\Delta t}{\Delta x_m + \Delta x_{m-1}} \cdot \frac{E_m \cdot A_m}{V_m}$$

$$DIF2_m = \frac{\Delta t}{\Delta x_m + \Delta x_{m+1}} \cdot \frac{E_{m+1} \cdot A_{m+1}}{V_m}$$

$$Q_m = AC_m \cdot U_m$$

$$Q_{m+1} = AC_{m+1} \cdot U_{m+1}$$

U_m = advective velocity

AC_m = conveyancy cross-sectional area

and similarly for the primed variables, equation (10) becomes

$$C'_m (1 - \alpha'_2 U'_{m+1} \cdot ADV2'_m + \alpha' U'_m \cdot ADV'_m + DIF'_m + DIF2'_m)$$

$$= C'_{m+1} (-\alpha'_2 U'_{m+1} \cdot ADV2'_m + DIF2'_m) + C'_{m-1} (\alpha' U'_m \cdot ADV'_m$$

$$+ DIF'_m) + C_m (1 + \alpha_2 U_{m+1} \cdot ADV2_m - \alpha U_m \cdot ADV_m$$

$$- DIF2_m - DIF_m) + C_{m+1} (-\alpha_2 U_{m+1} \cdot ADV2_m + DIF2_m)$$

$$+ C_{m-1} (\alpha U_m \cdot ADV_m + DIF_m) + \Delta t (Se_m + Si_m) - \frac{\Delta t}{V_m} Q_\ell C_m \qquad (11)$$

Equation (11) is further simplified to

$$(1 + COE_m)C'_m = COE2_m \cdot C'_{m+1} + COE1_m \cdot C'_{m-1}$$
$$+ CON_m \cdot C_m + CON2_m \cdot C_{m+1} + CON1_m \cdot C_{m-1}$$
$$+ \Delta t(Se_m + Si_m) - \frac{\Delta t}{V_m} Q_\ell C_m \qquad (12)$$

where

$$COE_m = \alpha' U'_m \cdot ADV'_m - \alpha'_2 U'_{m+1} \cdot ADV2'_m + DIF'_m + DIF2'_m$$

$$COE1_m = \alpha' U'_m \cdot ADV'_m + DIF'_m$$

$$COE2_m = -\alpha'_2 U'_{m+1} \cdot ADV2'_m + DIF2'_m$$

$$CON_m = 1 - \alpha U_m \cdot ADV_m + \alpha_2 U_{m+1} \cdot ADV2_m - DIF_m - DIF2_m$$

$$CON1_m = \alpha U_m \cdot ADV_m + DIF_m$$

$$CON2_m = -\alpha_2 U_{m+1} \cdot ADV2_m + DIF2_m$$

The lateral inflow, Q_ℓ, may be written as

$$Q_\ell = Q_t + Q_{sew}$$

where Q_t is the natural runoff (e.g. flow from tributaries) and Q_{sew} is the sewage flow. In a tidal estuary, Q_t may be positive or negative, depending on the phase of tide, with an average value over tidal cycle Q_f, the net freshwater inflow. Without the detailed information about the time variation of Q_t over tidal cycle, the net effect of lateral inflow is approximated by a constant value, $Q_f + Q_{sew}$. Therefore, the last term of equation (12) becomes

$$\frac{\Delta t}{V_m} (Q_f + Q_{sew}) C_m$$

The terms $\bar{Se}_m$ and $\bar{Si}_m$ will differ for different parameters. We have assumed that the biochemical processes follow Fick's law with first order decay rates, therefore, it will be shown in the later sections that all the mathematical expressions for Se and Si are algebraic functions, and no finite difference approximation is needed. However, there are choices in expressing Se and Si in terms of concentrations at the beginning or end of time increments. To avoid introducing extra unknows into the finite difference equation, $\bar{Se}$ and $\bar{Si}$ are expressed as known concentrations of water quality parameters other than the one under consideration. In case Se and/or Si depend on the concentration of the water quality parameter under consideration, the average of the concentrations at the beginning and end of time step is used.

In general, equation (12) may be written as

$$C'_m = a_m C'_{m+1} + b_m C'_{m-1} + c_m \qquad (13)$$

where

$$a_m = COE2_m/(1 + COE_m + \frac{\Delta t}{2} k)$$

$$b_m = COE1_m/(1 + COE_m + \frac{\Delta t}{2} k)$$

$$c_m = \{C_m\ (CON_m - \frac{\Delta t}{2} k - \frac{Q_f + Q_{sew}}{V_m} \cdot \Delta t)$$

$$+ C_{m+1} \cdot CON2_m + C_{m-1} \cdot CON1_m$$

$$+ \Delta t\ (Se^*_m + Si^*_m)\}/(1 + COE_m + \frac{\Delta t}{2} k)$$

$$Se^*_m + Si^*_m = \bar{Se}_m + \bar{Si}_m - k\ (C_m + C'_m)/2 \qquad (14)$$

In the above expression, Se + Si is separated into two parts, one depends on the average concentration of the water quality parameter under consideration and the other is the remainder.

C. Method of Solution

Because of advective and dispersive transport across the transects bounding each end of a particular reach of the estuary, the concentration of a substance in one reach will depend on the concentrations in two adjacent reaches. This interdependence of concentrations at neighboring reaches is manifested in equation (13). Therefore, the equation cannot be solved for the concentration at the mth reach by itself. Equations must be written for every reach of the estuary and solved for the concentrations in every reach simultaneously.

Suppose that the total length of the estuary to be modeled is divided into N reaches. (N-2) equations will be obtained by writing equation (13), for m = ML+1 to m = MU-1, where the MLth and MUth reaches are the most upstream and downstream ones, respectively. Since there are (N-2) equations for N unknowns, two boundary conditions must be specified. The principal operation of numerical computations in the model is then to compute the concentrations in each reach at time $t_o + \Delta t$ with a given initial concentration field at time t_o and appropriate boundary conditions. The computed concentration field at $t_o + \Delta t$ will then be used as the initial condition to compute the concentration field at time $t_o + 2\Delta t$, and so forth. Each computation cycle will advance the time by the

increment of Δt. Within each computation cycle, the (N-2) simultaneous equations are solved by an elimination method.

Given the upstream boundary condition C'_{ML}, C'_{ML+1} may be expressed in terms of C'_{ML+2} through equation (13) with m = ML+1, i.e.

$$C'_{ML+1} = a_{ML+1}C'_{ML+2} + b_{ML+1}C'_{ML} + c_{ML+1} \tag{15}$$

where the only unknown on the right hand side of the equation is C'_{ML+2}. Equation (15) may, in turn, be substituted back into equation (13) with m = ML+2, and thus one arrives at an expression for C'_{ML+2} in terms of C'_{ML+3}. In general, there exists the following relation

$$C'_m = P_m C'_{m+1} + O_m \tag{16}$$

where the recursion coefficients P_m and O_m may be calculated from the upstream boundary condition C'_{ML}.

With subscript m-1, equation (16) becomes

$$C'_{m-1} = P_{m-1}C'_m + O_{m-1}$$

Substituting this expression for C'_{m-1} in equation (13), it becomes

$$C'_m = a_m C'_{m+1} + b_m (P_{m-1}C'_m + O_{m-1}) + c_m$$

or

$$C'_m = \frac{a_m}{1 - b_m \cdot P_{m-1}} C'_{m+1} + \frac{b_m O_{m-1} + c_m}{1 - b_m \cdot P_{m-1}} \tag{17}$$

The comparison between equations (16) and (17) gives

$$P_m = \frac{a_m}{1 - b_m \cdot P_{m-1}}$$

$$O_m = \frac{b_m \cdot O_{m-1} + c_m}{1 - b_m \cdot P_{m-1}} \quad \} \qquad (18)$$

Since C'_{ML} is a known quantity, the comparison between equation (15) and (16) with m = ML+1 gives

$$P_{ML+1} = a_{ML+1}$$

$$O_{ML+1} = b_{ML+1} \cdot C'_{ML} + c_{ML+1}$$

and thus

$$P_{ML} = 0, \quad O_{ML} = C'_{ML}$$

In summary, the recursion coefficients and equation are

$$P_{ML} = 0, \quad O_{ML} = C'_{ML}$$

$$P_m = \frac{a_m}{1 - b_m \cdot P_{m-1}}$$

$$O_m = \frac{c_m + b_m \cdot O_{m-1}}{1 - b_m \cdot P_{m-1}} \quad \} \qquad (18)$$

and

$$C'_m = P_m C'_{m+1} + O_m \qquad (16)$$

with m = ML+1, ML+2, ---, MU-1.

Then, the order of numerical computations is (1) calculate the recursion coefficients by applying equations (18) repeatedly with m = ML+1, ML+2, ---, MU-1, and (2) with

C'_{MU} given as the downstream boundary condition, the concentrations of the interior reaches are calculated by applying equation (16) repeatedly with m = MU-1, MU-2, ---, ML+1.

D. Evaluation of Physical Parameters

(1) Velocity U: In an estuary, the current velocity may be divided into two parts,

$$U_m(t) = UF_m + Ut_m(t) \tag{19}$$

where UF is the non-tidal component generated by freshwater discharge and Ut is the oscillating tidal component. In the model, the tidal current is approximated by a sinusoidal function of time with period T and phase ϕ

$$Ut_m(t) = UT_m \sin \{\frac{2\pi}{T} t + \phi_m\} \tag{20}$$

where UT is the amplitude. UT_m and ϕ_m are obtained from field data. The non-tidal component UF is calculated by the equation

$$UF_m = \frac{Q_m}{AC_m} \tag{21}$$

where Q_m is the freshwater discharge from a drainage area upstream of the mth transect, Q_m is estimated from the record of a stream gauge station located upstream of the tidal limit, with freshwater discharge assumed to be proportional to drainage area.

(2) Dispersion coefficient E: The dominant mechanism of longitudinal dispersion is the interaction between turbulent diffusion and shearing current. Taylor's (1954) formulation of one-dimensional dispersion has been successfully modified and extended to homogeneous estuaries (Holley, et al., 1970; Harleman, 1971). The dispersion coefficient in the freshwater portion of a tidal estuary may be expressed as

$$E = \nu n|U|R^{5/6} \tag{22}$$

where n is Manning's friction coefficient, $|U|$ is the absolute value of velocity, R is hydraulic radius, and ν is a constant on the order of 100. It is known that the presence of density stratification due to salinity intrusion enhances the vertical shear while suppressing the turbulence, and therefore, increases the dispersion coefficient. Equation (22) is modified to

$$E = \nu n|U|R^{5/6}\left(1 + \nu' S + \nu'' \frac{\partial S}{\partial x}\right) \tag{23}$$

where ν' and ν'' are constants and S is the salinity. ν' and ν'' are determined by the model calibration, i.e. adjusting ν' and ν'' until the model results agree satisfactorily with the salinity distribution measured in the field.

(3) River geometry: Cross-sectional area, A, of the transect is determined by planimetry of the bottom profile, constructed from sounding data. Where extensive shoal areas exist, the shoals are subtracted from the total area to arrive at the conveyancy area, AC. It is assumed that water is transported through the conveyancy area alone and the shoaling area serves only for storage.

The transect depth is defined as the mean depth of the conveyancy area, obtained by dividing AC by the surface width of the conveyancy area. The reach depth is defined as the average of the mean depths of total cross-sections for the two bounding transects.

Reach length, Δx, or the distance between two adjacent transects, is determined from Coast & Geodetic Survey navigation charts. The volume of the reach is calculated as the reach length multiplied by the average cross-sectional area of the two bounding transects. In cases where there is a tributary junction in the reach, the volume of the tributary within one tidal excursion from the junction, is added to the reach volume. The reach depth is defined as the volume divided by the sum of surface areas of main channel and oxbow, or tributary.

E. The Kinematics of Ecosystem Model

This model treats the nitrogen, phosphorus, oxygen demanding material, dissolved oxygen and phytoplankton with an interacting system of eight components. Figure 3 is a schematic diagram showing the interaction of these components. Each rectangular box represents one component being simulated by the model, with its name in the computer program shown in parentheses. The arrow between components represents the biochemical transformation of one substance to the other. The arrows with one end not attached to any component represent the external sources (or sinks) or the internal sources (or sinks) due to the biochemical reactions. The mathematical represen-

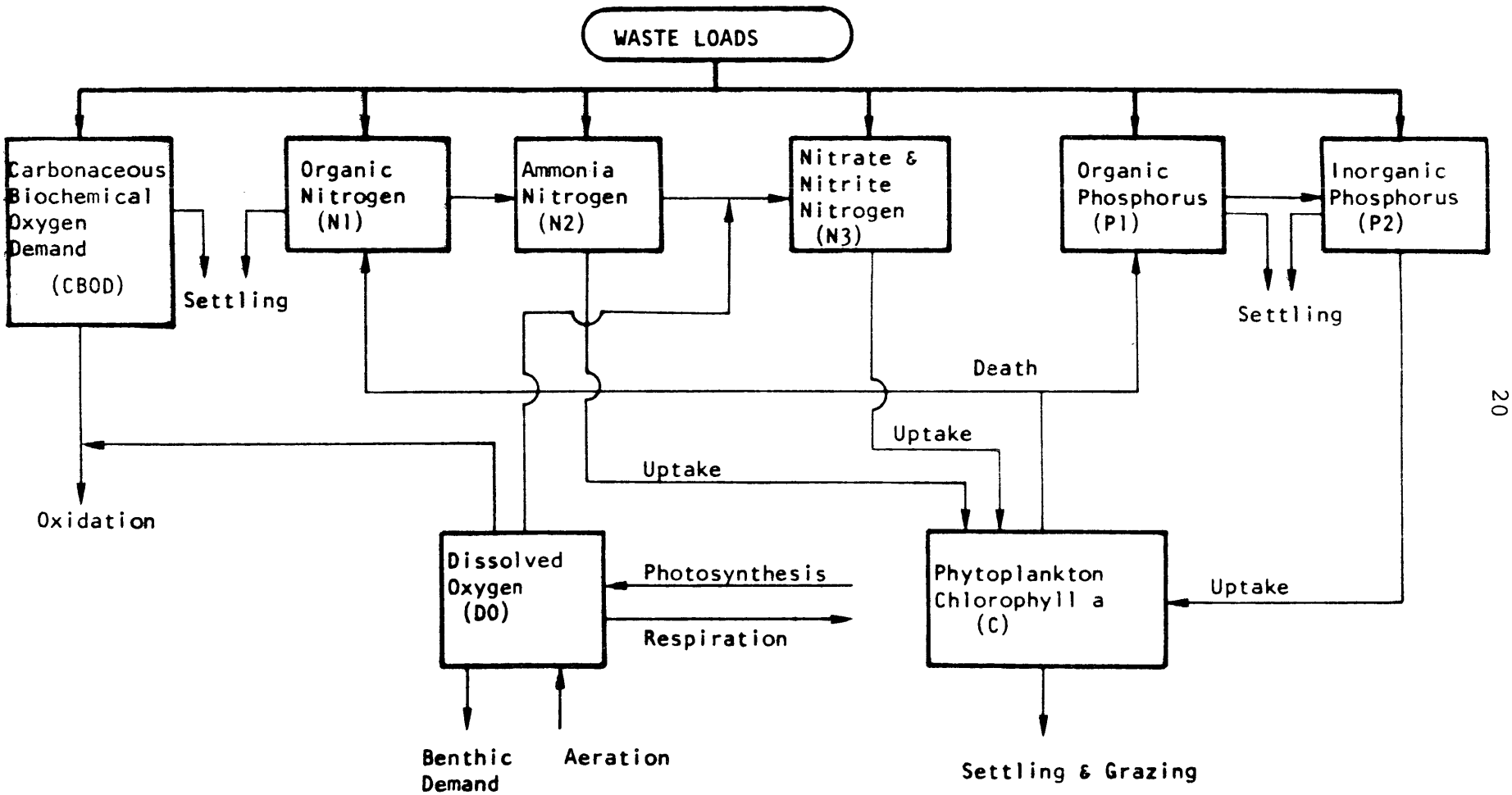

Figure 3. Schematic Diagram of Interaction of Ecosystem Model

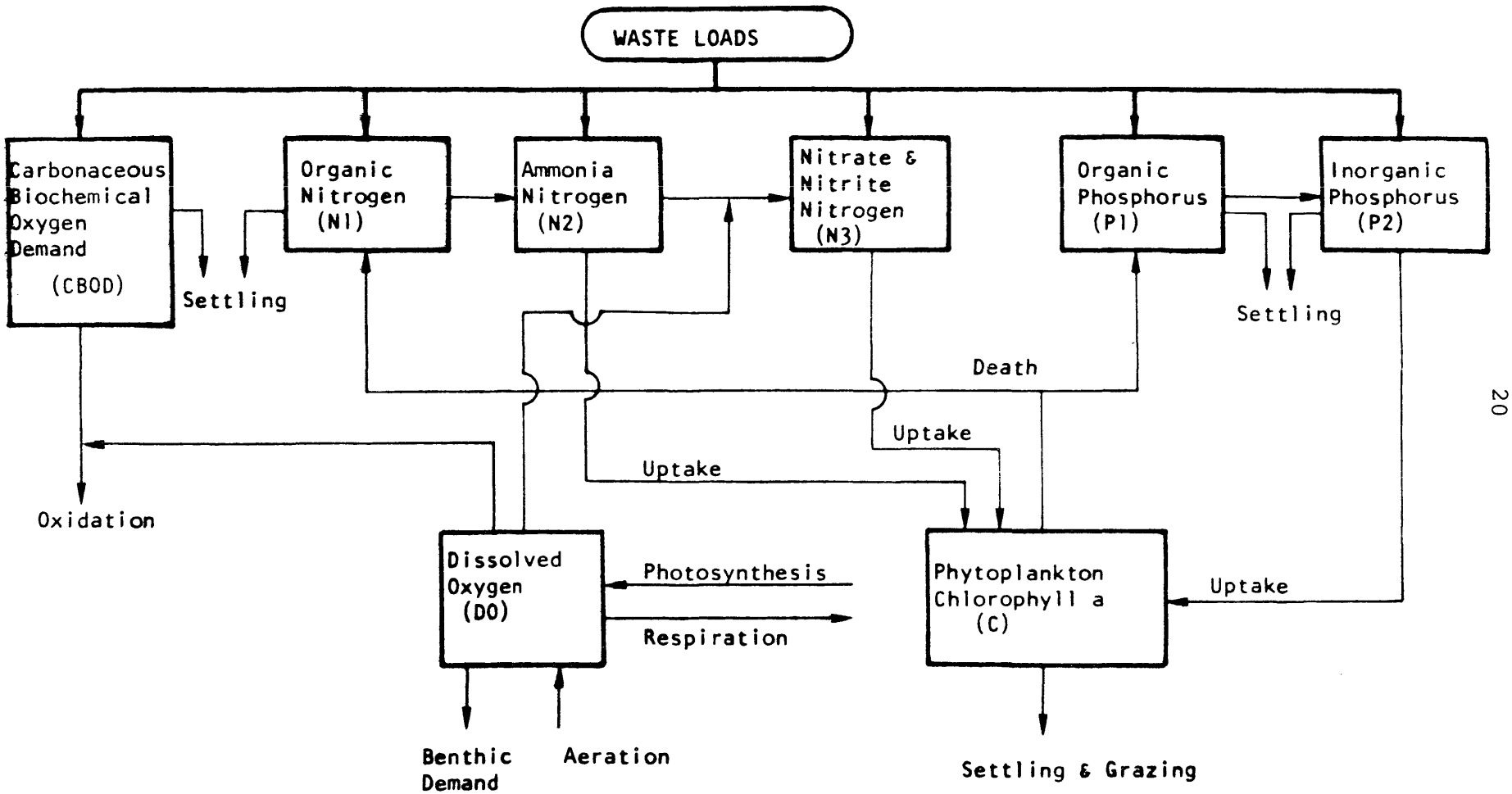

Figure 3. Schematic Diagram of Interaction of Ecosystem Model

tation of the terms Se and Si for each of the eight components are explained as follows:

(1) Phytoplankton concentration, C, measured as µg/ℓ of chlorophyll 'a'

$$Se = -k_{cs} \cdot C$$

where k_{cs} is the settling rate of phytoplankton.

$$Si = (g-d-kg)C$$

where g and d are the growth and endogenous respiration rates of phytoplankton respectively, kg is the grazing of phytoplankton by zooplankton.

(2) Organic Nitrogen, N1 in mg/ℓ

$$Se = W_{n1} - k_{n11} \cdot N1$$

where W_{n1} is the wasteload from point and non-point sources and k_{n11} is the settling rate.

$$Si = -k_{n12} \cdot N1 + a_n \cdot (d + 0.4\ kg)$$

where k_{n12} is the hydrolysis rate of organic nitrogen to ammonia nitrogen and a_n is the ratio of nitrogen to chlorophyll 'a' in mg-N/µg-C.

(3) Ammonia Nitrogen, N2 in mg/ℓ

$$Se = W_{n2}$$

where W_{n2} is the wasteload from point and non-point sources.

$$Si = k_{n12} \cdot N1 - k_{n23} \cdot N2 - a_n \cdot g \cdot C \cdot P_r$$

where k_{n23} is the NH_3 to NO_3 nitrification rate, P_r is ammonia preference by phytoplankton given by

$$P_r = \frac{N2}{N2 + K_{mn}}$$

when ammonia-nitrogen is preferred by the dominant algal species or

$$P_r = 1 - \frac{N3}{N3 + K_{mn}}$$

when nitrate-nitrogen is preferred by the dominant algal species. K_{mn} is the Michaelis constant.

(4) Nitrite - Nitrate Nitrogen, N3 in mg/ℓ

$$Se = W_{n3} - k_{n33} \cdot N3$$

where W_{n3} is wasteload from point and non-point sources, k_{n33} is the nitrate escape rate.

$$Si = k_{n23} \cdot N2 - (1 - P_r) \cdot a_n \cdot g \cdot C$$

where the first term represents the nitrification of ammonia nitrogen and the second term represents the uptake by phytoplankton.

(5) Organic Phosphorus, P1 in mg/ℓ

$$Se = W_{p1} - k_{p11} \cdot P1$$

where W_{p1} is wasteload from point and non-point sources, k_{p1} is the settling rate.

$$Si = -k_{p12} \cdot P1 + a_p \ (d + 0.4 \ kg)$$

where k_{p12} is the organic P to inorganic P conversion rate, a_p is the phosphorus to chlorophyll ratio, in mg - P/μg-C.

(6) Inorganic Phosphorus, P2 in mg/ℓ

$$Se = W_{p2} - k_{p22} \cdot P2$$

where W_{p2} is wasteload from point and non-point sources, k_{p22} is settling rate.

$$Si = k_{p12} \cdot P1 - a_p \cdot g \cdot C$$

where the first term represents the conversion of organic phosphorus to inorganic phosphorus, the second term represents the uptake by phytoplankton.

(7) Carbonaceous Biochemical Oxygen Demand, CBOD in mg/ℓ

$$Se = W_b - k_s \cdot CBOD$$

where W_b is the wasteload from point and non-point sources, k_s is the settling rate.

$$Si = -k_1 \cdot CBOD + 2.67\, a_c \cdot 0.4\, kg \cdot C$$

where k_1 is the oxidation rate of CBOD, a_c is the carbon-chlorophyll ratio.

(8) Dissolved Oxygen, DO in mg/ℓ

$$Se = k_2 \cdot (DO_s - DO) - BEN$$

where k_2 is reaeration rate, DO_s is the saturated oxygen concentration, BEN is the benthic oxygen demand.

$$Si = -k_1 \cdot CBOD - 4.57 \cdot k_{n23} \cdot N2 + a_d \cdot g \cdot C - a_r \cdot d \cdot C$$

where the first two terms represent the oxygen demands by oxidation of CBOD and by nitrification of ammonia nitrogen, the last two terms represents the source and sink due to photosynthesis and respiration of phytoplankton, a_d (or a_r) is the amount of oxygen produced per unit chlorophyll synthesized in the photosynthesis process.

The model treats the salinity and coliform bacteria as independent systems. The simulation of salinity distribution not only serves to calibrate the dispersion coefficient for the model, but also furnishes the required parameter to calculate saturated oxygen content of saline water.

(9) Salinity, S in parts per thousand

$$Se = 0$$

$$Si = 0$$

(10) Coliform Bacteria, BAC in MPN/100 ml

$$Se = W_{bac}$$

where W_{bac} is the loading from point and non-point sources.

$$Si = -k_b \cdot BAC$$

where k_b is the die-off rate.

F. Evaluation of Biochemical Parameters and Rate Constants

The biochemical parameters and rate constants are determined by one of three methods: (a) Calculate with empirical or semi-empirical formula, (b) Data from field measurement, (c) Model calibration. Most of the rate constants are determined through model calibration, with the average values reported in literatures as the guides.

(1) Reaeration coefficient k_2: O'Connor and Dobbins (1956) presented a theoretical derivation of the reaeration coefficient, in which fundamental turbulence parameters were taken into account. They derived the following formula

$$(k_2)_{20} = \frac{(D_c U)^{1/2}}{H^{3/2}} \qquad (24)$$

where D_c is the molecular diffusivity of oxygen in water, U and H are the cross-sectional mean velocity and depth respectively, and $(k_2)_{20}$ is the reaeration coefficient at $20^{\circ}C$. This formula has been shown to give a satisfactory estimate of k_2 for a reach of river with cross-sectional mean depth and velocity more or less uniform throughout the reach. In case the cross-section varies appreciably within a single reach, there is no reason to expect a satisfactory estimate from the formula by using the values of U and H at the two bounding transects of the reach. Therefore, equation (24) is modified as stated in the following paragraph.

Assuming that the O'Connor and Dobbins formula is valid locally then

$$f = k_2 h = \frac{(D_c u)^{1/2}}{h^{1/2}} \tag{25}$$

where f is the exchange coefficient, i.e., the exchange rate of oxygen through unit water surface area, u is the local depth-mean velocity and h is local depth. M, the exchange rate of oxygen through the water surface over an entire reach is

$$M = \int_{Ah} f\,(DO_s - DO)\,dAh \tag{26}$$

where Ah is the total surface area over a reach. By definition of k_2,

$$M = (k_2)_{20} V\,(DO_s - DO) \tag{27}$$

thus,

$$(k_2)_{20} = \frac{D_c^{1/2}}{V} \int_{Ah} \frac{u^{1/2}}{h^{1/2}}\,dAh = D_c^{1/2} \left\langle \frac{u^{1/2}}{h^{1/2}} \right\rangle \frac{AH}{V}$$

$$= D_c^{1/2} \left\langle \frac{u^{1/2}}{h^{1/2}} \right\rangle \frac{1}{\langle h \rangle} \tag{28}$$

where < > indicates the average over the surface area Ah, and <h> is the mean depth of the reach. Since the velocity data are available only at the end transects of a reach, no true $\left\langle \frac{u^{1/2}}{h^{1/2}} \right\rangle$ may be estimated. In this model, the average value

$\frac{U^{1/2}}{H^{1/2}}$ at the two end-transects is used.

To adjust k_2 for temperatures other than 20°C, Elmore and West's (1961) formula is used

$$k_2 = (k_2)_{20} \cdot 1.024^{(T-20)} \tag{29}$$

where T is the water temperature in centigrade degrees.

(2) Saturated oxygen content, DO_s: The saturation concentration of dissolved oxygen depends on temperature and salinity. From tables of saturation concentration (Carritt and Green, 1967) a polynomial equation was determined by a least-squares method.

$$DO_s = 14.6244 - 0.367134T + 0.0044972T^2 - 0.0966S + 0.00205TS + 0.0002739S^2$$

where S is salinity in parts per thousand and DO_s is in mg/liter.

(3) Benthic oxygen demand, BEN: The bottom sediment of an estuary may vary from deep deposits of sewage or industrial waste origin to relatively shallow deposits of natural material of plant origin and finally to clean rock and sand. The oxygen consumption rate of the bottom deposits must be determined with field measurements. Collection procedures and results are discussed in a previous section. The temperature effect was simulated by Thomann (1972).

$$BEN = (BEN)_{20} \cdot 1.065^{(T-20)}$$

where $(BEN)_{20}$ is the benthic demand at 20°C.

(4) CBOD oxidation rate, k_1: The oxidation rate of CBOD (carbonaceous biochemical oxygen demand) normally ranges from 0.1 to 0.6 per day (base e). The rate also depends on water temperature; the following formula is used for this temperature dependence.

$$k_1 = (k_1)_{20} \cdot 1.047^{(T-20)}$$

The value of $(k_1)_{20}$ is obtained by model calibration.

(5) CBOD settling rate, k_s: The net settling rate k_s is usually assumed to be negligible unless evidence shows the contrary.

(6) Coliform bacteria dieoff rate, k_b (day^{-1})

$$k_b = (k_b)_{20} \cdot 1.040^{(T-20)}$$

where $(k_b)_{20}$ is the dieoff rate at 20^oC and T is temperature in degrees centigrade. The value of $(k_b)_{20}$ is obtained by model calibration.

(7) Settling rate of organic nitrogen, k_{n11} (day^{-1})

The value of k_{n11} is obtained by model calibration.

(8) Organic N to NH_3 hydrolysis rate, k_{n12}

$$k_{n12} = aT$$

The value of $\underline{a}$ $(day^{-1} \cdot degree^{-1})$ is obtained by model calibration.

(9) NH_3 to NO_3 nitrification rate, k_{n23}

$$k_{n23} = aT$$

The value of $\underline{a}$ $(day^{-1} \cdot degree^{-1})$ is obtained by model calibration.

(10) NO_3 escaping rate, k_{n33} (day^{-1})

The value of k_{n33} is obtained by model calibration.

(11) Organic phosphorus setting rate, k_{p11} (day^{-1})

The value of k_{p11} is obtained by model calibration.

(12) Organic P to inorganic P conversion rate, k_{p12} (day^{-1})

$$k_{p12} = aT$$

The value of $\underline{a}$ ($day^{-1} \cdot degree^{-1}$) is obtained by model calibration.

(13) Inorganic phosphorus settling rate, k_{p22} (day^{-1})

The value of k_{p22} is obtained by model calibration.

(14) Nitrogen-chlorophyll ratio, a_n

a_n is of order of 0.01 mg N/μg C

(15) Phosphorus-chlorophyll ratio, a_p

a_p is of order of 0.001 mg P/μg C

(16) Carbon-chlorophyll ratio, a_c

a_c is of order of 0.05 mg carbon/μg C

(17) Oxygen produced per unit of chlorophyll growth, a_d

$$a_d = 2.67 \cdot a_c \cdot PQ$$

where PQ is photosynthesis quotient, PQ = 1 ~ 1.4.

(18) Oxygen consumed per unit of chlorophyll respired, a_r

$$a_r = 2.67 \cdot a_c/RQ$$

where RQ is respiration ratio.

(19) Phytoplankton settling rate, k_{cs}

$$k_{cs} = S_\ell/h$$

where S_ℓ is settling velocity, whose normal range is 15 to 150 cm/day (0.5 to 5 ft/day).

(20) Zooplankton grazing, kg: In general kg should depend on the concentration of herbivorous zooplankton biomass. Because zooplankton is not simulated in this ecosystem model, kg is expressed in day^{-1} and zooplankton is assumed to have come into equilibrium with phytoplankton.

(21) Endogenous respiration rate, R_s

$$R_s = aT$$

where a is of order of 0.005/day/degree.

(22) Growth rate, G_c: The growth rate expression is that developed by Di-Toro, O'Connor and Thomann (1974) and as used in this model is given by

$$G_c = \underbrace{K_{gr}(1.08)^{(T-20)}}_{\text{temperature effect}} \cdot \underbrace{I\ (I_a,\ I_s,\ k_e,\ C,\ h)}_{\text{light effect}} \cdot \underbrace{N\ (N2,\ N3,\ P2)}_{\text{nutrient effect}}$$

where k_{gr} is the optimum growth rate at $20^{\circ}C$ of the order of 2.0/day. The functional form, I, for the light effect incorporates vertical extinction of solar radiation and self-shading effect. The form is

$$I = \frac{2.718}{k_e h}\left(e^{-\alpha_1} - e^{-\alpha_o}\right)$$

where $k_e = k_e' + 0.0088 \cdot C + 0.054 \cdot C^{0.66}$

$$\alpha_1 = \frac{I_a}{I_s} e^{-k_e h}$$

$$\alpha_o = \frac{I_a}{I_s}$$

k_e' is the light extinction coefficient at zero chlorophyll concentration, k_e is the overall light extinction coefficient, I_a is the incoming solar radiation and I_s is the optimum light intensity, about 300 langleys per day. The nutrient effect makes use of product Michaelis - Mention kinetics and is given by

$$N = \frac{N2 + N3}{K_{mn} + N2 + N3} \cdot \frac{P2}{K_{mp} + P2}$$

where K_{mn} is the half saturation concentration for total inorganic nitrogen and K_{mp} is the half saturation concentration for inorganic phosphorus. K_{mn} and K_{mp} are determined from literature values or calibration.

III. WATER QUALITY DATA

A very large amount of data is required to apply a mathematical model to a particular estuary and even more data is required for the calibration and verification procedures. Calibration is defined as the process whereby the basic model is adjusted so that it reproduces the behavior of the prototype estuary. For verification the model is run a second time for a different set of environmental conditions. Often minor adjustments are required at this time in order to have the model reproduce both sets of field data.

The most important data set, the calibration water quality data, was gathered during an intensive survey on June 28 and 29, 1976. Salinity, temperature and dissolved oxygen were measured every hour at a series of stations. Nutrient, chlorophyll "a", fecal coliform and BOD (biochemical oxygen demand) samples were collected every three hours. An analysis of the field data was presented in a separate report to the 208 Agency. The verification data set consists of data from a low water slack survey on August 23, 1976 and a high water slack survey the following day.

In addition to the in-stream water quality data, a variety of other factors must be monitored, measured or estimated. These data sets are the subject of this chapter.

A. Bathymetry

VIMS has conducted bathymetric surveys of the Pagan River for the Cooperative State Agencies (CSA) Program. Eleven profiles were determined in the spring of 1974, and three more

bottom profiles were added in the spring of 1975. The transect locations are shown in figure 4. A Raytheon model DE 719 fathometer was used for profiling. The accuracy of the depth soundings is 0.5 feet (15 centimeters). The bathymetric profiles were corrected to mean tide level according to tide tables and time of sounding. Longitudinal distance from the river mouth was determined from a National Ocean Survey (NOS) navigation chart.

B. Base Freshwater Discharge

For a variety of reasons, it is difficult to calculate net water flows in tidal portions of rivers and estuaries. Consequently, stream gauging stations are normally located at or upstream of the fall line. Unfortunately, there are no gauging stations along the Pagan River, so no freshwater discharge record is available. The base flow from groundwater and delayed subsurface runoff has been estimated by assuming the ratios of discharge to drainage area for the James at Richmond and for the Pagan River to be equal. The values used for base flow to the most upstream segment were 10.5 cfs for the calibration period and 5.0 cfs for the time of verification.

Since poor water quality conditions have been observed in the Pagan River, it is recommended that a permanent gauging station be established to facilitate future studies. The method used to calculate base flows may overestimate values slightly since the James basin is many times larger than the Pagan River basin and the geology and land uses differ. However, this cannot be verified since no data are available for the Pagan River.

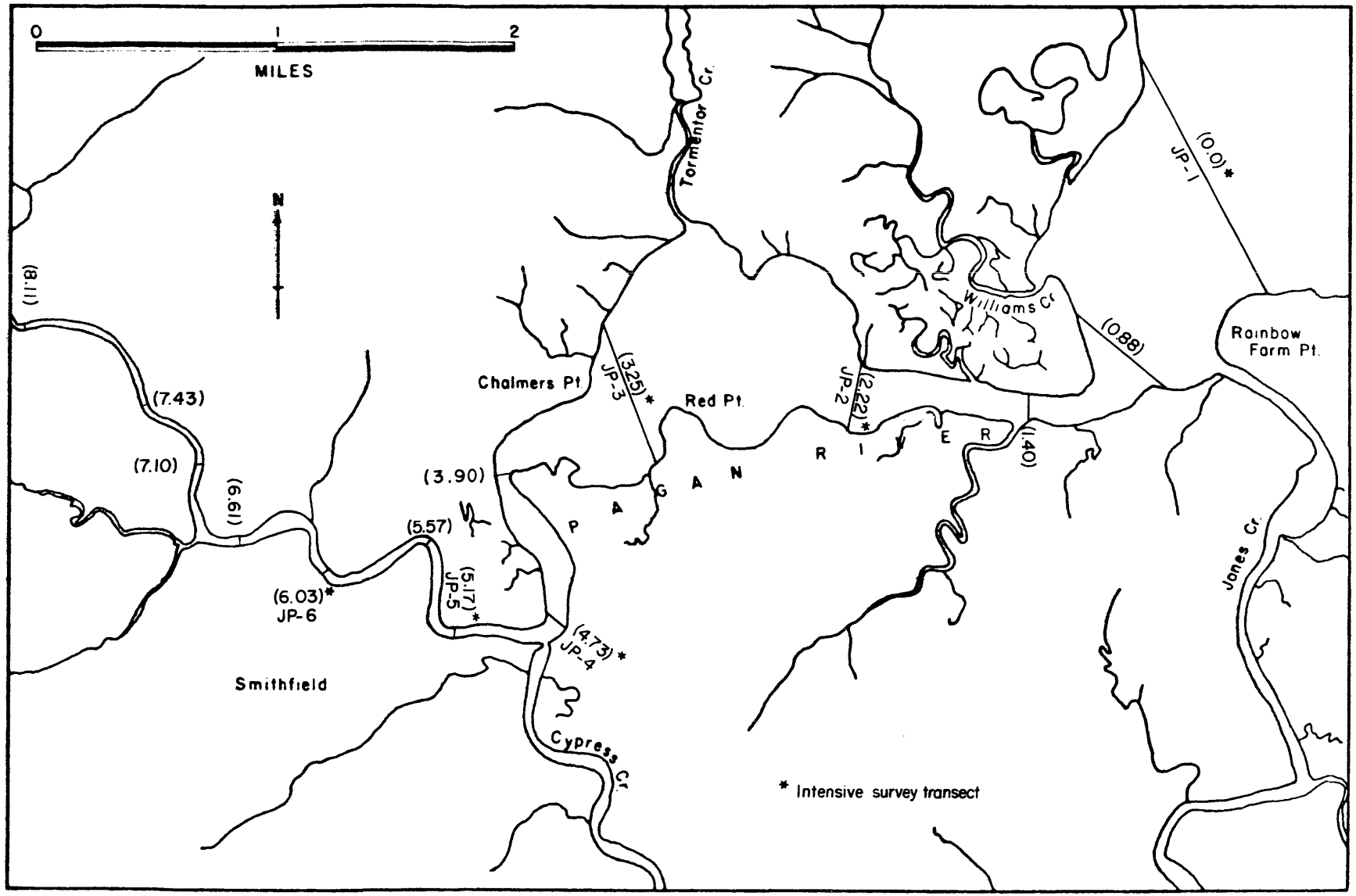

Figure 4. Locations of transects at which the bathymetric profiles and water quality data were measured. (The numbers in parentheses indicate the distances from river mouth in statute miles, 1 mile = 1.61 kilometers).

C. Tidal Current

In August 1974 during the CSA field survey, VIMS placed current meters in three vertical strings at stations located at miles 0.0, 4.73 and 6.61 (0.0, 7.6 and 10.6 kilometers). The meters were Braincon Model 1381, Histogram types, which record average speed and direction at twenty-minute intervals on photographic film. They were kept in place for nine to fifteen days. The data collected for the CSA program were supplemented with tidal prism data (Cronin, 1971) to estimate tidal current amplitude values for input to the model.

D. Point Source Waste Loads

There are only 5 point source discharges to the Pagan River; locations are indicated in Figure 5. Table 1 is a listing of the major waste discharges that were used as input data for the Pagan River ecosystem model calibration, based on the June 28-29, 1976 intensive water quality survey.

Values for the first three parameters listed are based on a study conducted by the State Water Control Board (SWCB) which included daily sampling (24-hour composites) of both dischargers for the period May 20-26, 1976. CBOD was calculated from BOD_5 using a 0.1/day decay rate (base e). This decay rate was determined from 30 day BOD tests using water samples from the river near the two meat packing plants at the time of the intensive survey.

The mass emission rates were calculated using the SWCB reported monthly average flow rate for June, 1976. The concentrations used to calculate the next three loading rates are

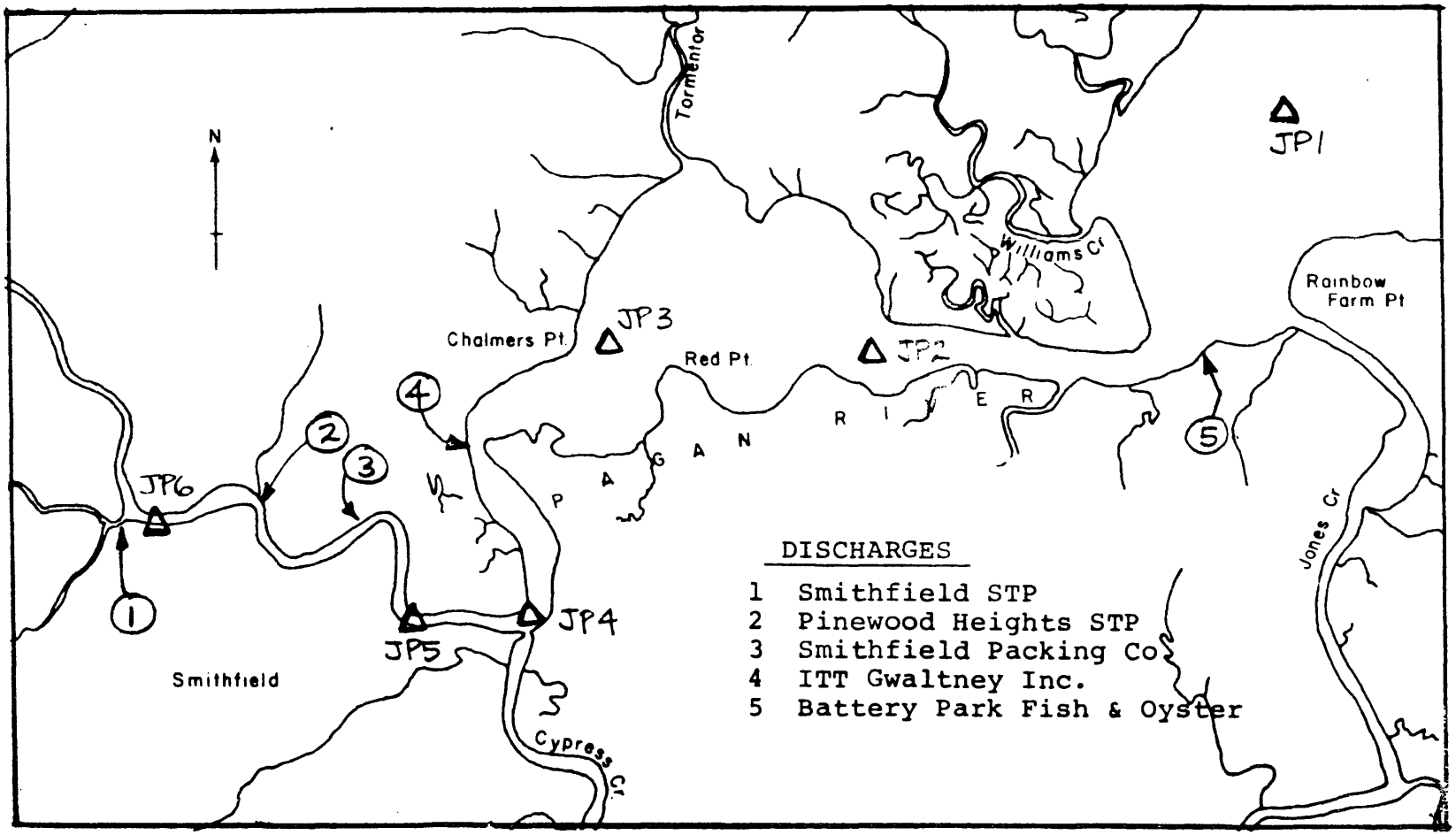

Figure 5. Locations of point sources of pollutants and intensive survey sampling stations.

based on a SWCB July 20-21, 1976, study of Smithfield Packing Company and a SWCB January 20, 1976, study of I. T. T. Gwaltney. In both cases samples consisted of four 6-hour composites taken

TABLE 1. MAJOR DISCHARGES

Loading Rate (lbs/day)	Smithfield Packing	I. T. T. Gwaltney
CBOD	828.	3947
Organic Nitrogen	214.	163
Ammonia Nitrogen	537.	379
Nitrite and Nitrate-N	1.3	0.5
Organic Phosphorus	22.	63
Inorganic Phosphorus	346.	114
Fecal Coliform*	5904.	158

* billions/day

over a 24-hour period. Again the SWCB monthly average flow rates were used to calculate loads.

The fecal coliform value for Smithfield Packing is based on a SWCB April 12-13, 1976, study in which the coliform concentration was determined from the average of 4 grab samples. The I. T. T. Gwaltney value is from a SWCB March 8, 1976, study. Once again the model loading rates were based on the June monthly average flow rates. It should be noted that the quality of the effluent streams was variable during the spring and summer of 1976. It is recommended that future studies include monitoring of major dischargers before and during field surveys.

Because of their small discharge rates the Smithfield STP, the Pinewood Heights STP and the Battery Park Fish and Oyster Company probably have a negligible effect on dissolved oxygen and chlorophyll "a" concentrations in the river. If an effluent fecal coliform level of 200 MPN/100 ml is assumed, the fecal coliform contribution also is negligible. Therefore, these discharges were not included in the modeling study. The following are the reported loadings from the minor waste dischargers:

	CBOD (lbs/day)
Smithfield-Cary Street Lagoon	122*
Pinewood Heights	2.0*
Battery Park Fish and Oyster Co.**	11.1

* Monthly average, June, 1976.
** Betz report of present conditions.

To determine the loading rates for the model verification, based on the August 23 and 24, 1976 slack water surveys, the calibration rates were adjusted to the August monthly average flow rates. In addition, an adjustment was made in the delineation of total Kjeldahl nitrogen (TKN) between organic nitrogen and ammonia nitrogen, such that all the TKN load was attributed to organic nitrogen. The reason for the latter adjustment was a judgement based on examination of the field data in the absence of specific information about the effluent at the time.

E. Nonpoint Source Waste Loads

Field observations of stormwater runoff quality and quantity for a variety of land uses within the 208 study area were made by VIMS during the period March to October, 1976. The resulting data were used by Malcolm Pirnie Engineers, Inc. (MPEI) to calibrate the mathematical model of land runoff, STORM. Once this model had been calibrated, it was used to generate nonpoint source loadings for the drainage basins for the 30 day period prior to the estuarine sampling surveys. These STORM model outputs were used as inputs to the water quality models of the estuary in order to reproduce the water quality conditions which existed during the intensive survey and the slack water surveys.

The 185 square kilometer (71 square miles) drainage basin is about 54% forested, 32% agricultural, 4% pasture, 6% marsh, 3% non-urban residential and 1% non-urban commercial and industrial. Table 2 contains the nonpoint loads used in the model application. The Pagan River drainage basin was divided into 10 subbasins by MPEI to calculate nonpoint loads. Natural drainage patterns tend to collect nonpoint loads in much the same way as storm sewers. Consequently, these loads entered the river via only 8 of the 32 model segments.

F. Comparison of Point and Nonpoint Source Pollutant Discharges

In Table 3 the sum of the major point discharges (June, 1976) and the STORM model predictions (the August 8, 1976, rainfall event) are compared. The rainfall was 0.57 inches following a five-day dry period. For every constituent the

TABLE 2. NONPOINT LOADS TO PAGAN RIVER
PRECEDING FIELD SURVEYS

Date 1976	Rainfall (inches)	Flow (cfs/day)	Nitrogen Org. (lb)	Nitrogen Ammonia (lb)	Nitrogen NO_2-NO_3 (lb)	Phosphorus Org. (lb)	Phosphorus Inorg (lb)	CBOD (lb)	Fecal Coliforms (billions)
Calibration									
June 17	0.33	100.2	2236	547	312	623	266	7187	43,159
June 19	0.12	3.2	75	19	10	24	11	252	1,626
June 21	0.13	44.7	1171	285	164	323	137	3763	22,397
Verification									
Aug. 3	0.09	25.0	464	190	110	195	84	2435	12,738
Aug. 8	0.56	171.3	5589	1373	776	1358	584	17536	87,548
Aug. 9	0.57	134.1	3552	881	494	813	346	11032	49,939
Aug. 16	----	0.6	21	12	3	5	3	69	404

nonpoint load exceeds the point source load, in many cases by more than an order of magnitude. In addition, the rain event results in nearly a 2.5-fold increase in the discharge rate of freshwater into the estuary. One would expect loads of this magnitude to cause a significant, albeit transient, deterioration in water quality. Also, the data for June and August indicate that nonpoint loads, when averaged over dry as well as wet days, are of the same order of magnitude as point loads. Thus, one would assume that equilibrium or steady state nutrient levels would reflect both types of inputs.

TABLE 3. COMPARISON OF POINT AND NONPOINT SOURCE POLLUTANT LOADS IN THE PAGAN RIVER

Loads (pounds)	Daily Point Discharges	Aug. 8, 1976 Nonpoint Discharges
CBOD	4775	17536
Organic Nitrogen	377	5589
Ammonia Nitrogen	916	1373
Nitrite and Nitrate-N	1.8	776
Organic Phosphorus	85	1358
Inorganic Phosphorus	460	584
Fecal coliform*	6062	87548
Flow (cfs/day)	69.7*	171

* Base freshwater discharge to all river segments.

G. Solar Radiation and Turbidity

Because the process of phytosynthesis by phytoplankton requires light of wavelengths between about 400 and 700 mu as an energy source, the amount of light available to these organisms is important input information for the ecosystem model. The two aspects of light availability are the amount of natural light reaching the water surface and the portion of that light penetrating the water column where the phytoplankton reside.

The former of these two values was determined directly with a pyranometer that measures solar and scattered radiation (global radiation) and relfected radiation from the earth's surface (albedo) in the wave range of 300-3000 mu. The information was generously supplied by personnel from the Langley Research Center of the National Aeronautics and Space Administration. Table 4 shows the daily solar radiation values for the 21 days preceding and including the days of the 1976 study.

The latter of these two values is determined indirectly. Relative magnitudes of the light extinction coefficient throughout the estuary were determined from secchi disk readings (see table 5). Because light attenuation due to self-shading of phytoplankton is calculated in the model from the time-varying chlorophyll "a" concentrations, relative extinction coefficients were corrected for chlorophyll "a" concentrations to reflect only "non-phytoplankton turbidity". Because the phytoplankton can migrate up and down the water column in response to the available light, the organisms tend to concentrate at locations

TABLE 4. DAILY SOLAR RADIATION DURING MODEL SIMULATION PERIODS

Calibration Application		Verification Application	
Date	langleys/day	Date	langleys/day
June 9, 1976	419	August 2, 1976	221
10	355	3	214
11	351	4	545
12	435	5	569
13	307	6	478
14	499	7	470
15	527	8	158
16	473	9	79
17	209	10	377
18	448	11	403
19	452	12	491
20	359	13	459
21	312	14	360
22	407	15	403
23	491	16	347
24	430	17	511
25	519	18	429
26	479	19	433
27	541	20	445
28	479	21	287
29	550	22	399
		23	408
		24	444

TABLE 5. TURBIDITY READINGS AND CALCULATIONS FOR THE MODEL SIMULATIONS.

Station	Average Secchi Disk Visibility (range) meters	Extinction Coefficient (1.7/disk visibility) meters^{-1}	Extinction Coefficient Corrected for Chlorophyll "a" Concentration meters^{-1}
Intensive Survey			
JP1	0.73 (0.4-1.0)	2.34	2.00
JP2	0.24 (0.2-0.3)	7.08	6.52
JP3	0.20 (--)	8.50	7.77
JP4	0.40 (--)	4.25	3.12
JP5	0.30 (0.2-0.4)	5.67	4.56
JP6	0.46 (0.4-0.6)	3.70	2.01
Slack Water Surveys			
JP1*	0.9	1.89	1.69
JP2*	0.4	4.25	3.67
JP3	0.35 (0.3-0.4)	4.86 (4.25-5.67)	4.51
JP4*	0.3	5.67	5.38
JP5	0.3 (--)	5.67	4.99
JP6	0.25 (0.2-0.3)	6.8 (5.67-8.50)	6.00

* Only one reading taken.

of near optimum light levels rather than spreading evenly throughout the water column. Thus, some of the effect on phytoplankton of light attenuation due to turbidity is overcome; an extinction coefficient based solely on actual turbidity tends to overestimate the effect. The "effective extinction coefficient" used in the model was, therefore, determined from model calibration.

H. Benthic Oxygen Demand

Benthic oxygen demand is the uptake of dissolved oxygen from the water column by the bottom material. This consumption of oxygen takes place when the products of anaerobic decomposition in the sediment are exposed to dissolved oxygen in the water, either by bubbling up, in the case of gases such as H_2S, or by downward percolation of aerated water, in the case of solids such as FeS. This sink of dissolved oxygen can be quite substantial. For example, an oxygen demand of 1.0 $gm/m^2/day$ in two meters depth of water is equivalent to a BOD of 2.5 mg/l with a decay constant of $0.2/day^{-1}$.

The apparatus used for determining the benthic demand consisted of a cylindrical chamber fitted with a self-contained battery-powered stirrer and a dissolved oxygen probe (YSI-15) plugged into the top of the chamber. The chamber was open at the bottom and weighted so that it settled into the sediment and effectively isolated a unit bottom area and a parcel of overlying water. The stirrer provided gentle agitation to keep water moving past the membrane on the probe without stirring up the sediment. The dissolved oxygen concentration of the

trapped water parcel was monitored for a sufficient length of time to obtain a dissolved oxygen versus time slope (m). The bottom oxygen demand was calculated according to the following formula:

$$BD\left(\frac{gm}{mg^2 \cdot day}\right) = \frac{m\left(\frac{mg}{\ell \cdot hr}\right) H \cdot 24}{10^2}$$, where H is the mean depth of the chamber in cm, allowing for the volume displaced by the stirrer.

Three correction factors need to be considered:

1. Calibration of the DO probe. This was accomplished by air calibration.

2. Correction for BOD (f_b) in the water. The formula used for this correction was:

$$f_b = 1 - \frac{K_1 B \ (1.047)^{T-20}}{24m}$$

where K_1 = BOD decay constant at $20^{o}C$ (day^{-1})

B = ultimate BOD (ppm)

m = slope of DO curve (ppm/hr)

T = water temperature in degrees centigrade

3. Correction for temperature (f_T). The formula used for temperature correction was (Thomann, 1972):

$f_T = (1.065)^{T-20}$, where T is the water temperature in degrees centigrade.

The benthal oxygen demand was measured at three locations in the Pagan River at the time of the intensive survey, and the results were as follows:

Station	Distance from River Mouth miles	(km)	Benthic Oxygen Demand $gm/m^2/day$ at 20^oC and 5 mg/l DO
1	0.0	(0.0)	1.6
3	2.2	(3.5)	2.2
6	5.8	(9.3)	3.8

It was found that clear and dark chambers gave essentially identical results, indicating that planktonic activity was not affecting the determination.

IV. MODEL APPLICATION

A. Segmentation of the River

The river was divided into 32 reaches of equal length. Transects were located 0.25 miles (0.4 kilometers) apart as shown in Figure 6. The geometric parameters of the transects were obtained by interpolating the field data of the 14 bathymetric profiles. Figure 7 shows the total cross-sectional areas of the transects as a function of distance from the river mouth. The values from the linear interpolation actually were used in the model. A similar procedure was followed for the conveyancy cross-sectional areas.

B. Calibration

Calibration is the adjustment of the model so that the model results correspond closely to actual field observations. In particular parameters which are difficult to measure directly are varied. For this study, the data collected during the intensive water quality survey described in section III were used as the basis of the model calibration. Input data measured directly or estimated from field measurements have been presented and discussed in section III. A water temperature of 28.39^{o}C, the average temperature throughout the study area during the intensive survey was used.

The downstream boundary concentrations and concentrations of freshwater inflows were estimated from field data and are listed in table 5. The model was configured so that it was not necessary to define the upstream boundary concentrations explicitly. Rather the upstream flux was defined to be zero.

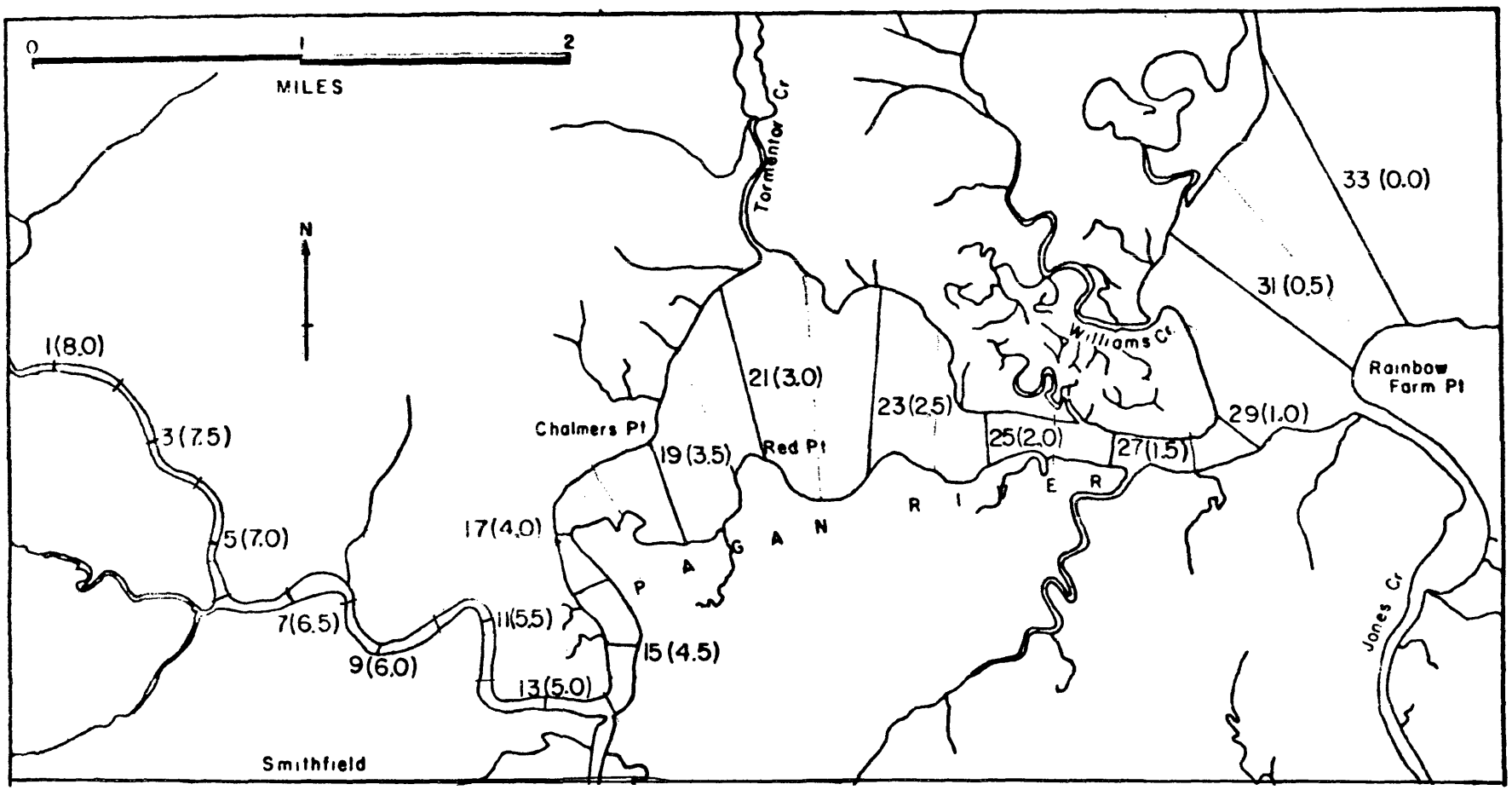

Figure 6. Locations of transects dividing the river into model segments. The numbers outside parentheses indicate the transect numbers of the model, those inside the parenthese indicate the distances from mouth in miles (1 mile = 1.61 kilometers).

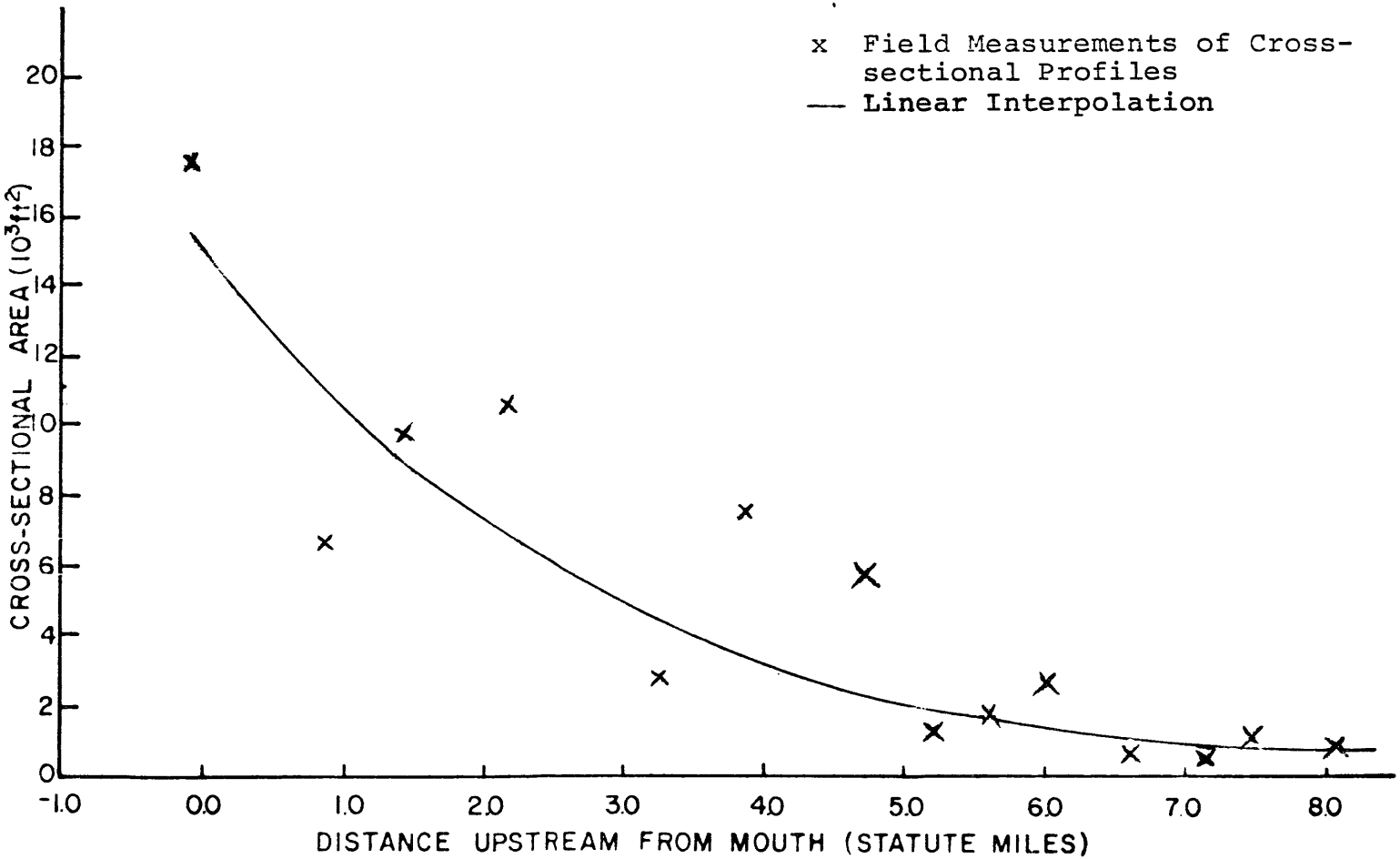

Figure 7. Cross-sectional areas versus distance along the river. (1 statute mile = 1.61 kilometers)

TABLE 6. DOWNSTREAM BOUNDARY AND FRESHWATER INFLOW CONCENTRATIONS USED IN THE MODEL CALIBRATION APPLICATION

Parameter (mg/l - except as noted	Downstream Boundary	Freshwater Inflow
Salinity (ppt)	11.5	0.1
Organic nitrogen	0.18	1.2
Ammonia-N	0.23	0.01
Nitrite & Nitrate-N	0.73	0.01
Organic phosphorus	0.11	1.2
Inorganic-P	0.027	0.045
Chlorophyll "a" (µg/l)	5.	100
CBOD	2.5	12
DO	6.5	10.6
Fecal coliform (MPN/100 ml)	4.0	1.

TABLE 7. INPUT VALUES OF PHYTOPLANKTON-RELATED COEFFICIENTS FOR THE ECOSYSTEM MODEL JULY, 1976 SIMULATION

Coefficient	Value
R_s	0.005/day/degree C (Thomann, et al., 1974)
K_{mn}	0.025 mg/l (Thomann, et al., 1974)
K_{mp}	0.005 mg/l (Thomann, et al., 1974; Halmann and Stills, 1974)
K_{gr}	0.1/day/degree C (Thomann, et al., 1974)
RIS	250 langleys/day (McAllister, et al., 1961)

The field data indicated that there was a large population of phytoplankton upstream from station JP-6. Chlorophyll "a" concentrations at that station increased dramatically during ebb tide and decreased during flood tide. Therefore, the freshwater inflow concentrations for organic nitrogen, organic phosphorus, CBOD, dissolved oxygen and chlorophyll "a" are high and reflect the presence of this algal bloom.

Some of the phytoplankton-related parameters were derived from literature values, which have been listed and referenced in Table 6. Unfortunately, many of the phytoplankton parameters vary from species to species and are not well known for most species. Moreover, the species composition of the population can change with changing conditions. The use of literature values generally assures an order-of-magnitude accuracy for a parameter, but a rigorous analysis of phytoplankton dynamics is beyond the scope of this study. Because of the large phytoplankton population and its significant effect on the dissolved oxygen concentrations in the upper portion of the study area, the development of more specific information about the population in future studies is recommended.

The calibrated values of the other parameters are presented in Table 7. For the rate constants K_{n12} (conversion of organic nitrogen to ammonia nitrogen) and K_{n23}(conversion of ammonia nitrogen to nitrite and nitrate nitrogen) there appear to be 3 different zones. One of these is upstream of and including the major point source discharge locations from kilometer 7.2 to km 12.8 (mile 4.5 to 8.0). The second is

TABLE 8. CALIBRATION VALUES OF VARIOUS MODEL PARAMETERS FOR JUNE, 1976 SIMULATION

Parameter	Value
a_d	1.4
a_r	1.0
K_{cs}	0.0/day
K_g	0.5/day
nitrogen preference	NO_3-N
K_{n11}	0.05/day
$Kn_{12}(a)$	mile 0.0 to mile 3.25: 0.100/day/degree C mile 3.25 to mile 4.50: 0.016/day/degree C mile 4.50 to mile 8.00: 0.0005/day/degree C
$K_{n23}(a)$	mile 0.0 to mile 4.00: 0.005/day/degree C mile 4.00 to mile 8.00: 0.025/day/degree C
K_{n33}	0.05/day
K_{p11}	0.0/day
$K_{p12}(a)$	0.003/day/degree C
K_{p22}	0.20/day
ν'	0.0
ν''	500.
KBAC	1.5/day
CKC_{20^oC}	0.12/day
Turbidity extinction coefficient proportion	0.15-0.20

from just downstream of this area to approximately the point where the river surface width increases substantially from km 7.2 to km 5.2 (mile 4.5 to mile 3.25). The third is from this widening point to the mouth, kilometer 5.2 to km 0.0 (mile 3.25 to mile 0.0).

Tidal average model predictions are presented along with the averages and ranges for the field data in Figures 8 through 17. Model results are consistent with the trends of the field data and generally fall well within the range of observed values. A few minor discrepancies do exist. In great part these are due to lack of data or freshwater flow, limited information concerning the phytoplankton community, and the one-dimensionality of the model. Additionally, there are numerous physical, chemical, biological and geological processes occurring simultaneously in the river. It is difficult to characterize conditions, much less model most of these processes. Given the complexity of the situation and the ecosystem model, the calibration actually is quite good. The discrepancies between field observations and model predictions tend to be in nutrient fractions, such as organic nitrogen or ammonia nitrogen. Predictions for parameters which integrate several processes are very good. In particular, the calibration for chlorophyll "a" (Figure 15) and dissolved oxygen (Figure 16) are very good. The latter includes a DO sag with minimum at km 7 (mile 4.4) which matches closely with the corresponding observed field values.

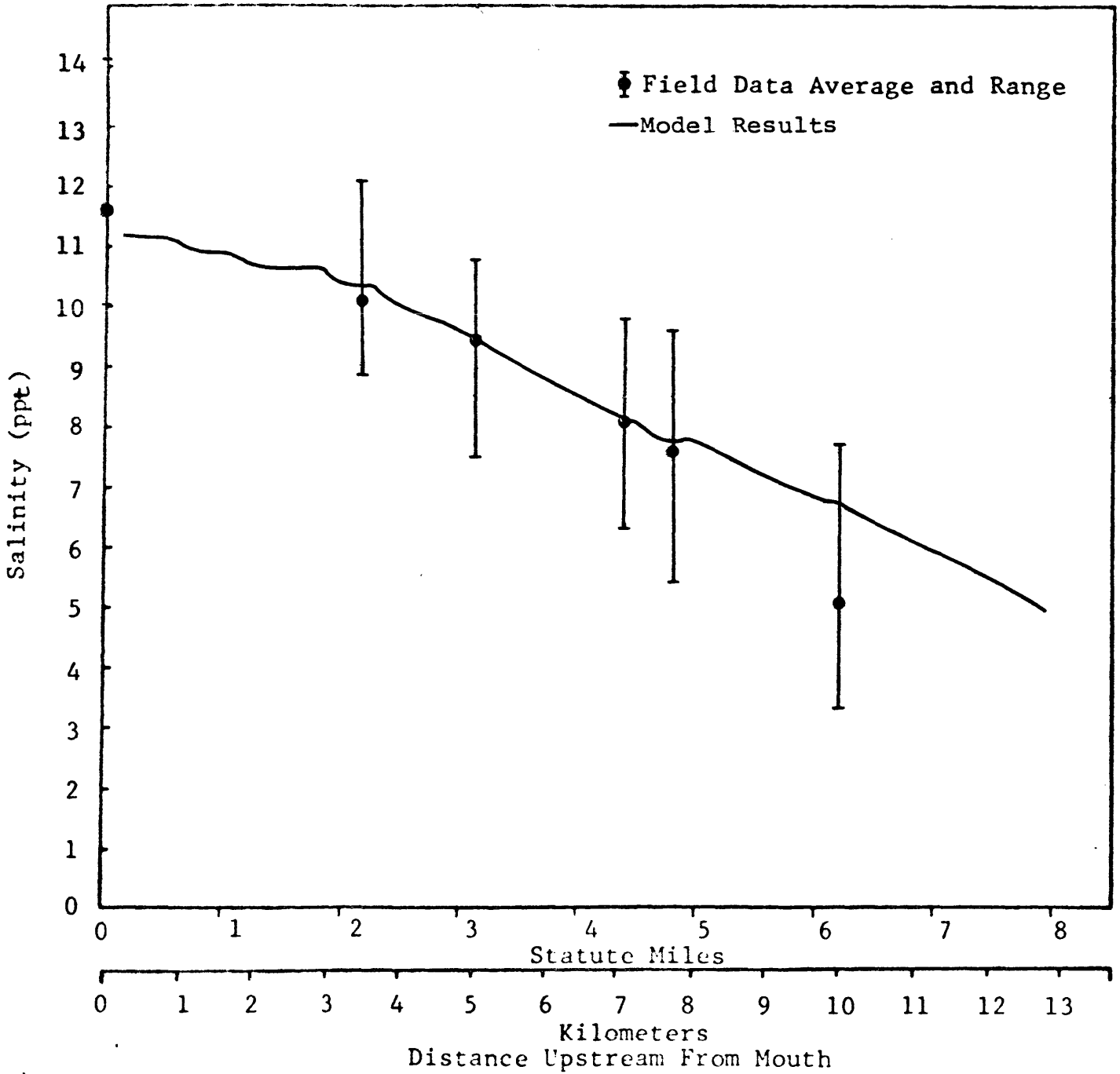

Figure 8. Comparison between computed salinity distribution and field data, June 28 and 29, 1976.

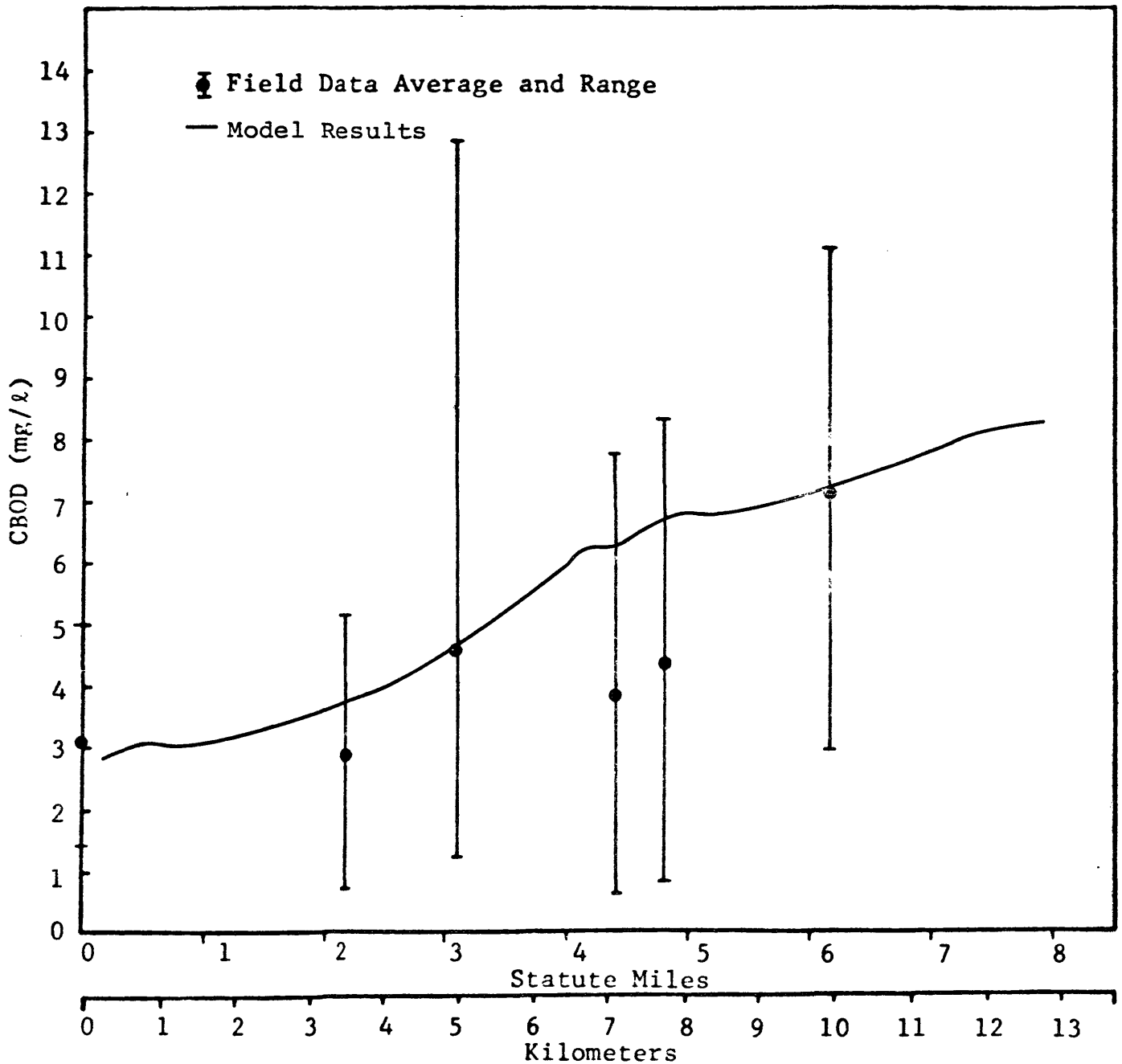

Figure 9. Comparison between computed CBOD distribution and field data, June 28 and 29, 1976.

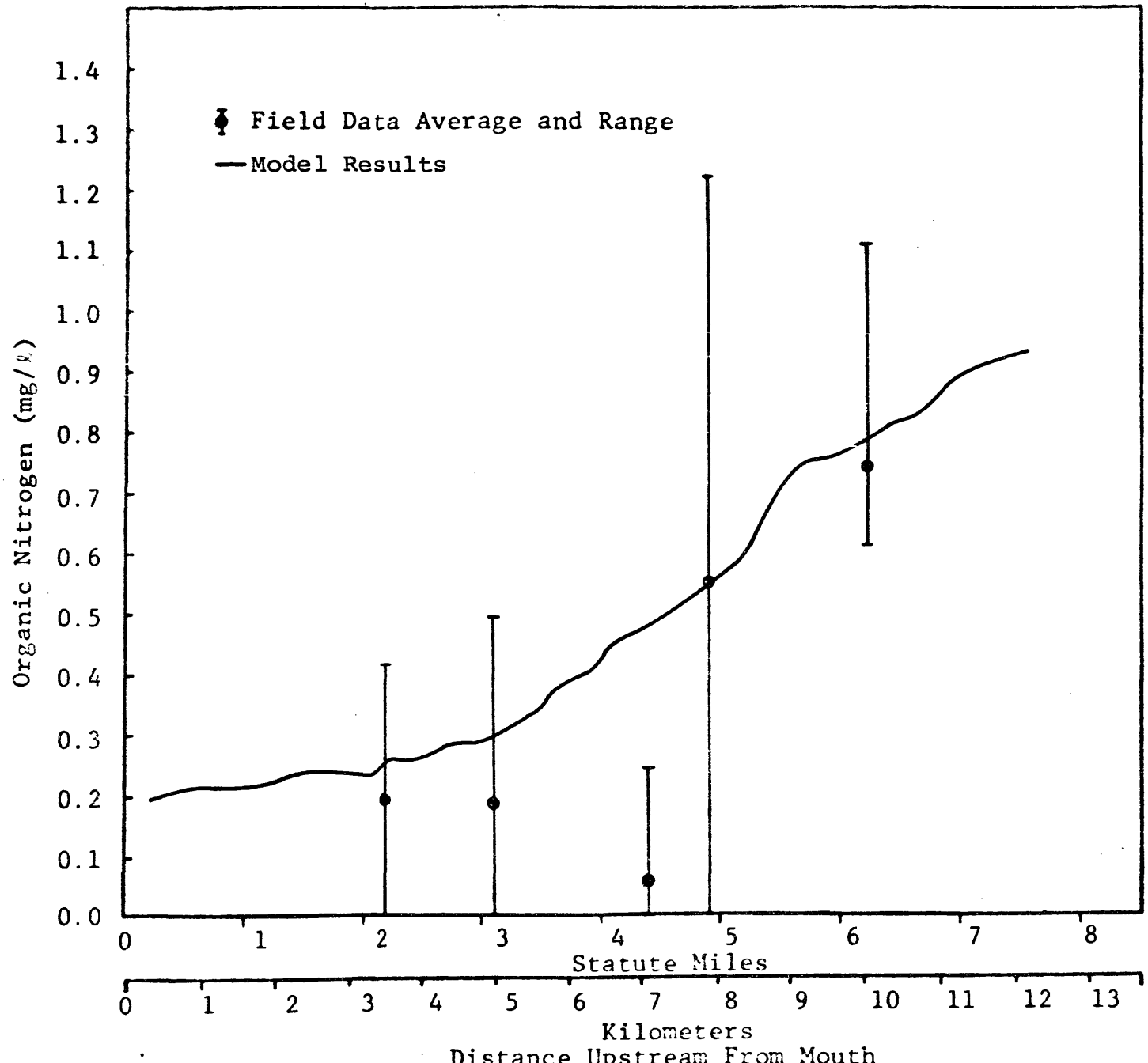

Figure 10. Comparison between computed Organic Nitrogen distribution and field data, June 28 and 29, 1976.

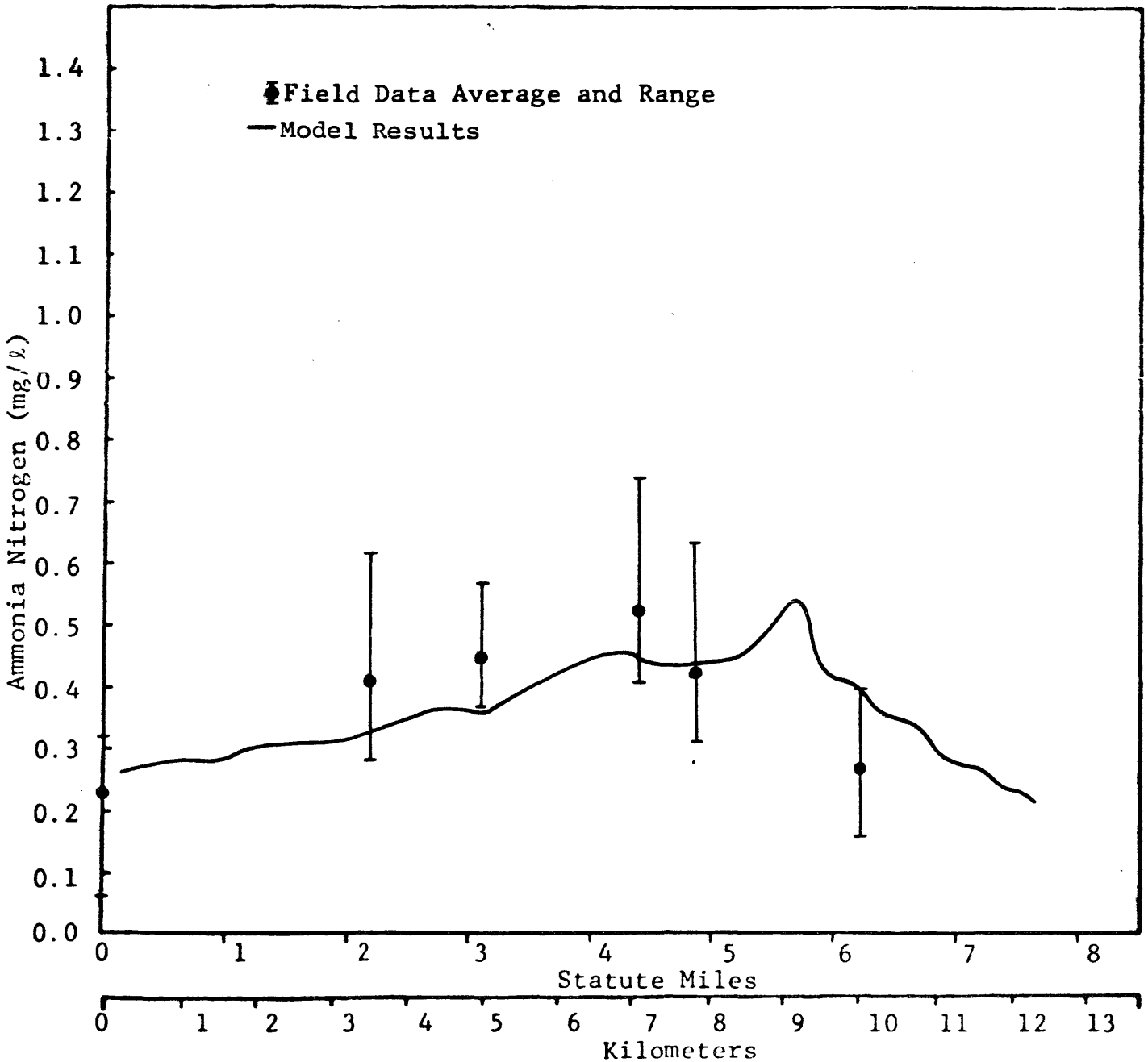

Figure 11. Comparison between computed Ammonia Nitrogen distribution and field data, June 28 and 29, 1976.

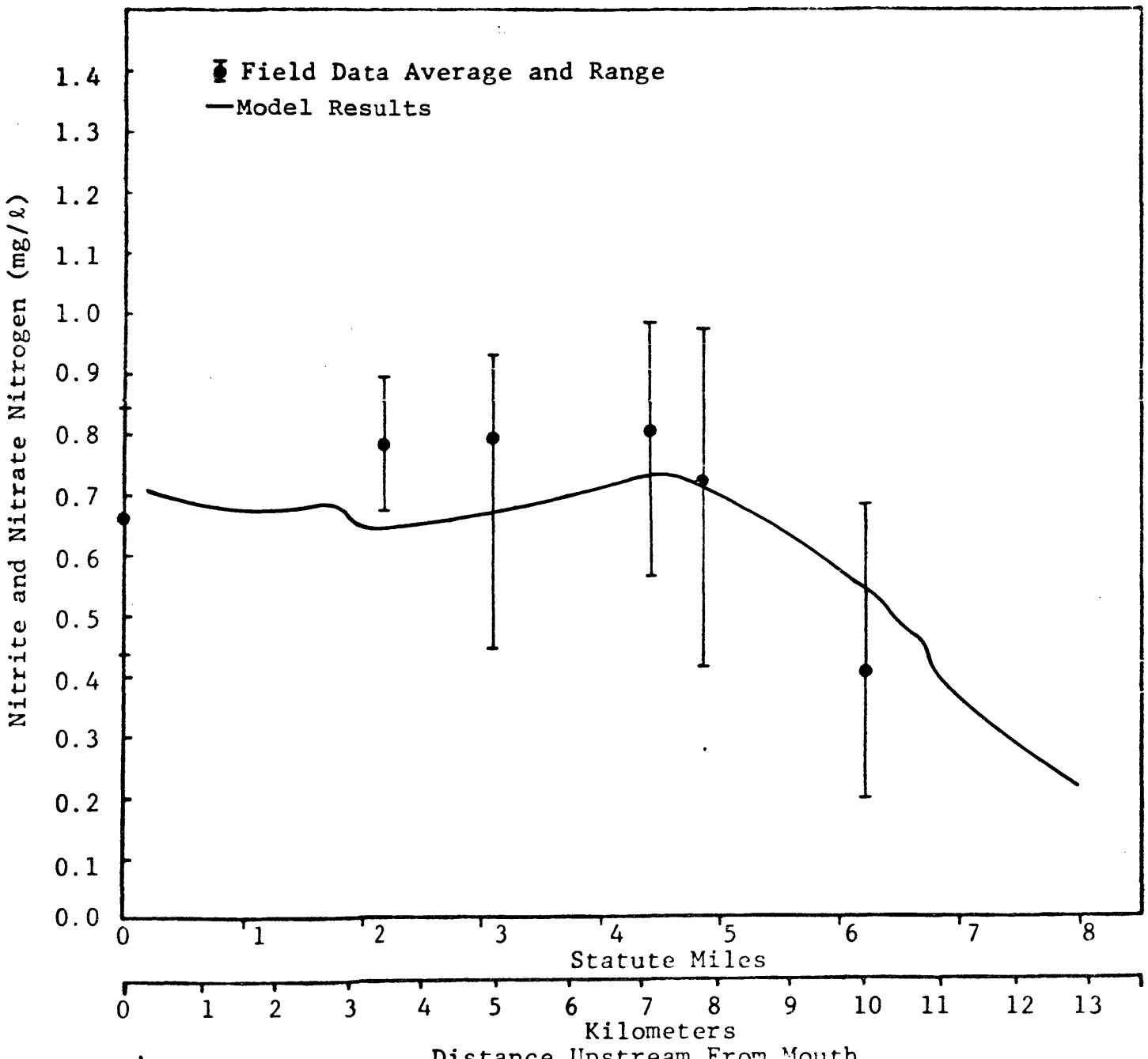

Figure 12. Comparison between computed Nitrite and Nitrate Nitrogen distribution and field data, June 28 and 29, 1976.

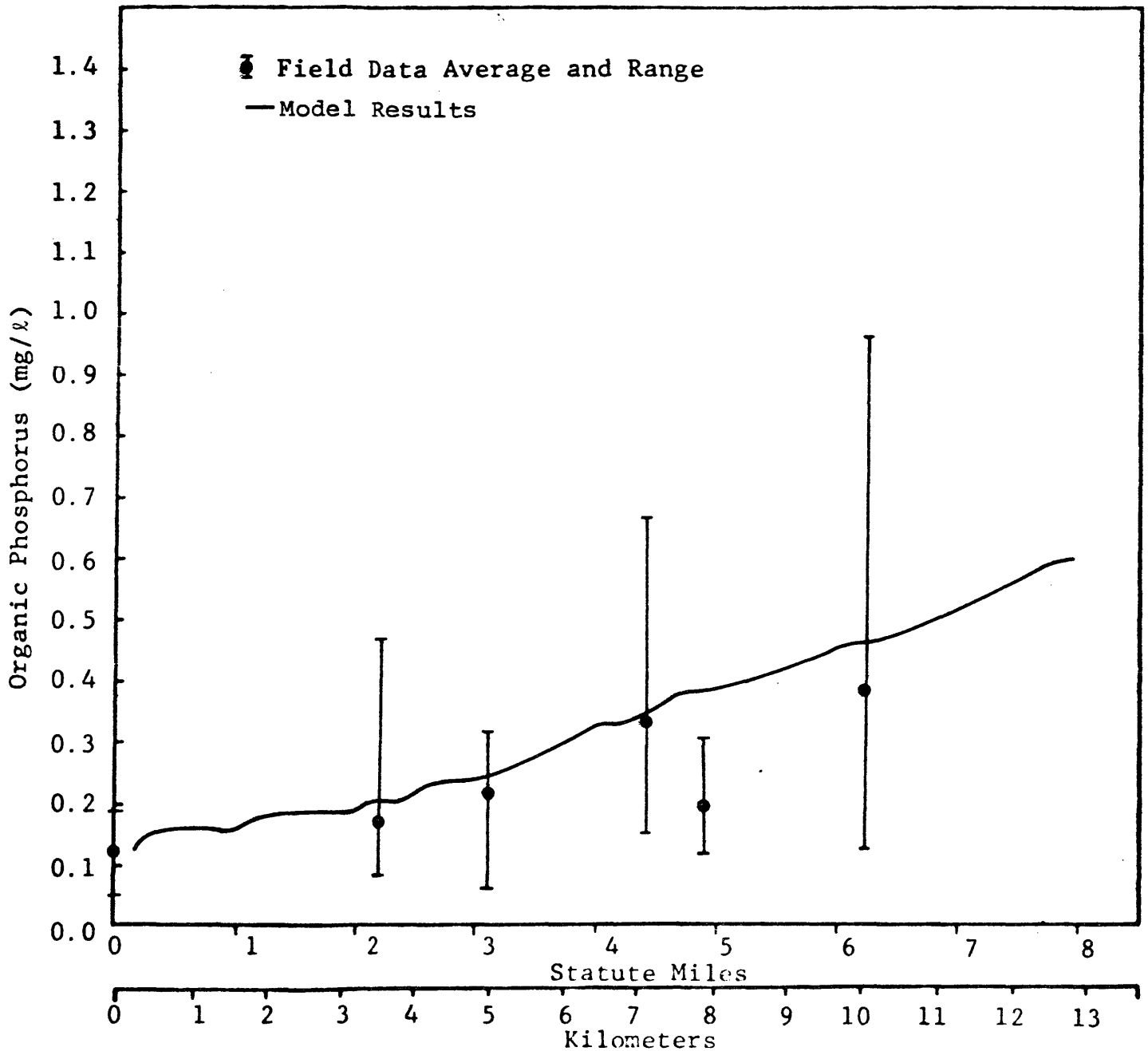

Figure 13. Comparison between computed Organic Phosphorus distribution and field data, June 28,and29, 1976.

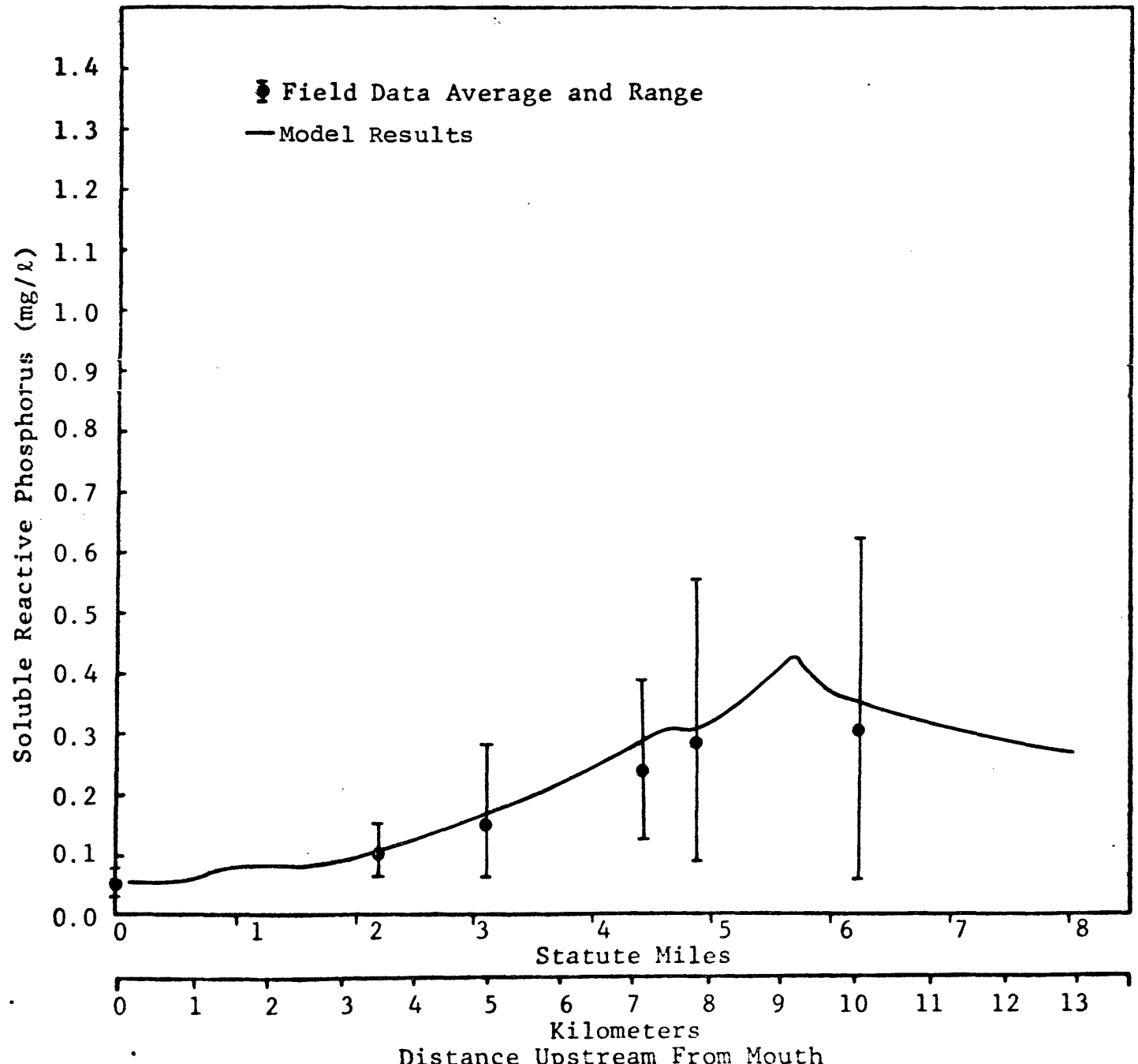

Figure 14. Comparison between computed Soluble Reactive Phosphorus distribution and field data, June 28 and 29, 1976.

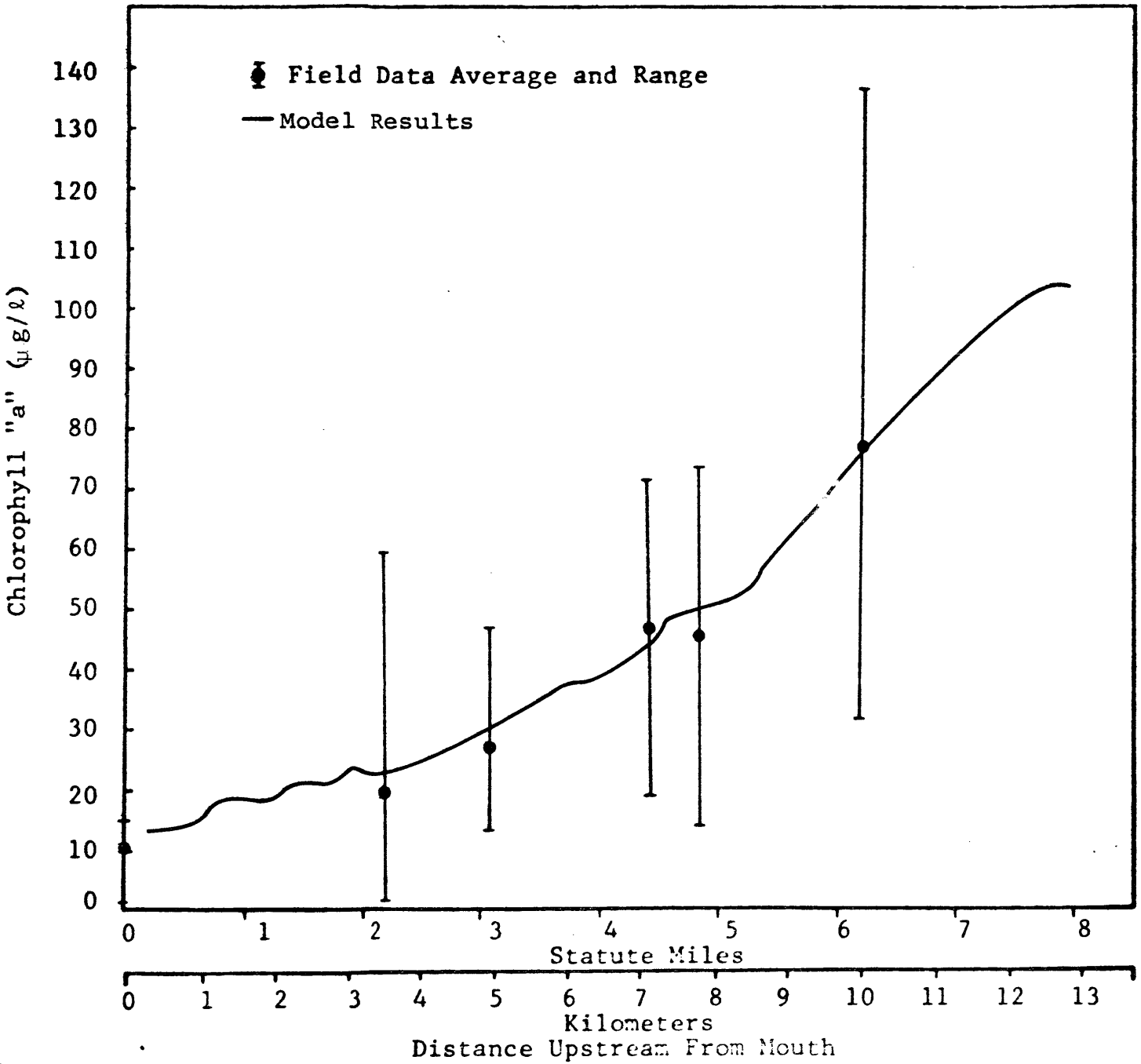

Figure 15. Comparison between computed Chlorophyll "a" distribution and field data, June 28 and 29, 1976.

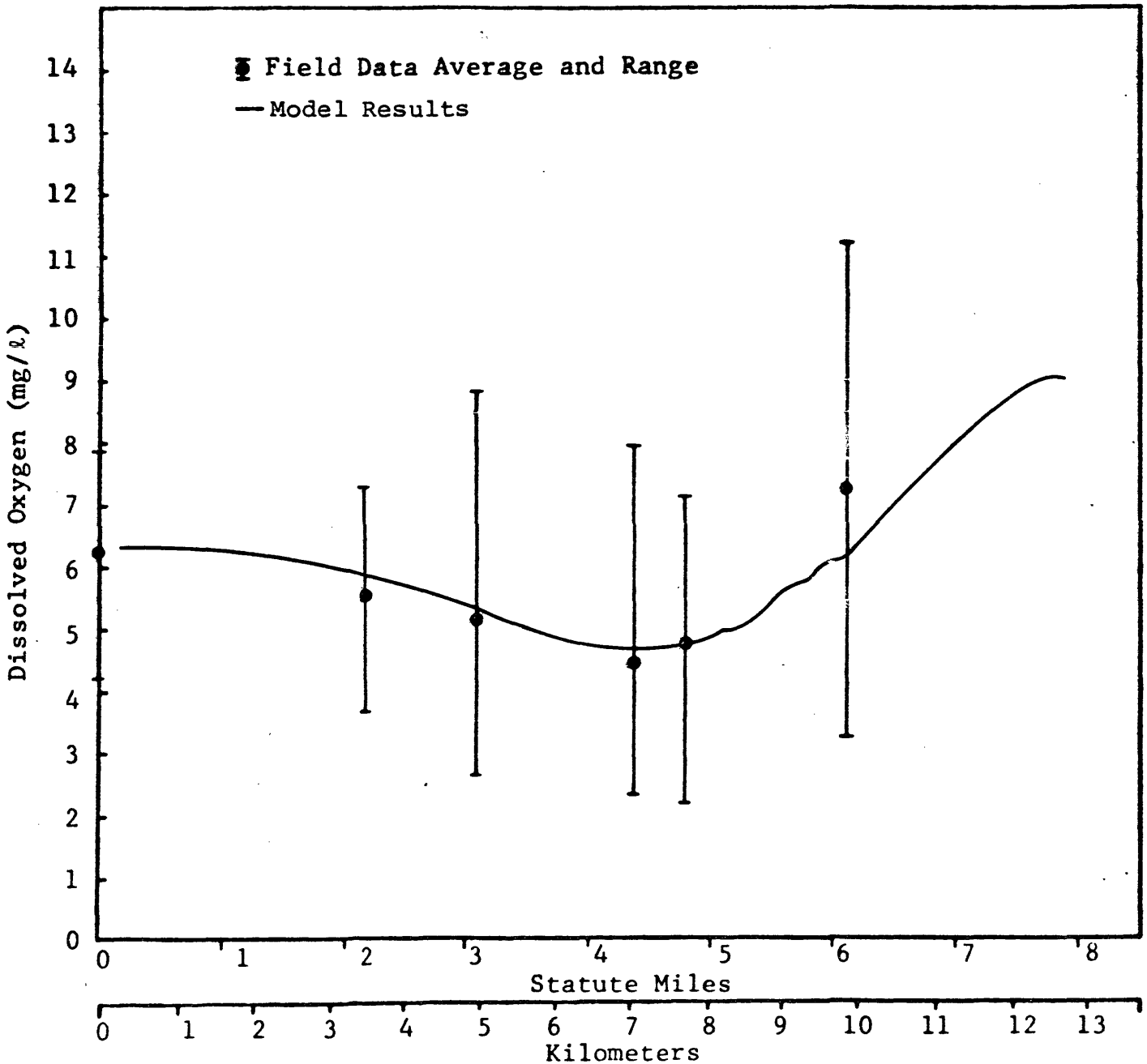

Figure 16. Comparison between computed Dissolved Oxygen distribution and field data, June 28 and 29, 1976.

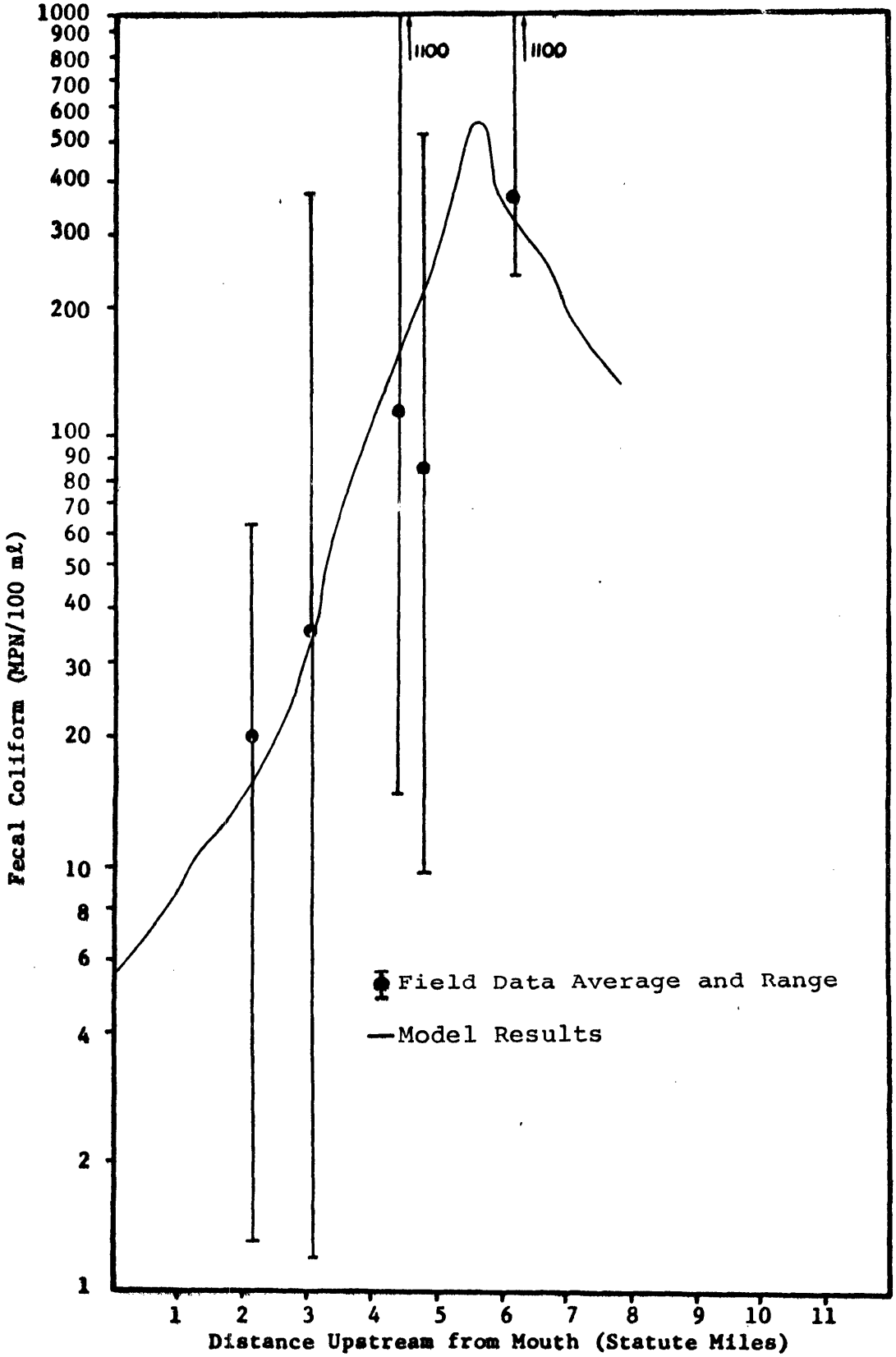

Figure 17. Comparison between computed Fecal Coliform distribution and field data, June 28 and 29, 1976.

C. Verification

For this model application all literature values and calibrated values of parameters were kept the same as for the calibration application as were the values of benthic oxygen demand. Field data values of turbidity were used with the calibrated proportion value. Solar radiation values measured in field for the relevant period are listed in Table 4. STORM model predictions of nonpoint source loads for the relevant period are listed in Table 2. Boundary and freshwater inflow concentrations were determined by examination of the field data and are listed in Table 8. Examination of the average value of chlorophyll "a" at each station for the two slack water surveys (figure 24), both conducted during daylight hours when maximum phytoplankton growth is expected, compared to the corresponding intensive survey values (figure 15) reflecting both day and night concentrations, suggests that the phytoplankton population was somewhat smaller during the August period. This is reflected in lower concentrations of organic nitrogen, chlorophyll "a", CBOD and DO in the lateral inflow. A temperature of 27.85, reflecting average field measurements, was used.

Field data for the model verification were obtained on August 23, 1976, during low water slack and during a high water slack on the following day.

Figures 18 through 26 show comparisons of tidal average model predictions with observed field data for the two slack water surveys. (Organic phosphorus field values could not be determined because total phosphorus water samples were misplaced.)

TABLE 9. BOUNDARY AND FRESHWATER INFLOW CONCENTRATIONS USED IN THE MODEL VERIFICATION APPLICATION

	Downstream Boundary	Freshwater Inflow
Salinity ppt	16.0	0.1
Organic nitrogen mg/l	0.20	0.2
Ammonia nitrogen mg/l	0.25	0.1
Nitrite & Nitrate nitrogen mg/l	0.15	0.01
Inorganic phorphorus mg/l	0.05	0.1
Chlorophyll "a" µg/l	5.0	80.
CBOD mg/l	1.0	1.0
DO mg/l	6.5	5.0
Fecal coliform MPN/100 ml	3.0	1.0

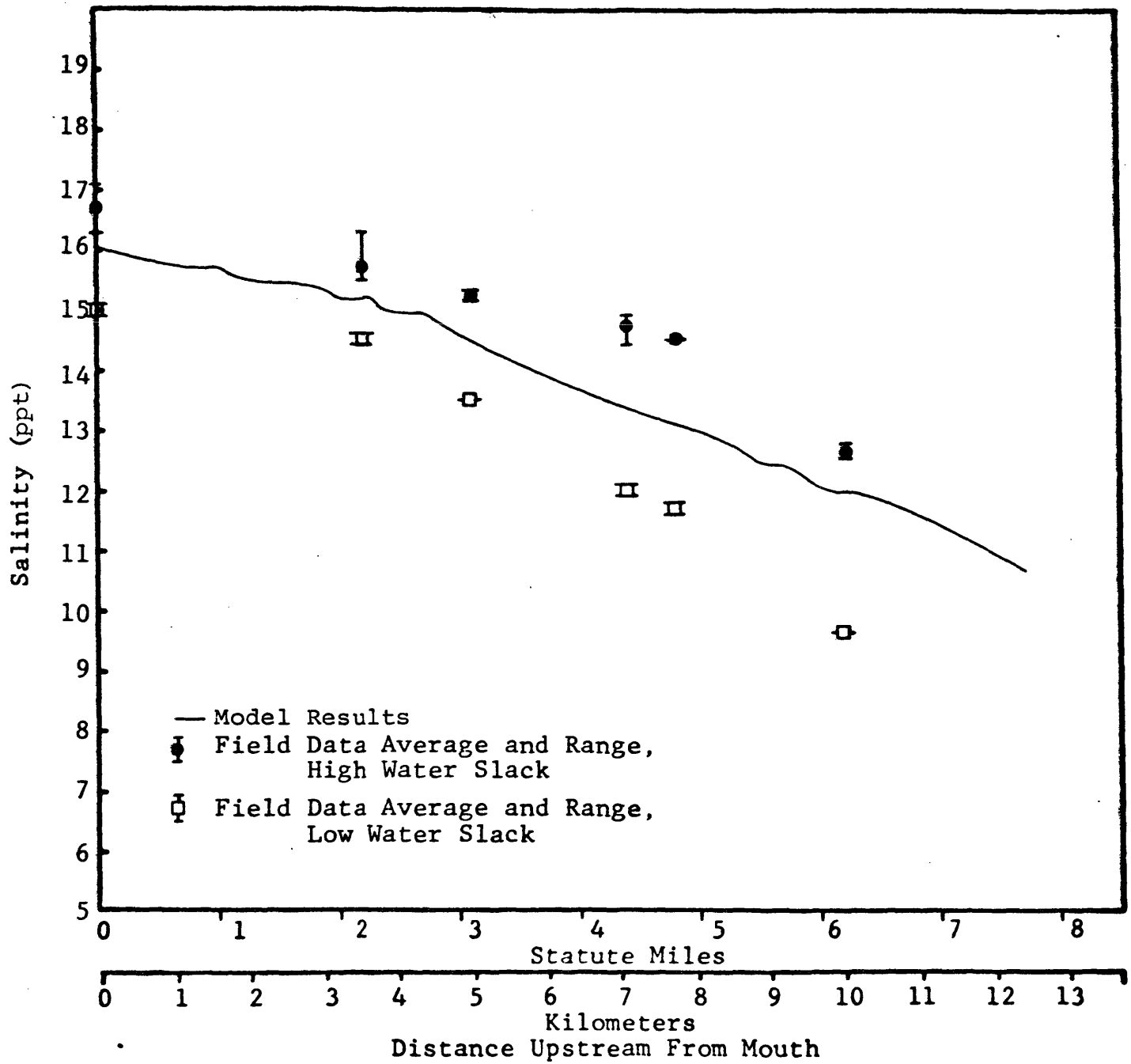

Figure 18. Comparison of computed salinity distribution with field data, August 23, and 24, 1976.

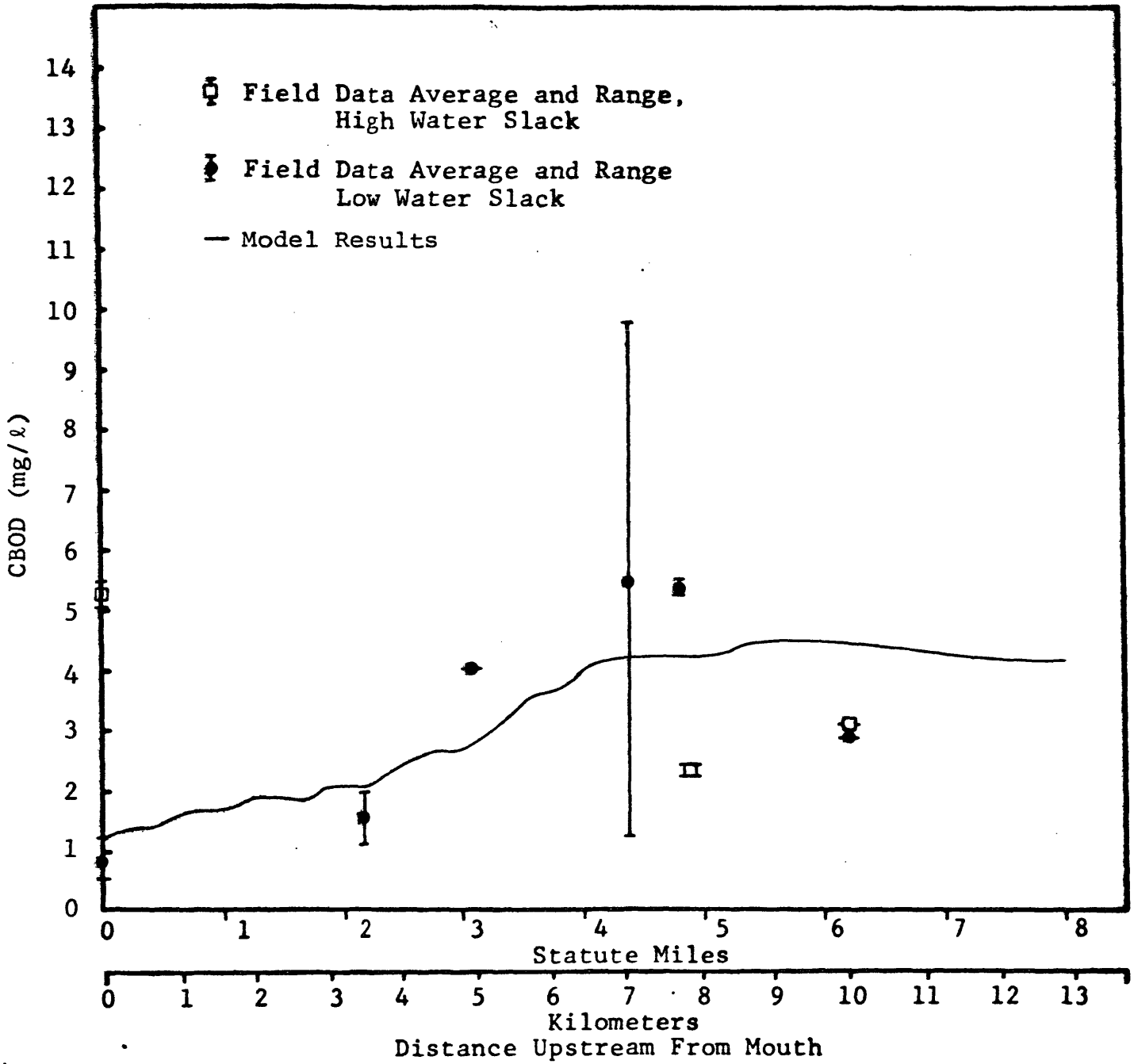

Figure 19. Comparison of computed CBOD distribution with field data, August 23, and 24, 1976.

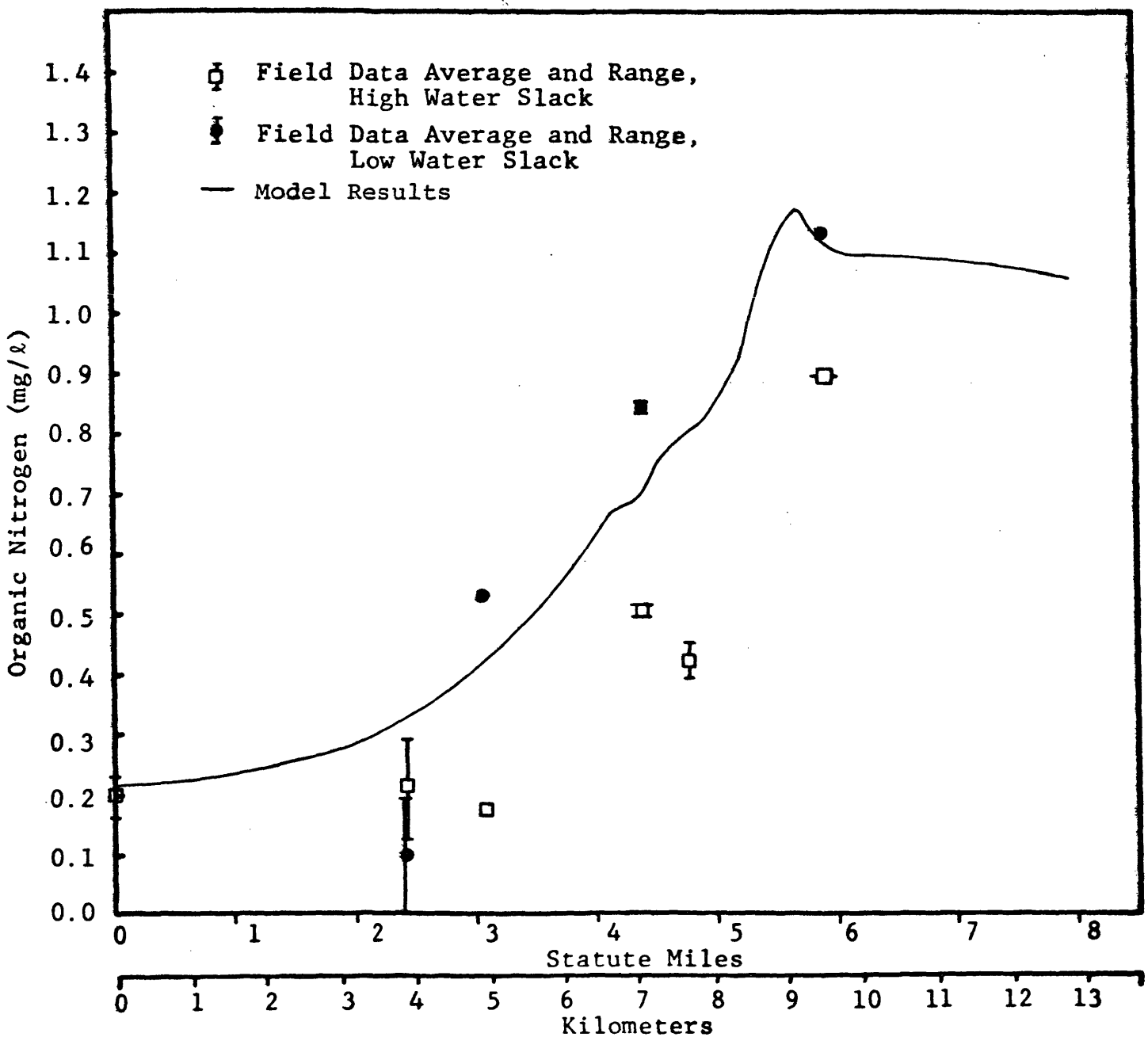

Figure 20. Comparison of computed Organic Nitrogen distribution with field data, August 23 and 24, 1976.

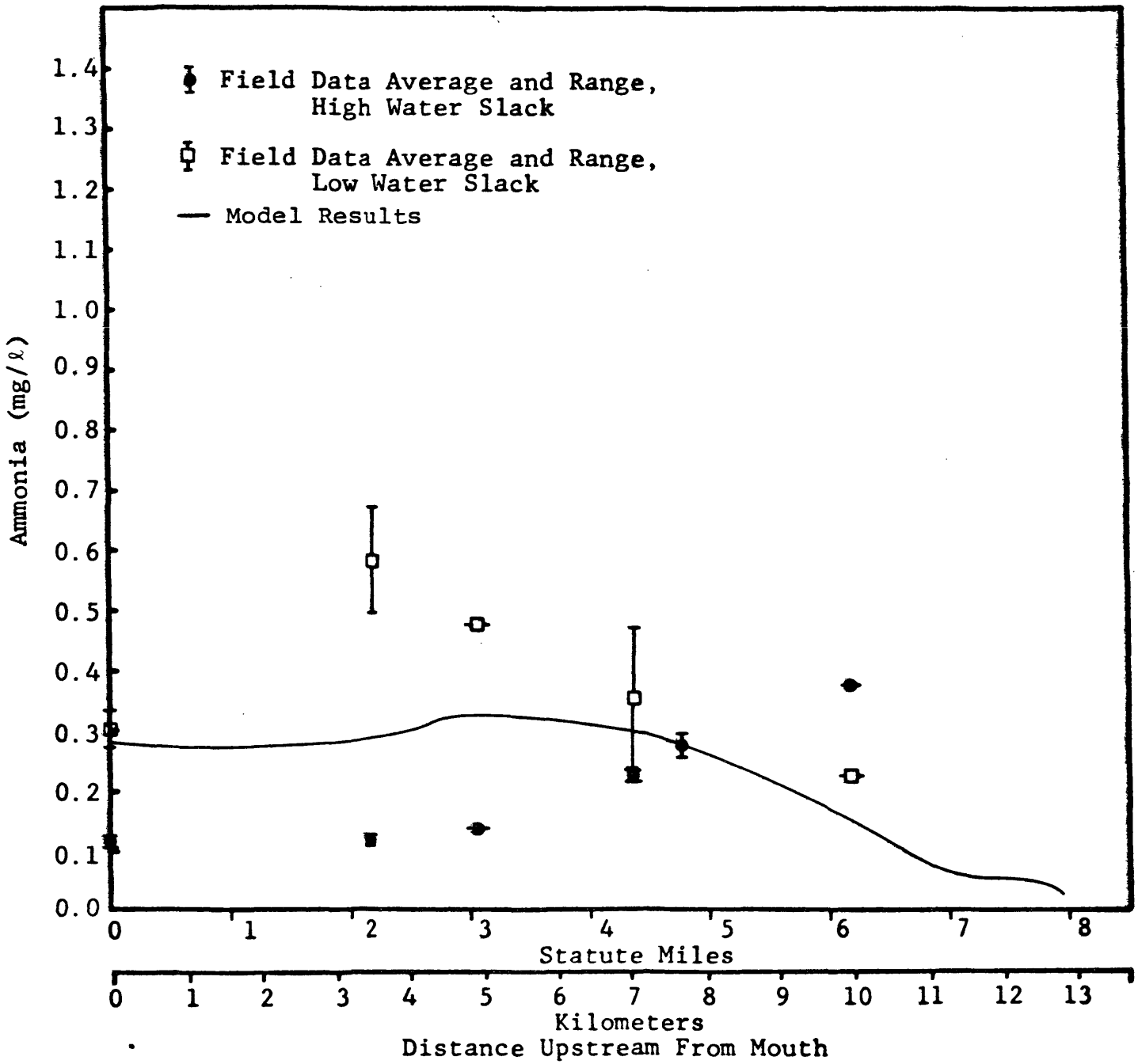

Figure 21. Comparison of computed Ammonia distribution with field data, August 23 and 24, 1976.

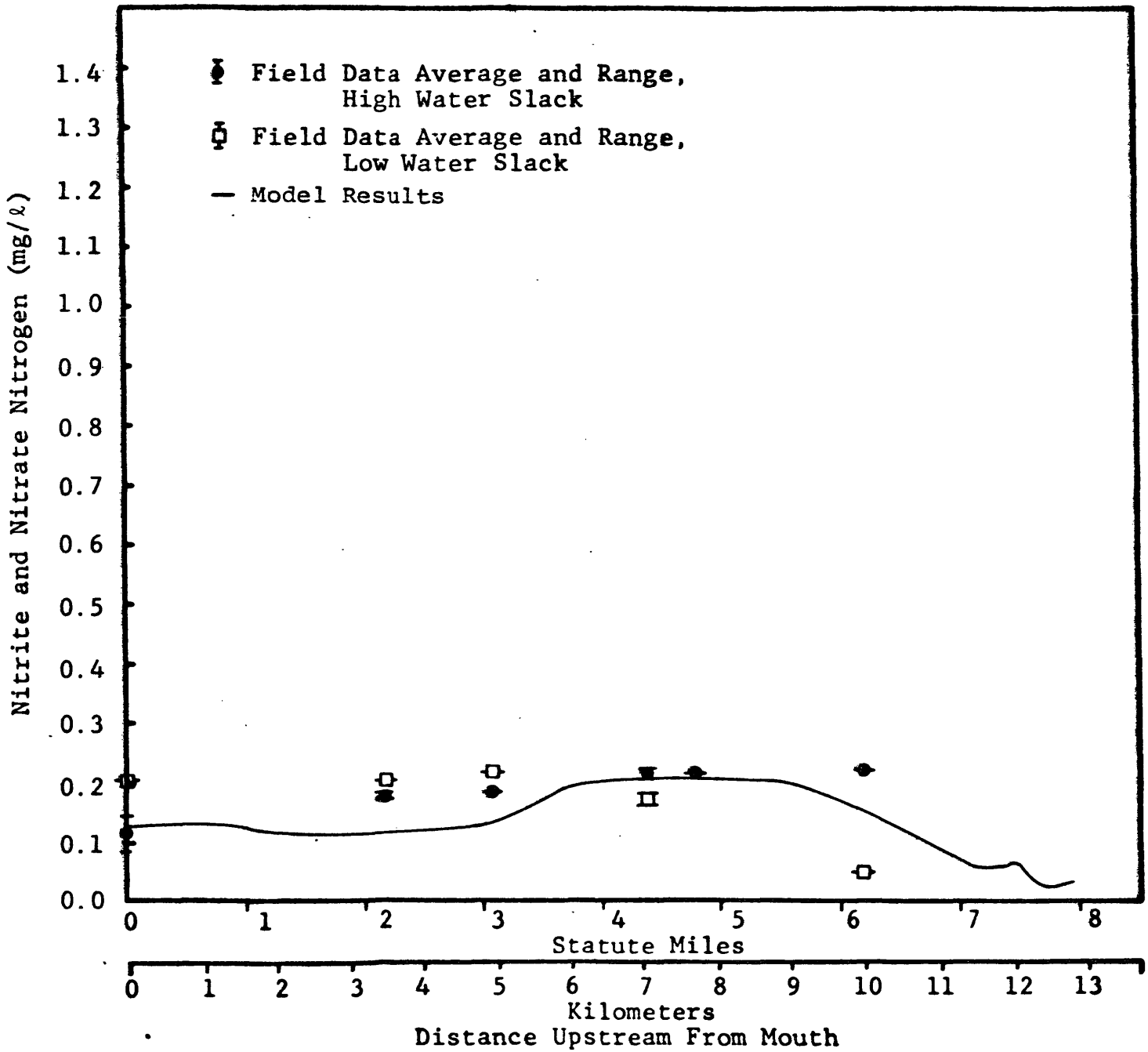

Figure 22. Comparison of computed Nitrite and Nitrate Nitrogen distribution with field data, August 23 and 24, 1976.

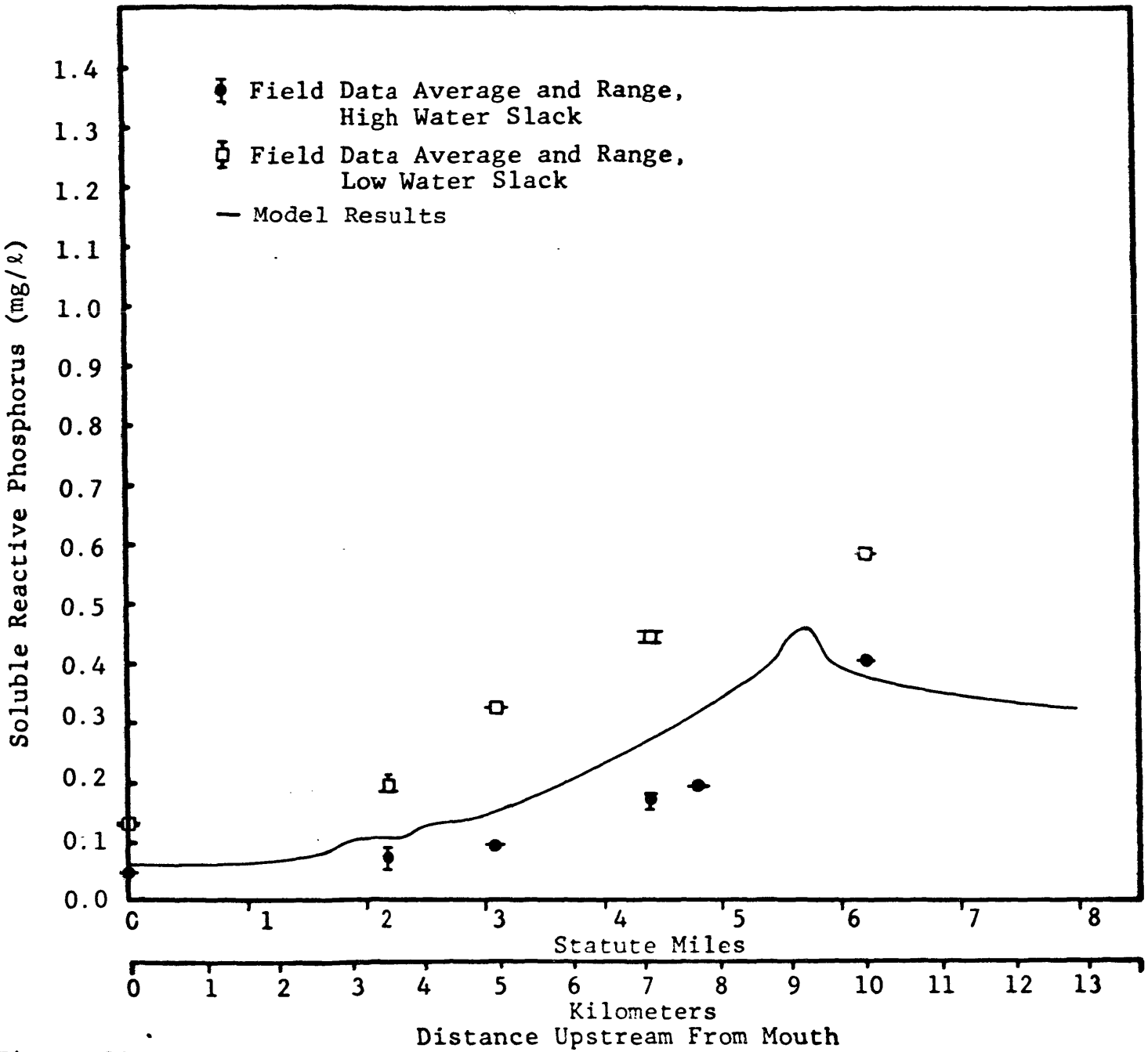

Figure 23. Comparison of computed Soluble Reactive Phosphorus distribution with field data, August 23 and 24, 1976.

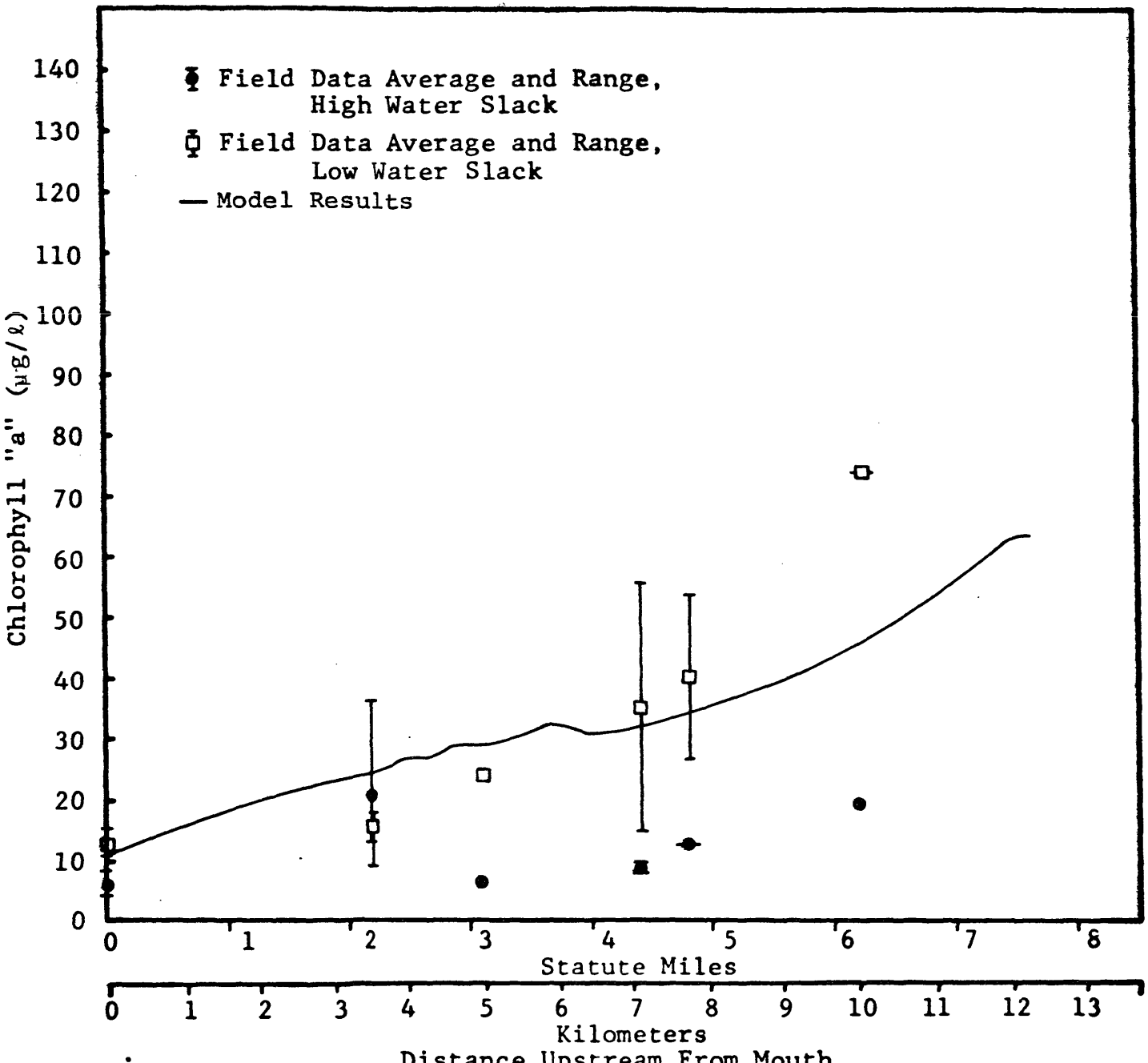

Figure 24. Comparison of computed Chlorophyll "a" distribution with field data, August 23 and 24, 1976.

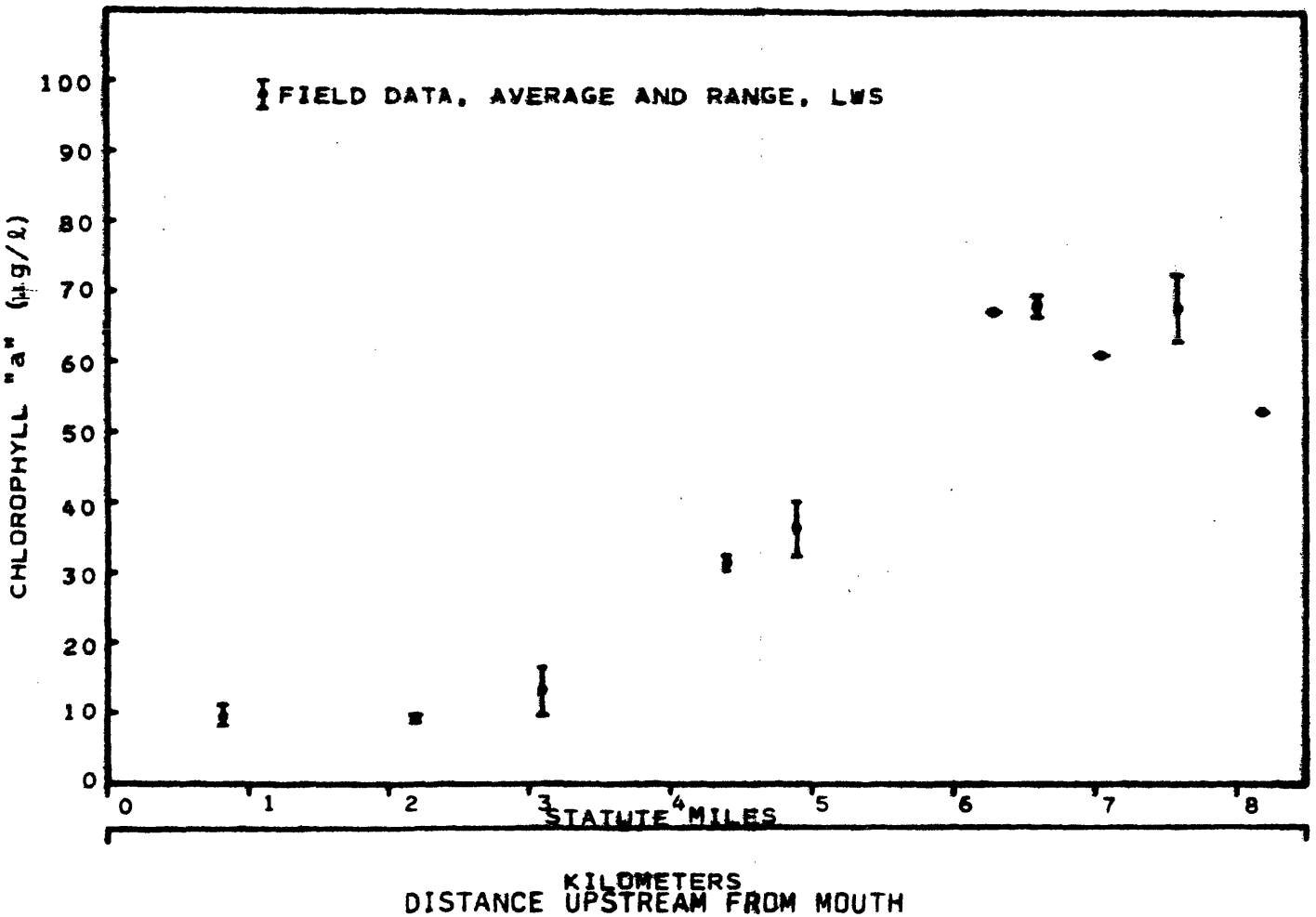

Figure 24A. Chlorophyll "a" distribution, June 22, 1977.

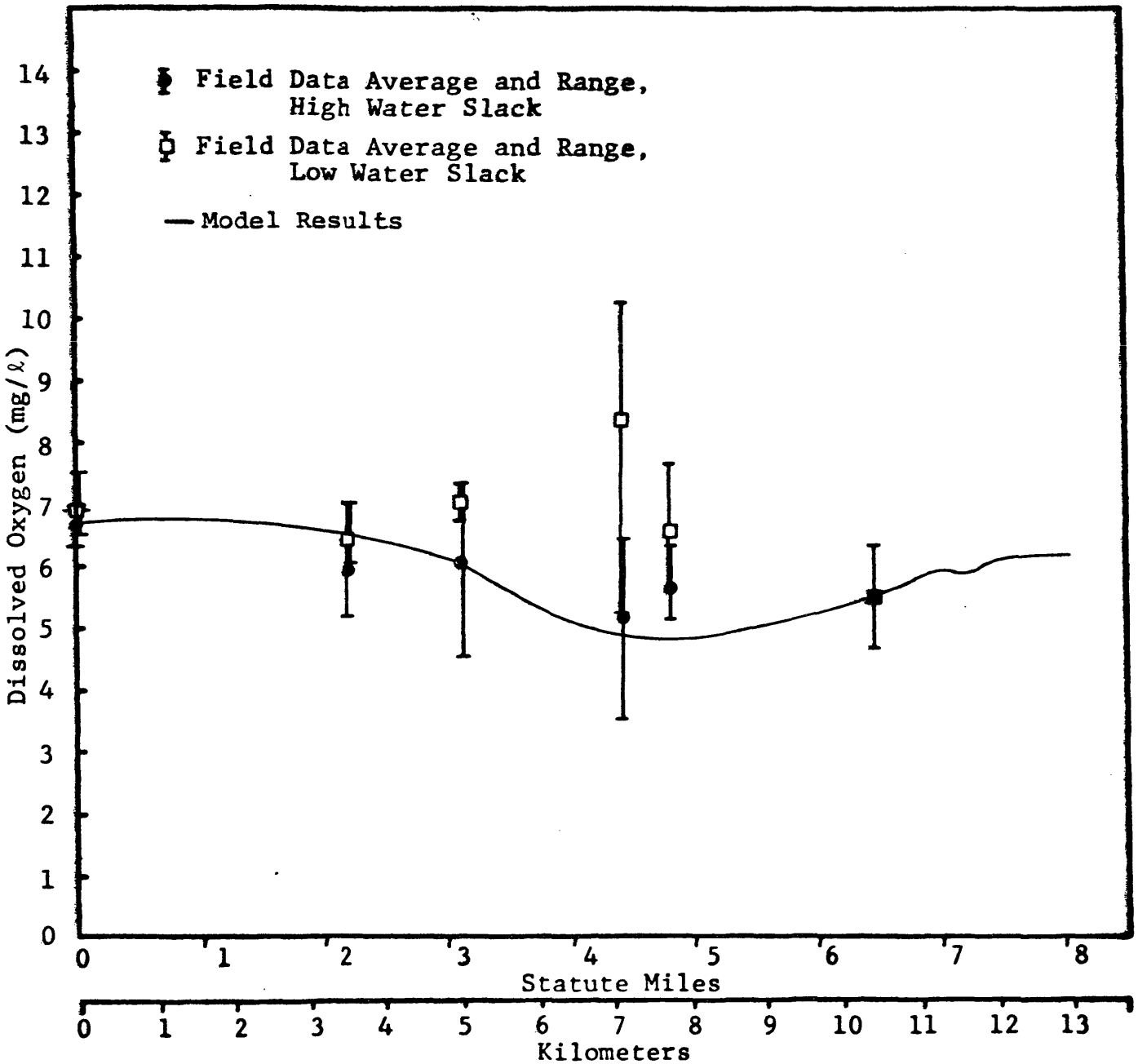

Figure 25. Comparison of computed Dissolved Oxygen distribution with field data, August 23 and 24, 1976.

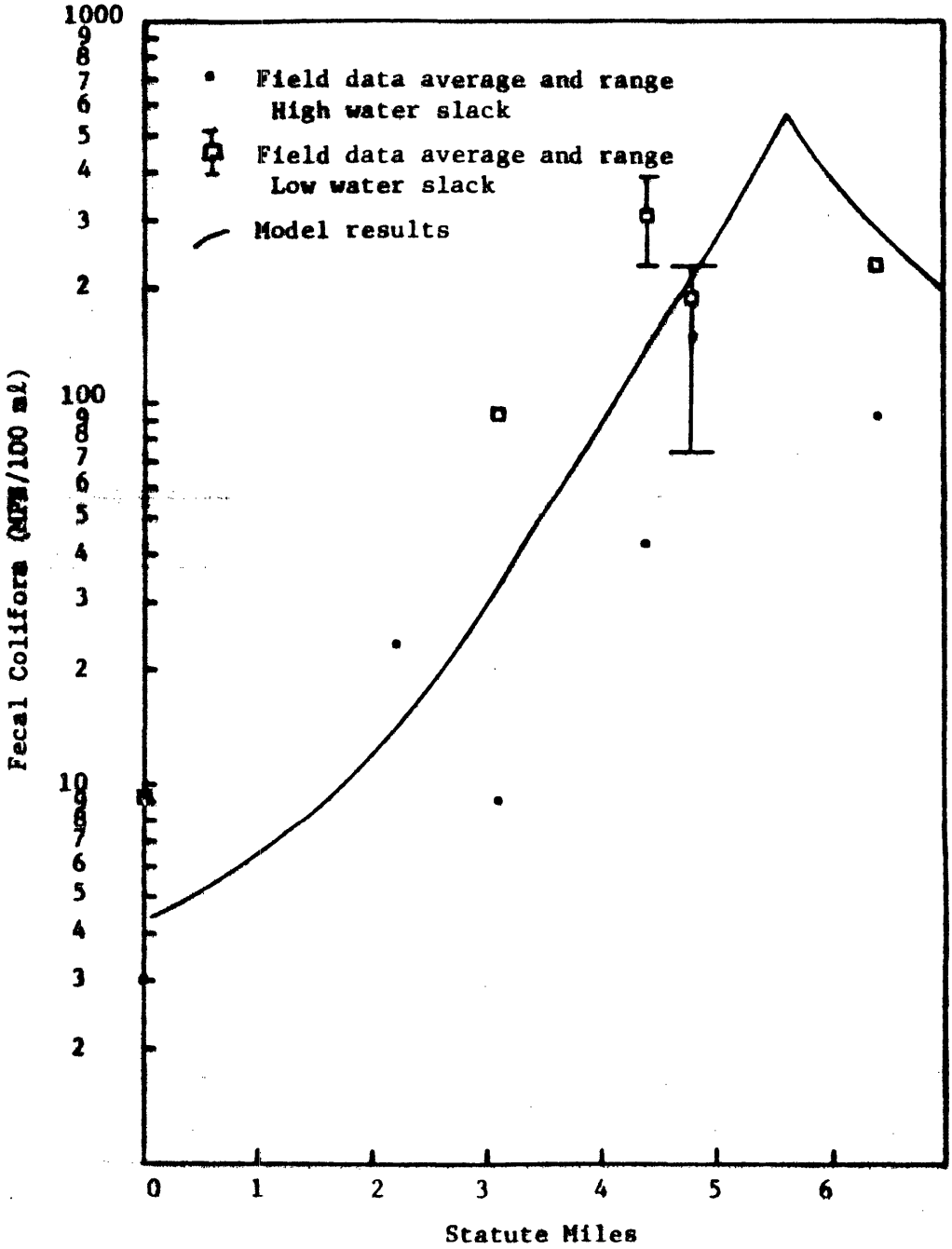

Figure 26. Comparison of computed coliform distribution with field data, August 23 and 24, 1976.

The verification model predictions do reflect the general longitudinal trends of the water quality constituents. The predicted tidal average values usually lie between the values observed at high water slack and at low water slack. However, the agreement is not as good as for the calibration runs. Part of the discrepancy results from the limited data set. The intensive survey data show large variations in concentrations of most constituents in response to tides and sunlight. Only a part of these variations can be reflected in field data collected at only two times during the diurnal and tidal cycles.

Field observations sometimes are difficult to interpret and/or explain. For example, chlorophyll "a" concentrations at high water slack are only about a fifth of the values observed at low water slack (Figure 24). Although dilution at high slack is to be expected, the degree of change normally is not so large. Field measurements from an additional slack survey on June 22, 1977, show intermediate values but the same general trend. That is chlorophyll "a" concentrations increase monotonically in the upriver direction.

The DO levels which are significantly above the model predictions also are at or above the saturation value. This indicates that phytosynthetic oxygen production was strong. Algal masses are "patchy" whereas the model predicts cross-sectional average values. Thus, there always is the possibility of minor variances between the predictions and field observations.

D. Sensitivity Analysis

A series of model runs was made to determine the sensitivity of the model to various input values. Figures 27 through 40 show the effect of varying those parameters determined during the calibration process. For example, the effect that doubling (or halving) the dispersion coefficient has on the salinity gradient is shown in Figure 27.

The increased mixing that an increase in dispersion coefficient signifies results in an upstream movement of salt. Therefore, for the salinity regime the impact of changing dispersion coefficient increases in the upriver direction. The impact on DO, on the other hand, varies throughout the river with maximum changes of about 0.5 mg/l (Figure 28).

Altering the CBOD decay rate has a dramatic effect on the BOD levels, but a less pronounced impact on DO levels (Figures 29 and 30). Increasing the hydrolysis rate for nitrogen decreases the levels of organic nitrogen appreciably, and results in increased concentrations of ammonia. The increase in ammonia levels is smaller than the decrease in organic nitrogen levels, presumably because ammonia oxidized and taken up by plankton at a fairly rapid rate (Figures 31 and 32). Similarly an increase in the rate of nitrification reduces ammonia levels and increases concentrations of nitrite and nitrate nitrogen. In this case the changes are roughly equal (Figures 33 and 34). The increased rate of nitrification also reduces the DO levels throughout the river. DO levels in the middle portion of the river increased about 0.5 mg/l when the nitrification rate was reduced by 50% (Figure 35).

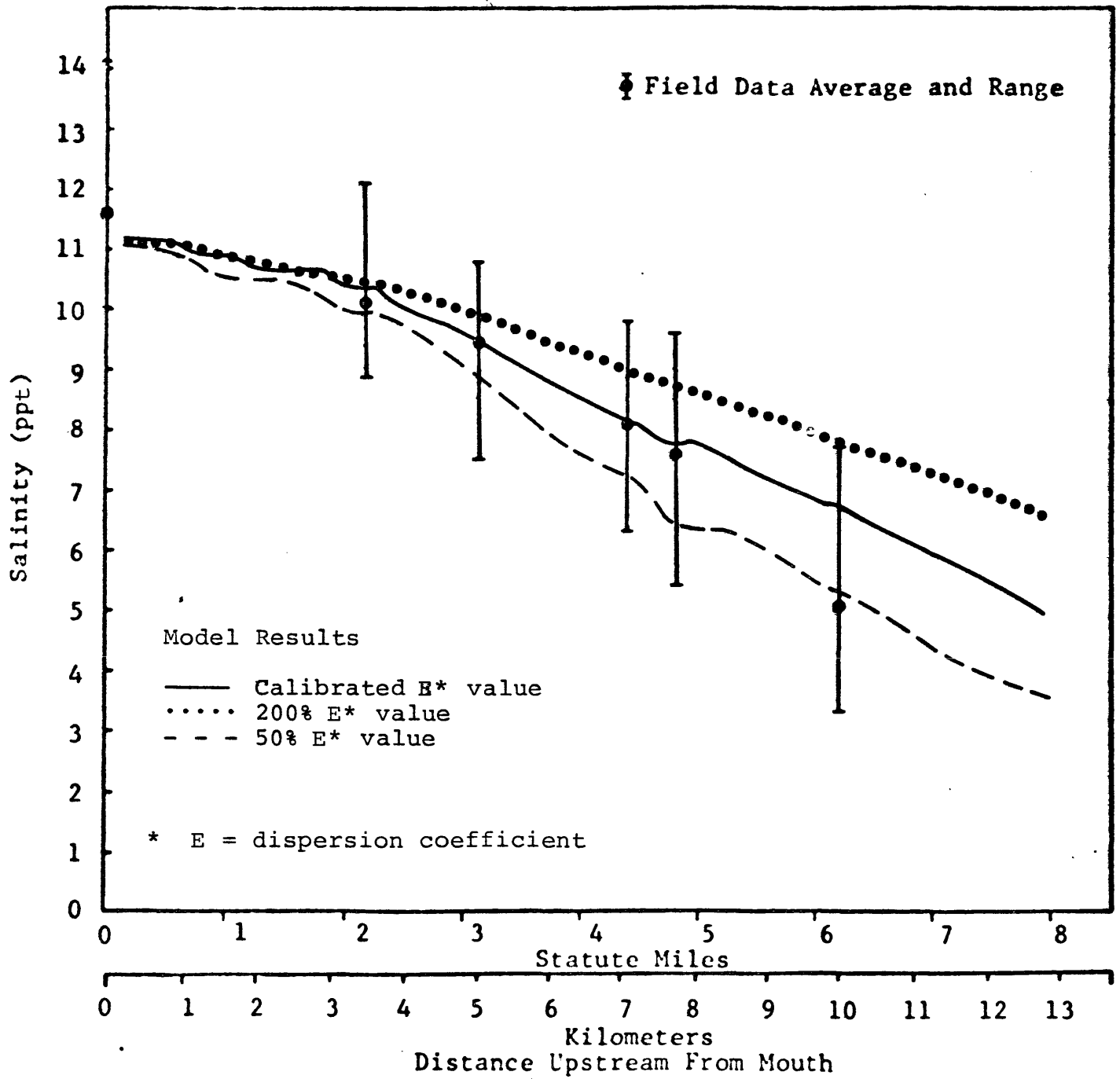

Figure 27. Effect of dispersion coefficient on salinity.

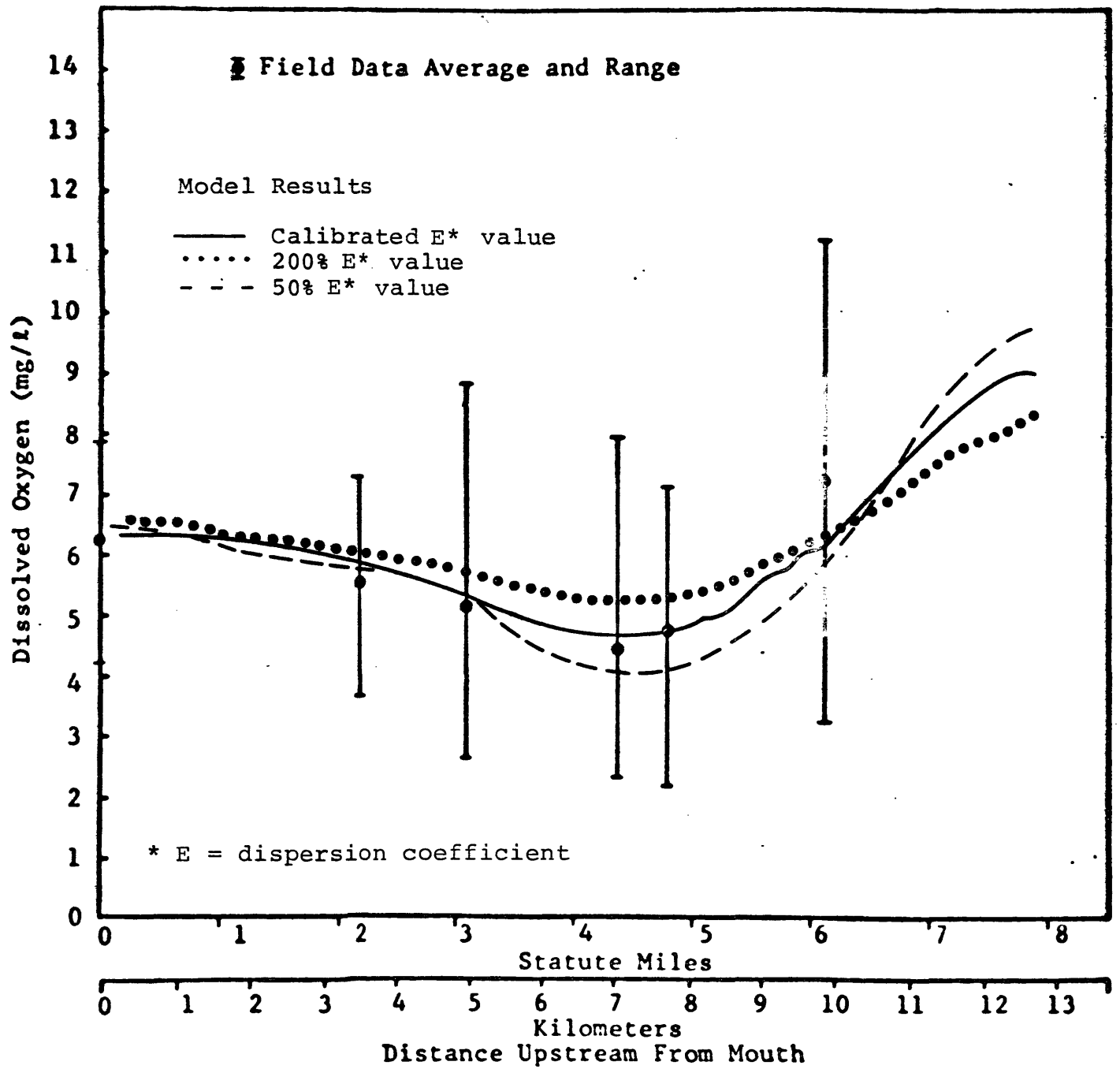

Figure 28. Effect of dispersion coefficient on DO concentration.

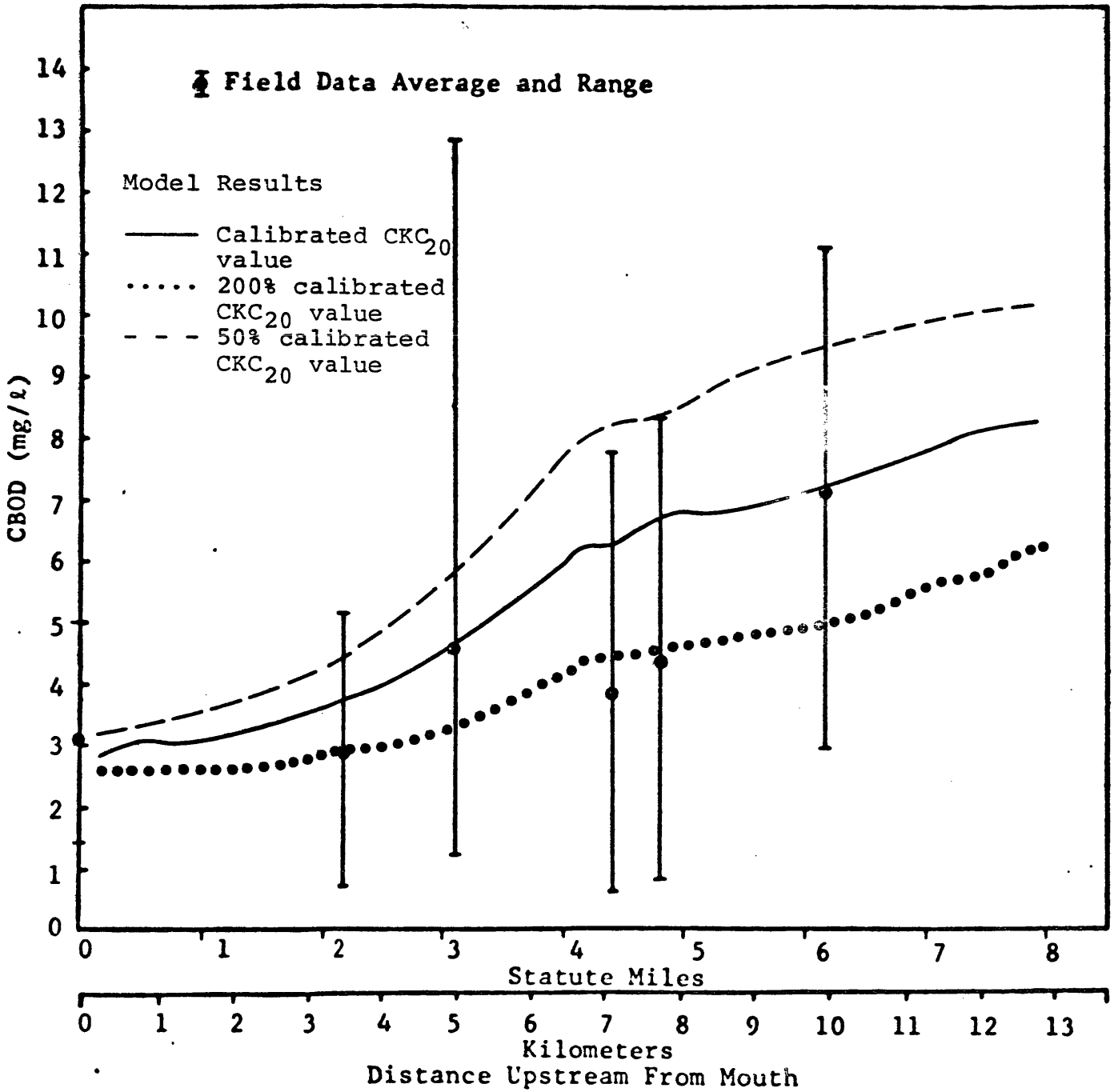

Figure 29. Effect of CBOD decay rate on CBOD concentration.

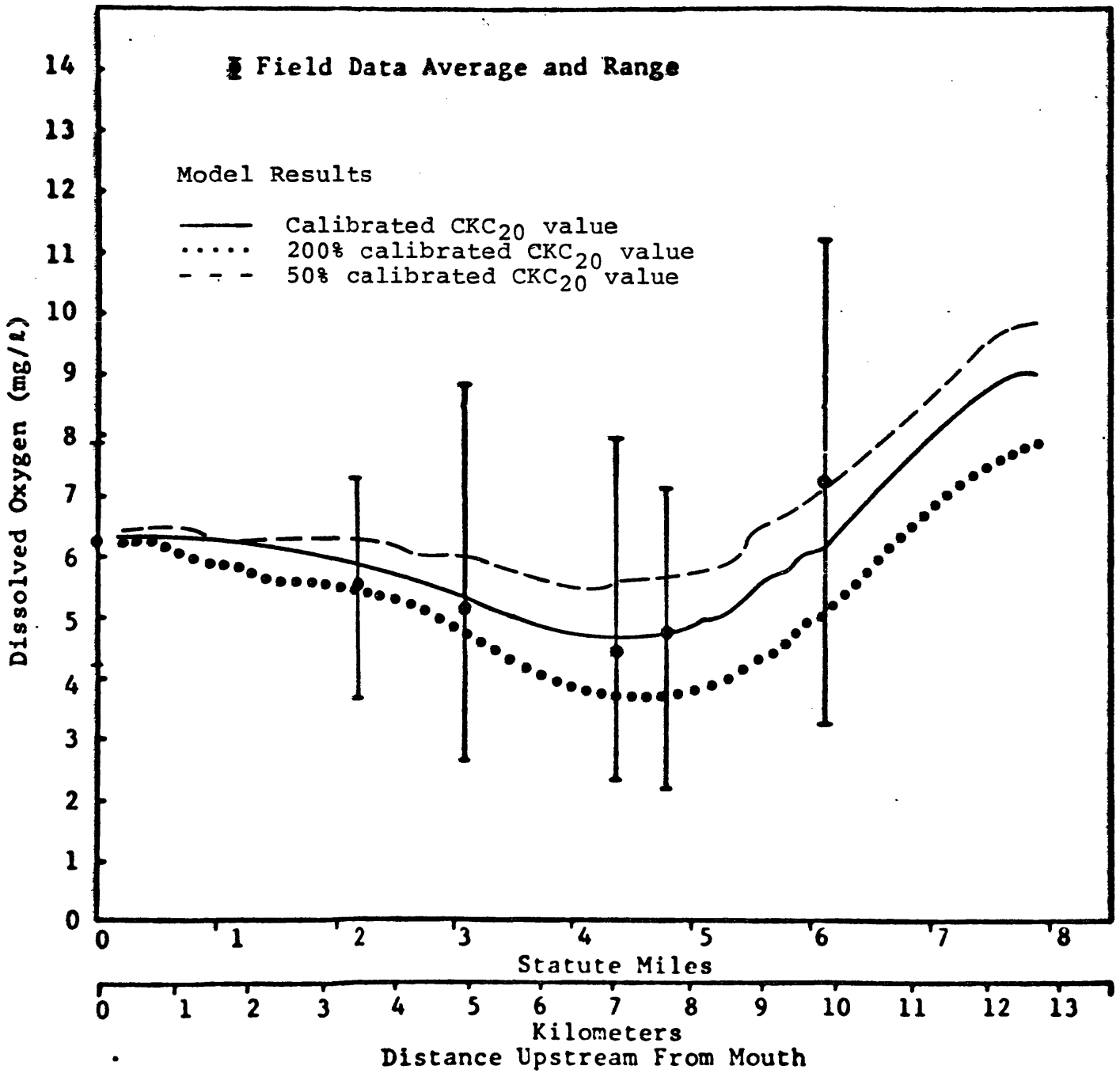

Figure 30. Effect of CBOD decay rate on DO concentration.

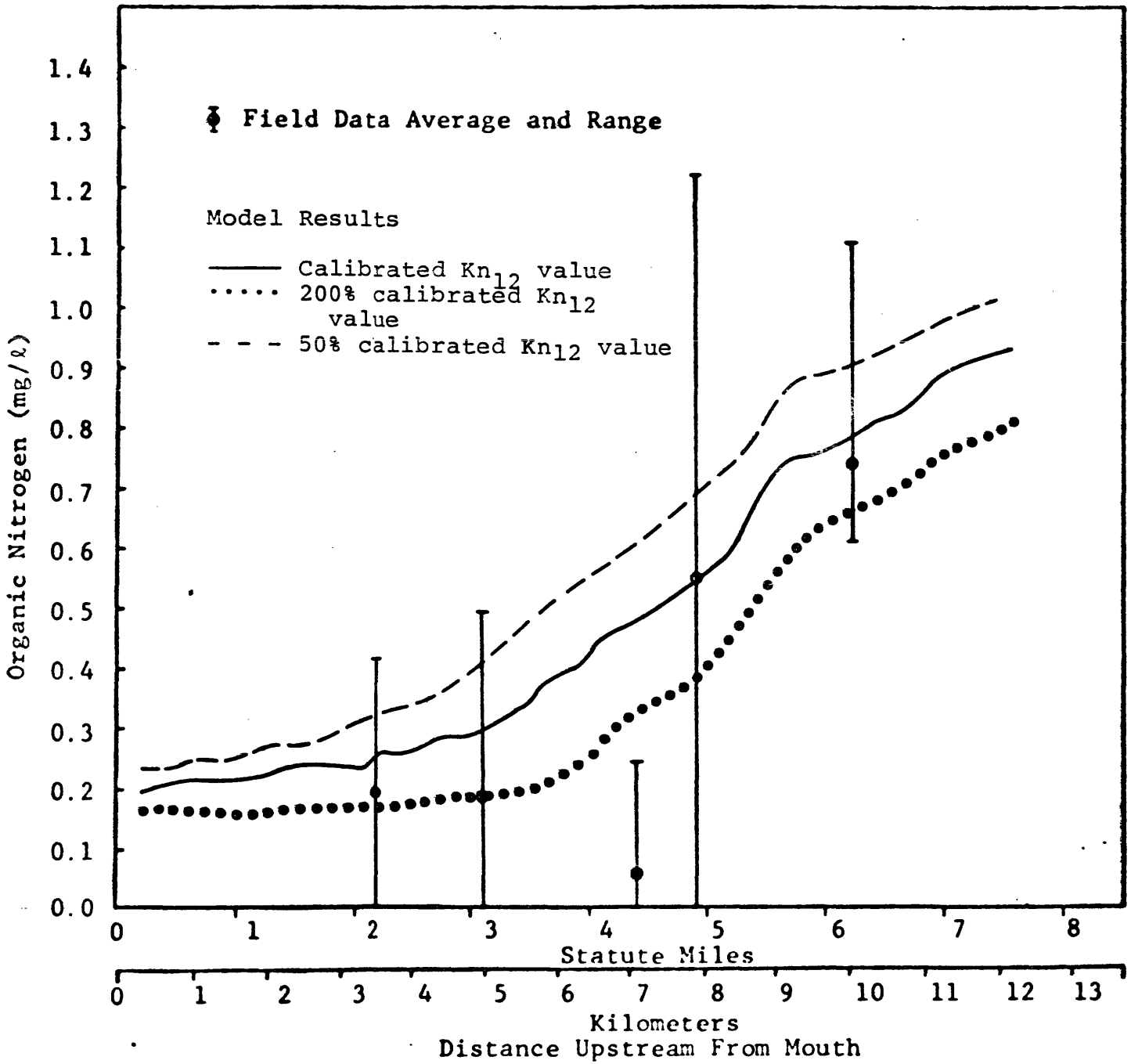

Figure 31. The effect of hydrolysis rate on organic nitrogen concentration.

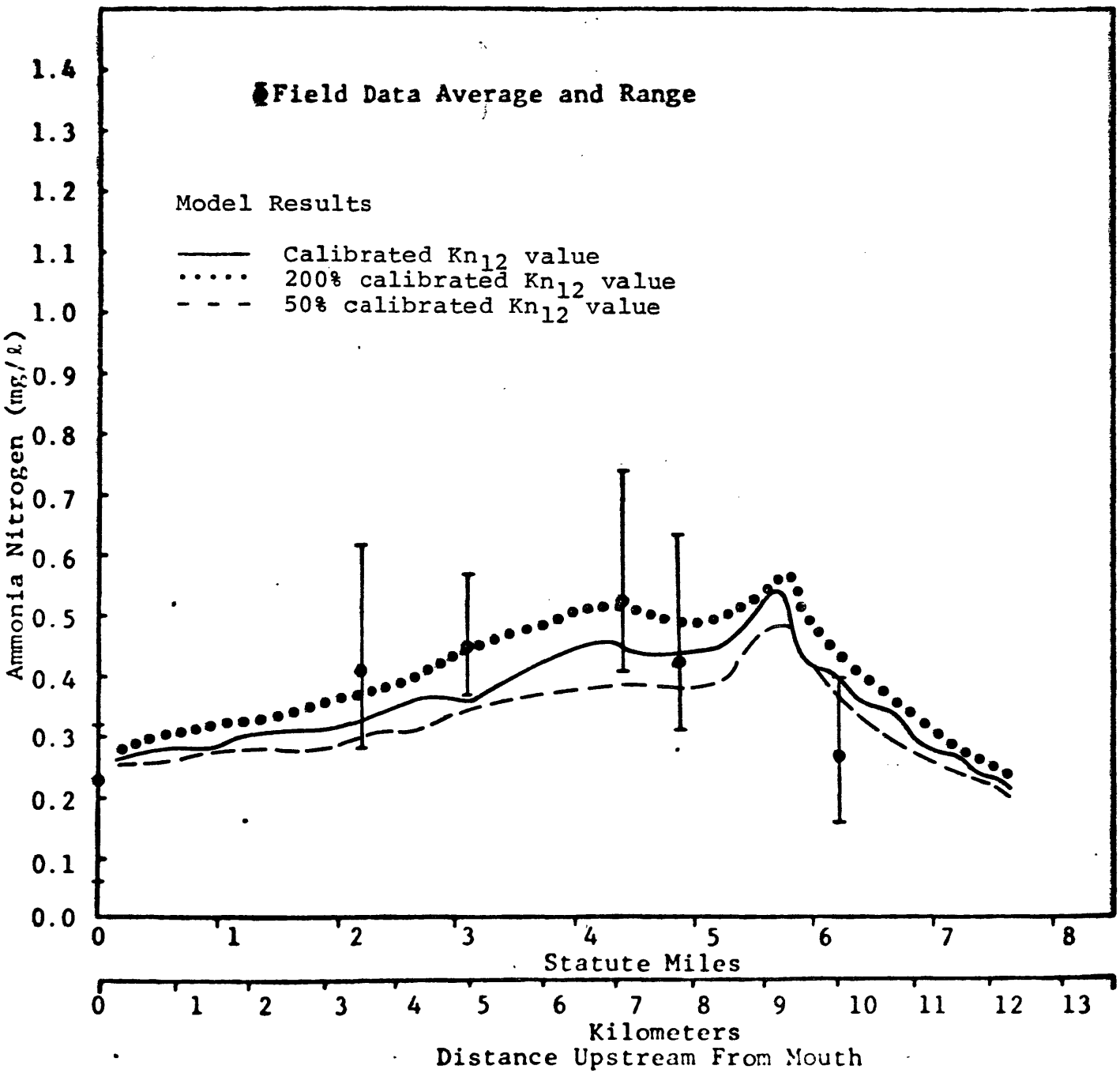

Figure 32. The effect of hydrolysis rate on ammonia nitrogen concentration.

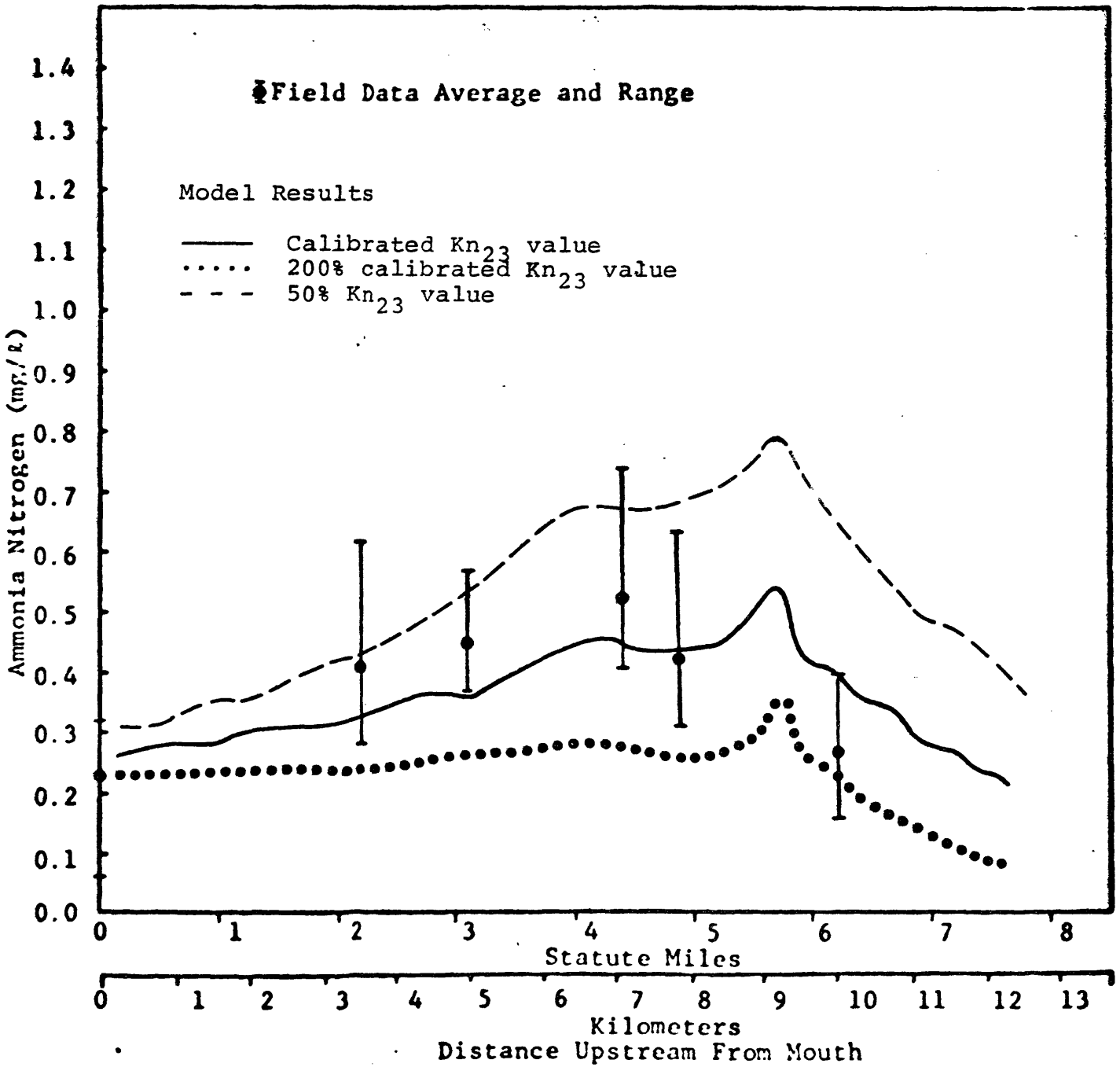

Figure 33. Effect of nitrification rate on ammonia nitrogen concentration.

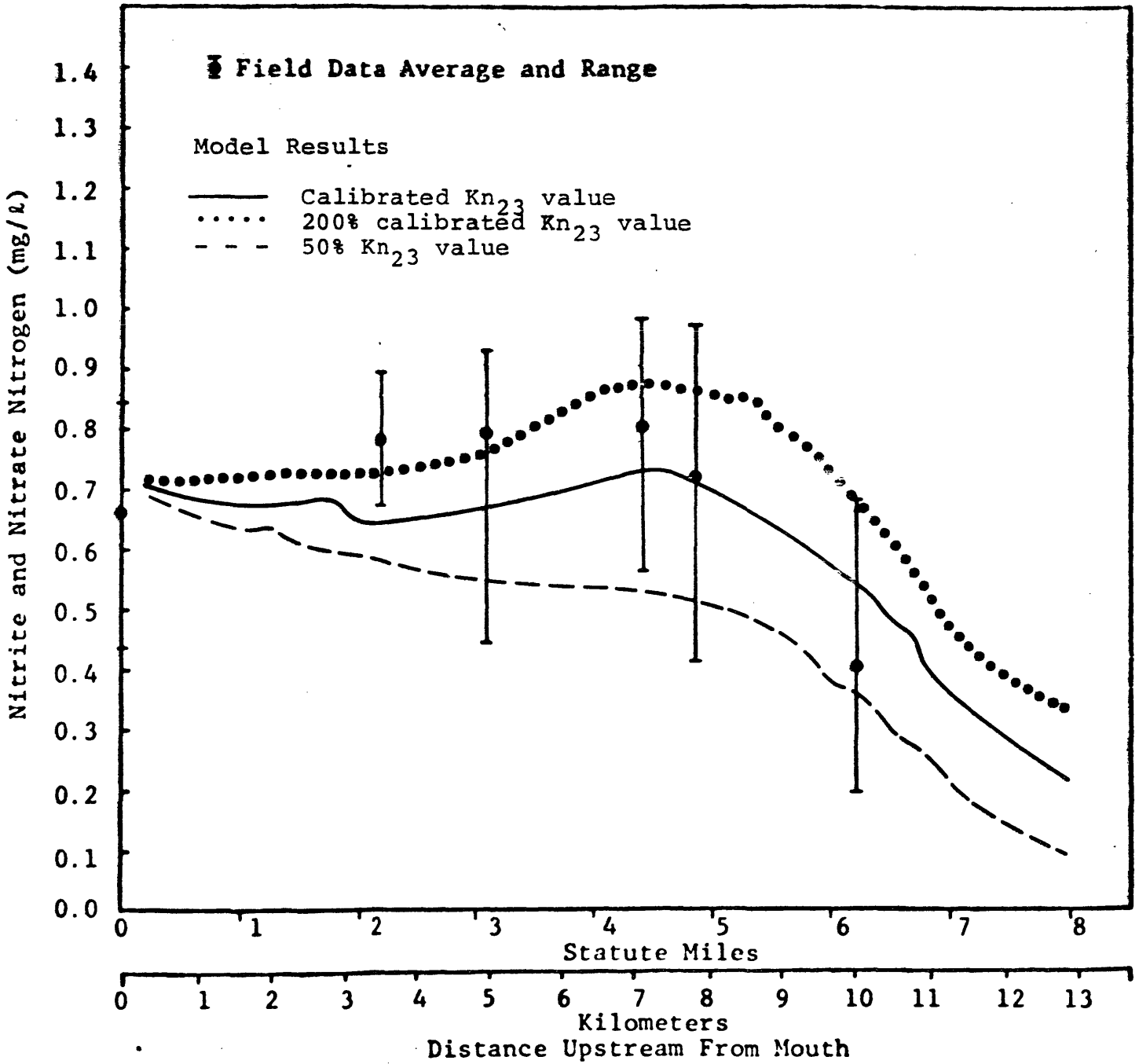

Figure 34. Effect of nitrification rate on nitrite and nitrate nitrogen concentration.

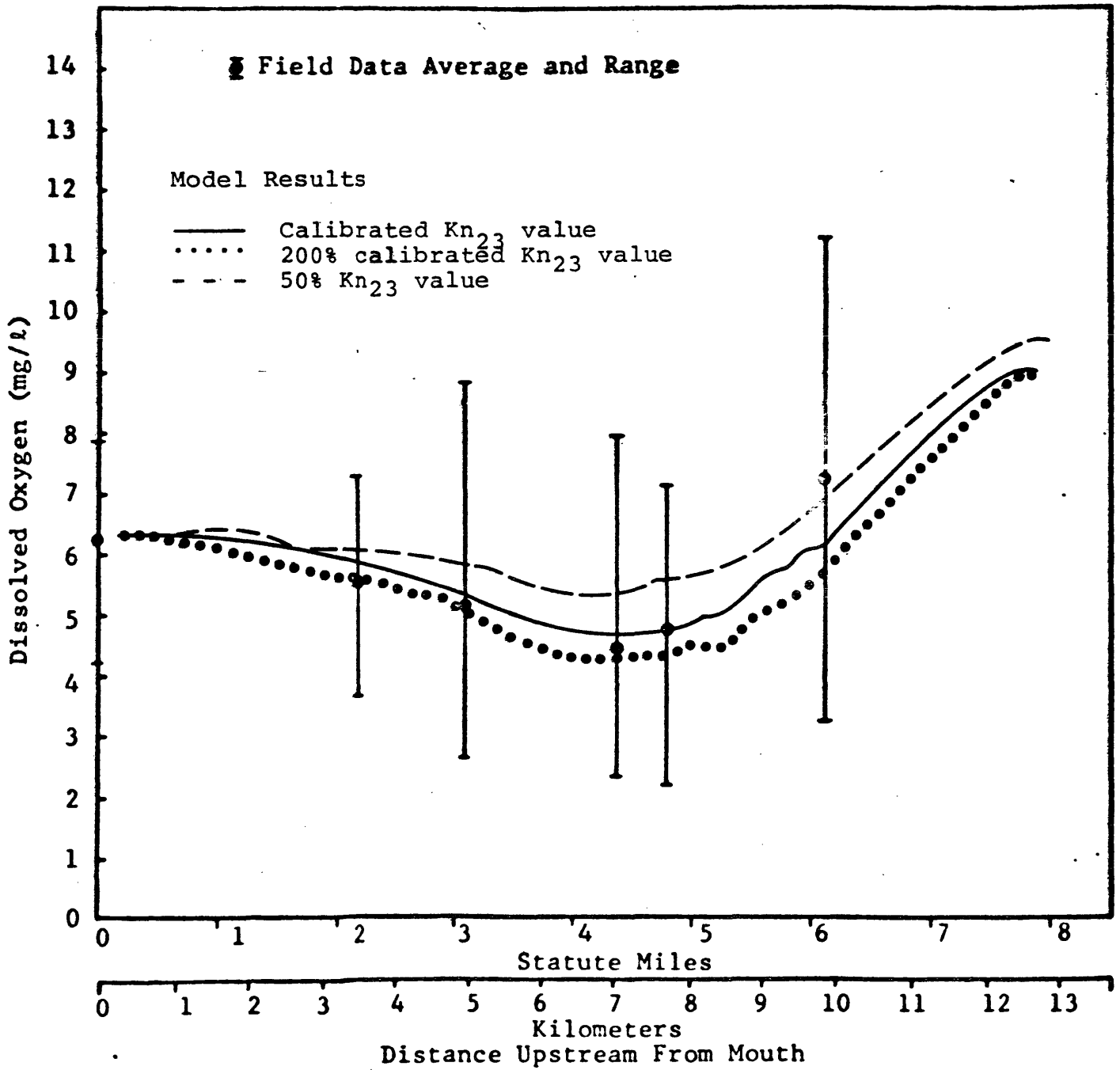

Figure 35. Effect of nitrification rate on DO concentration.

An increase in the transfer rate for phosphorus results in a decrease in organic phosphorus concentrations, a smaller increase in inorganic phosphorus levels, and a very small change in DO levels (Figures 36, 37 and 38).

Phytoplankton concentrations are sensitive to the rate of grazing by zooplankters. A 20% increase in the grazing rate reduces the plankton levels by as much as 10 µg of chlorophyll "a" per liter of water (Figure 39). Fecal coliform concentrations similarly are sensitive to the die-off rate. A change in die-off rate will result in an opposite change in fecal coliform levels of nearly the same magnitude. In Figure 40, it can be seen that a doubling of the die-off rate reduces the bacterial levels by about a half, and halving the die-off rate roughly doubles the coliform counts.

Figures 41 through 45 show the effect of a change in certain natural conditions such as base freshwater flow, turbidity, and benthic oxygen demand. Figure 41 demonstrates the important role of the benthic oxygen demand in determining the DO profile in the middle and upstream portions of the study area. Eliminating the benthal uptake increased DO levels by about 4 mg/l. This large increase also reflects the impact of the high phytoplankton levels and the long days during summer, which together result in a large net input of oxygen due to photosynthesis. It is likely that dead plankton settle to the bottom and that decomposition of these cells contributes to the benthal demand. Therefore, a high plankton level and no benthal demand seems unlikely ever to occur in nature. The model simulation, however, does demonstrate the importance of

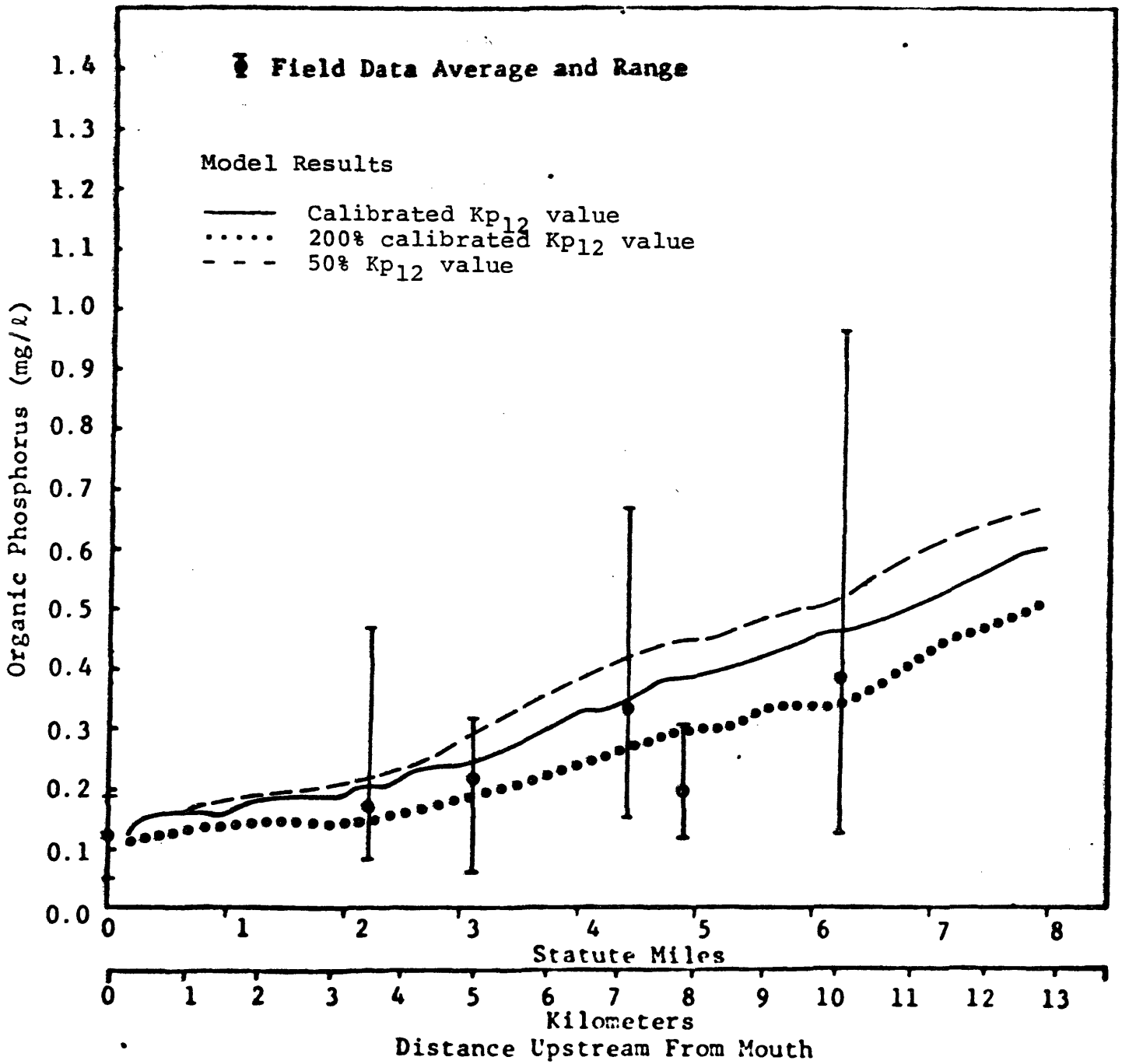

Figure 36. Effect of K_{p12} on organic-P concentration.

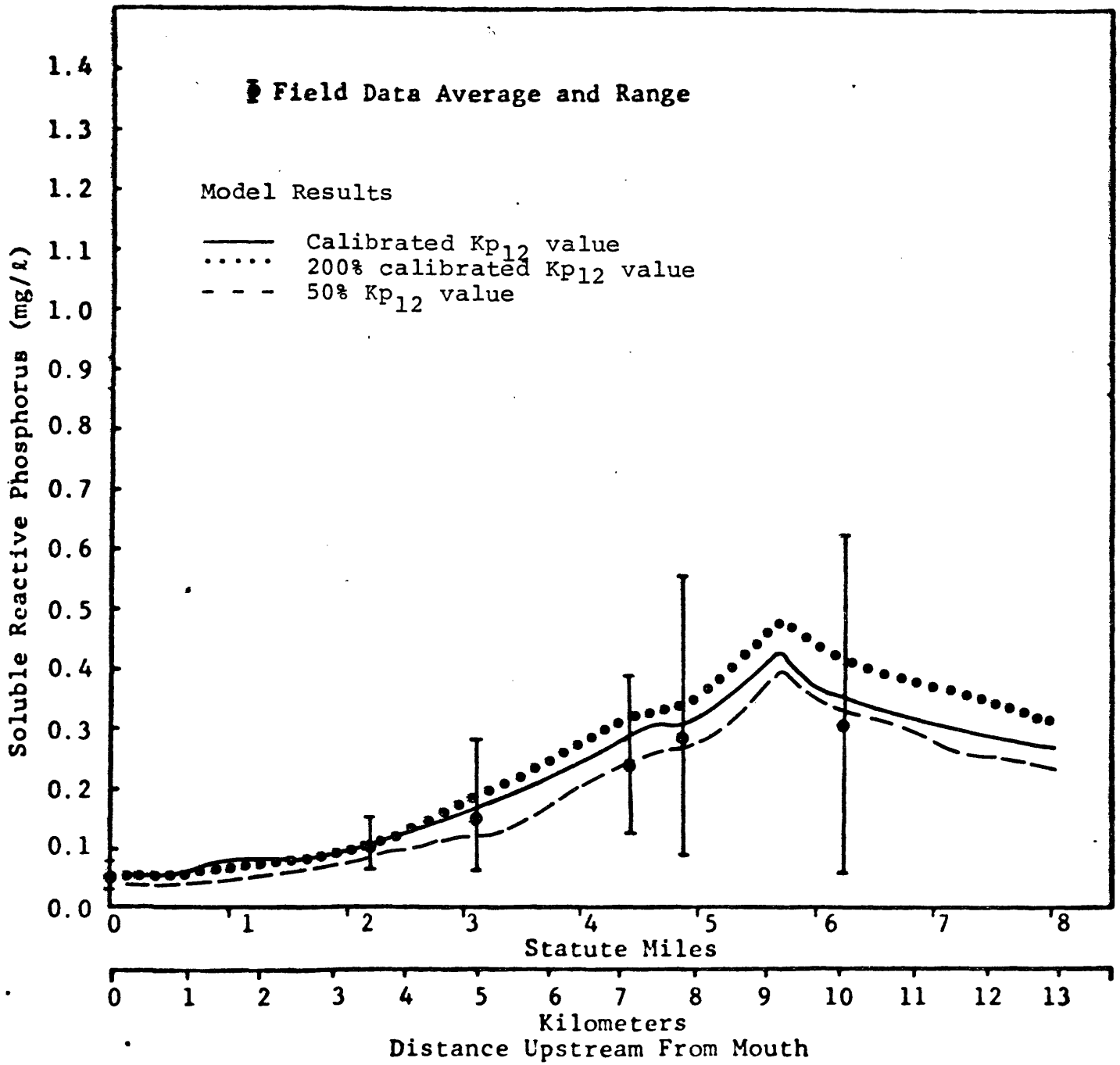

Figure 37. Effect of Kp_{12} on SRP concentration.

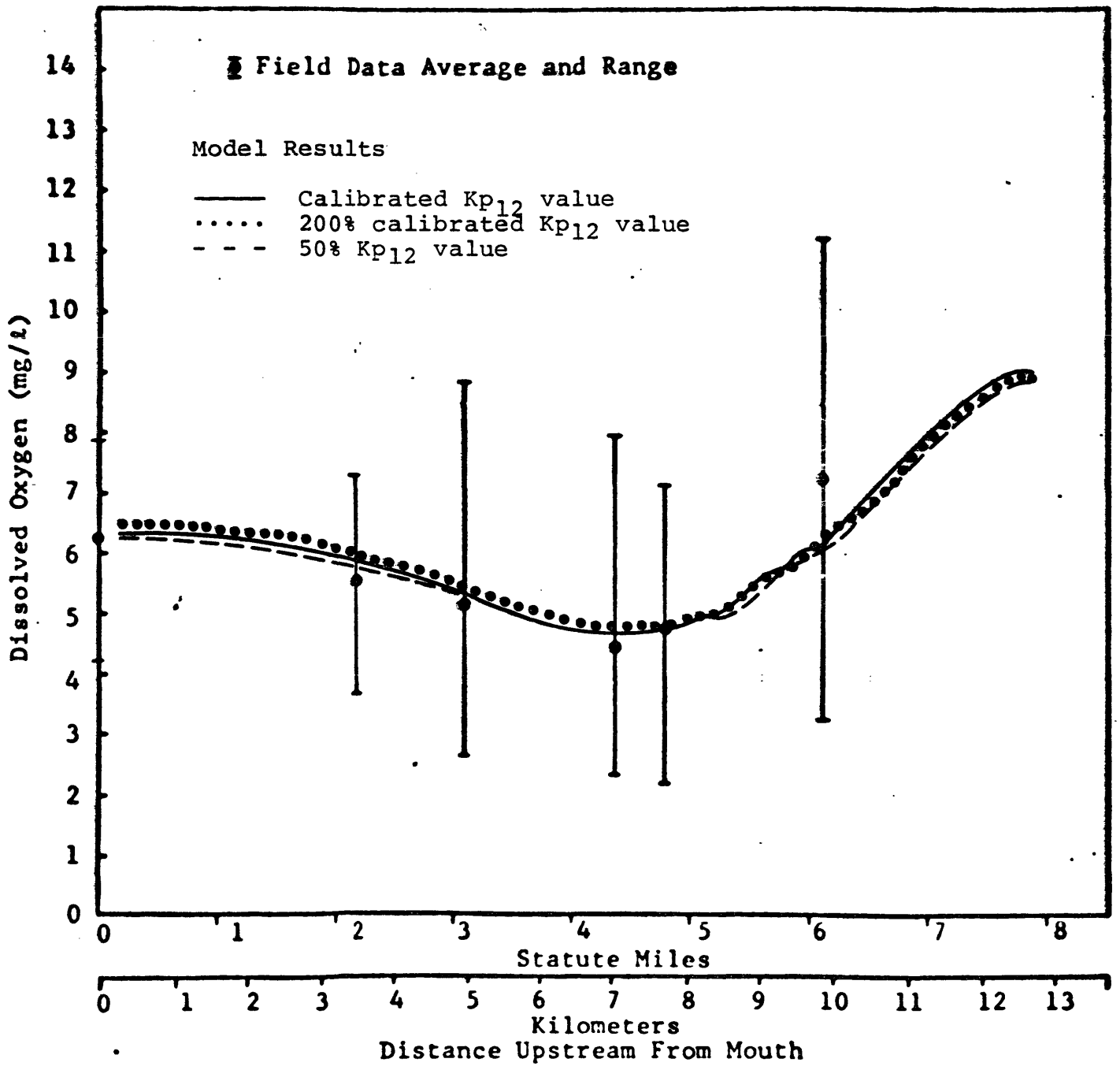

Figure 38. Effect of Kp_{12} on DO concentration.

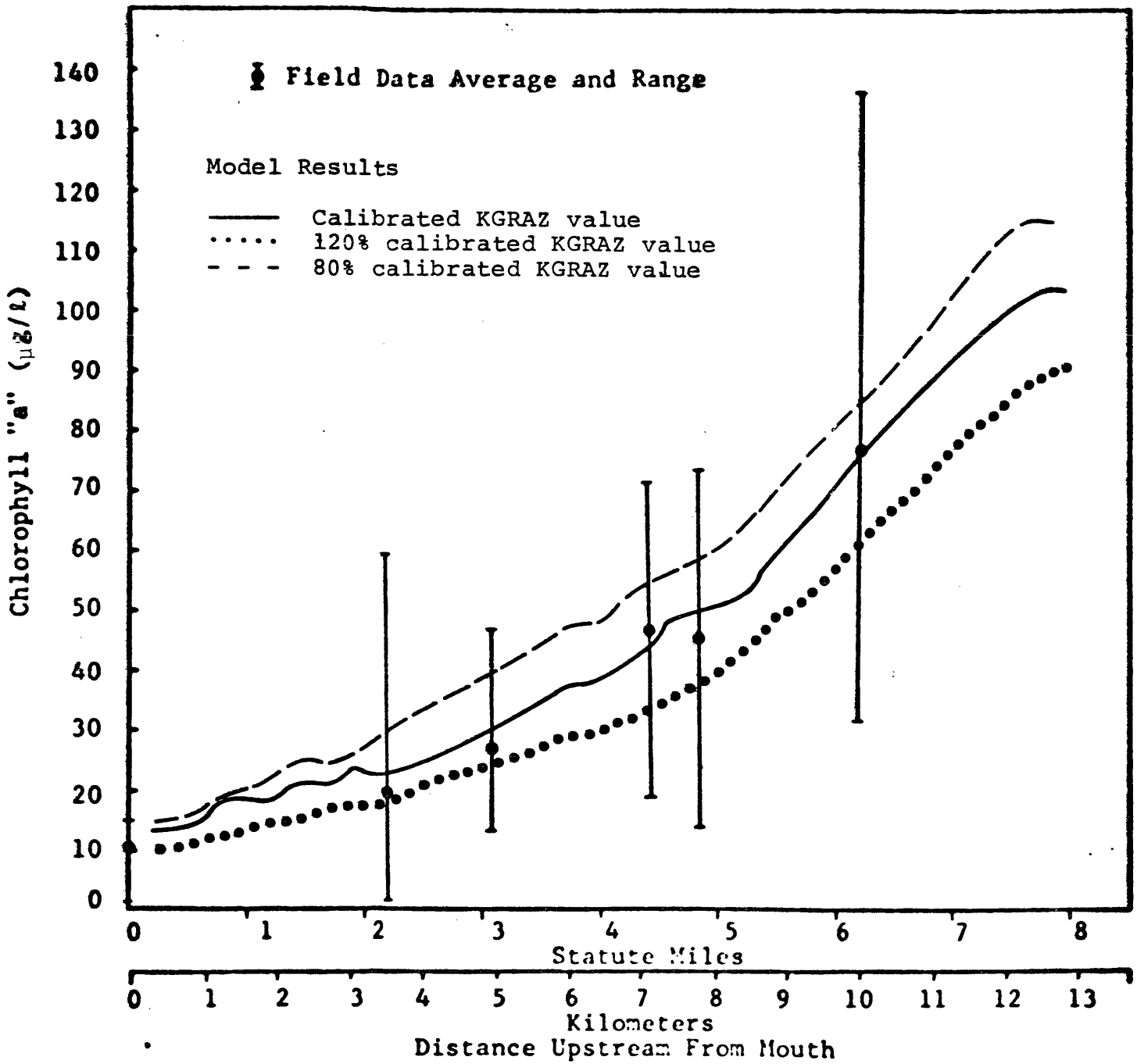

Figure 39. Effect of grazing rate on chlorophyll "a" concentration.

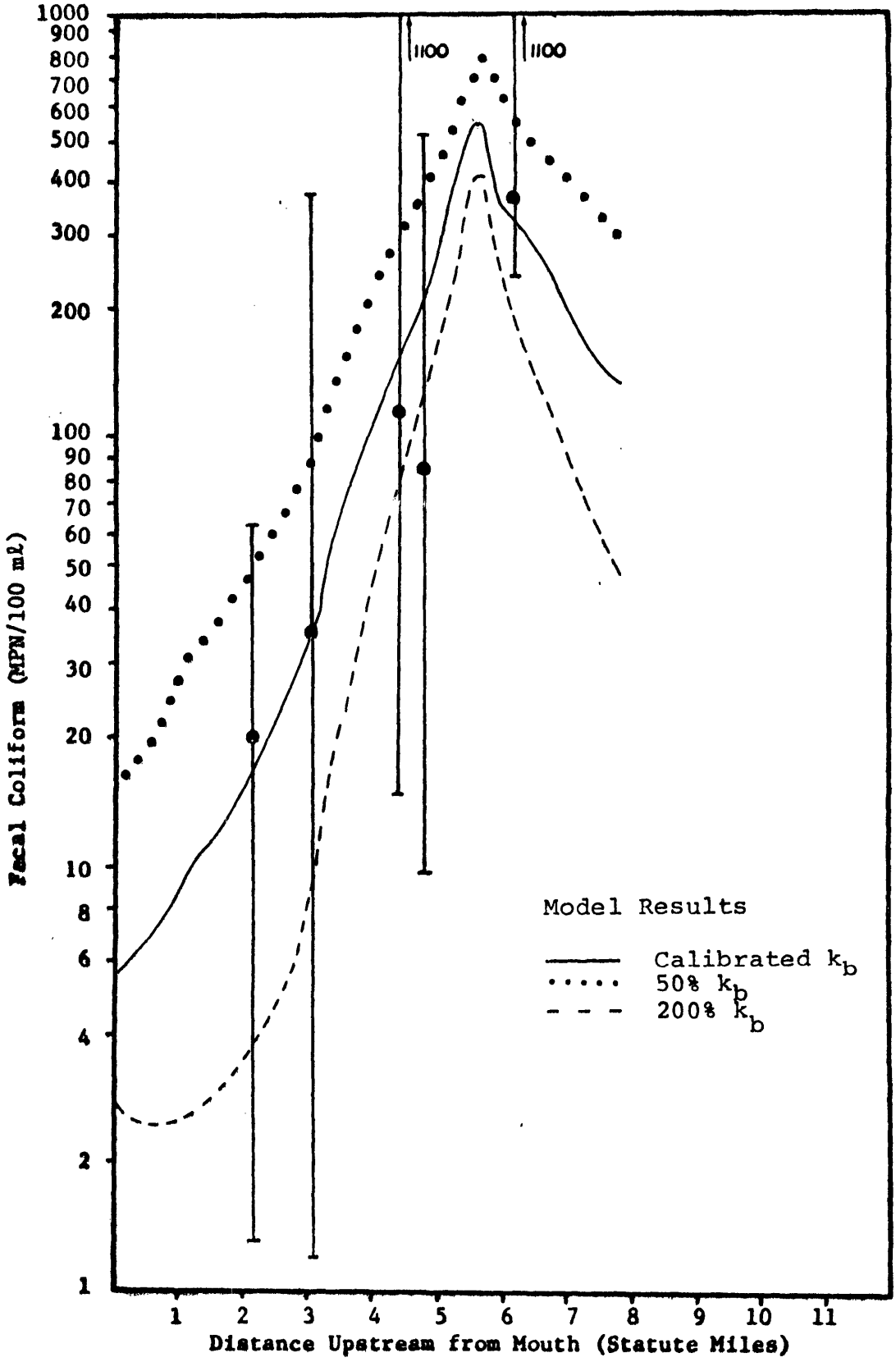

Figure 40. Effect of die-off rate on coliform concentration.

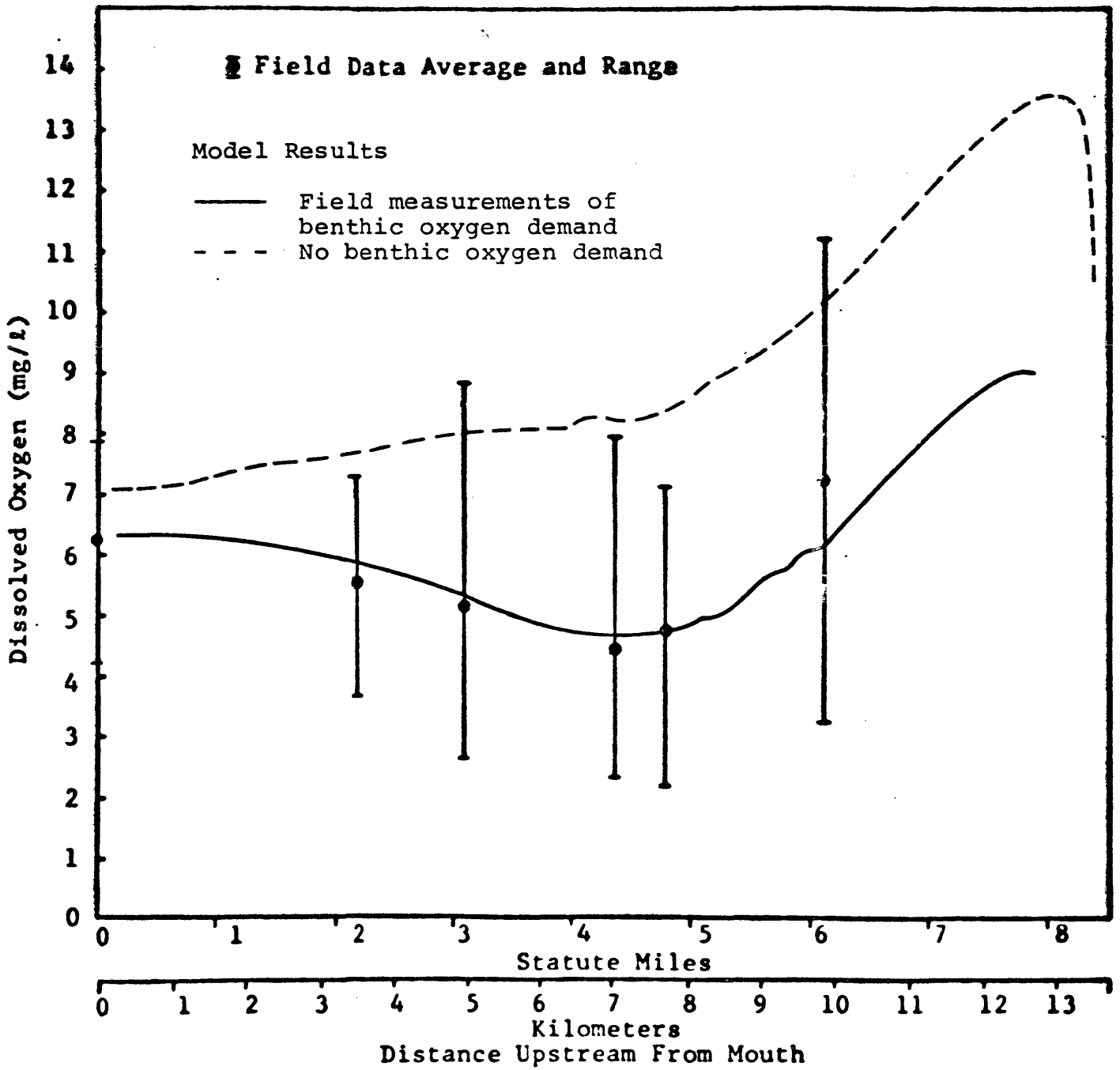

Figure 41. Effect of benthic oxygen demand on dissolved oxygen concentration.

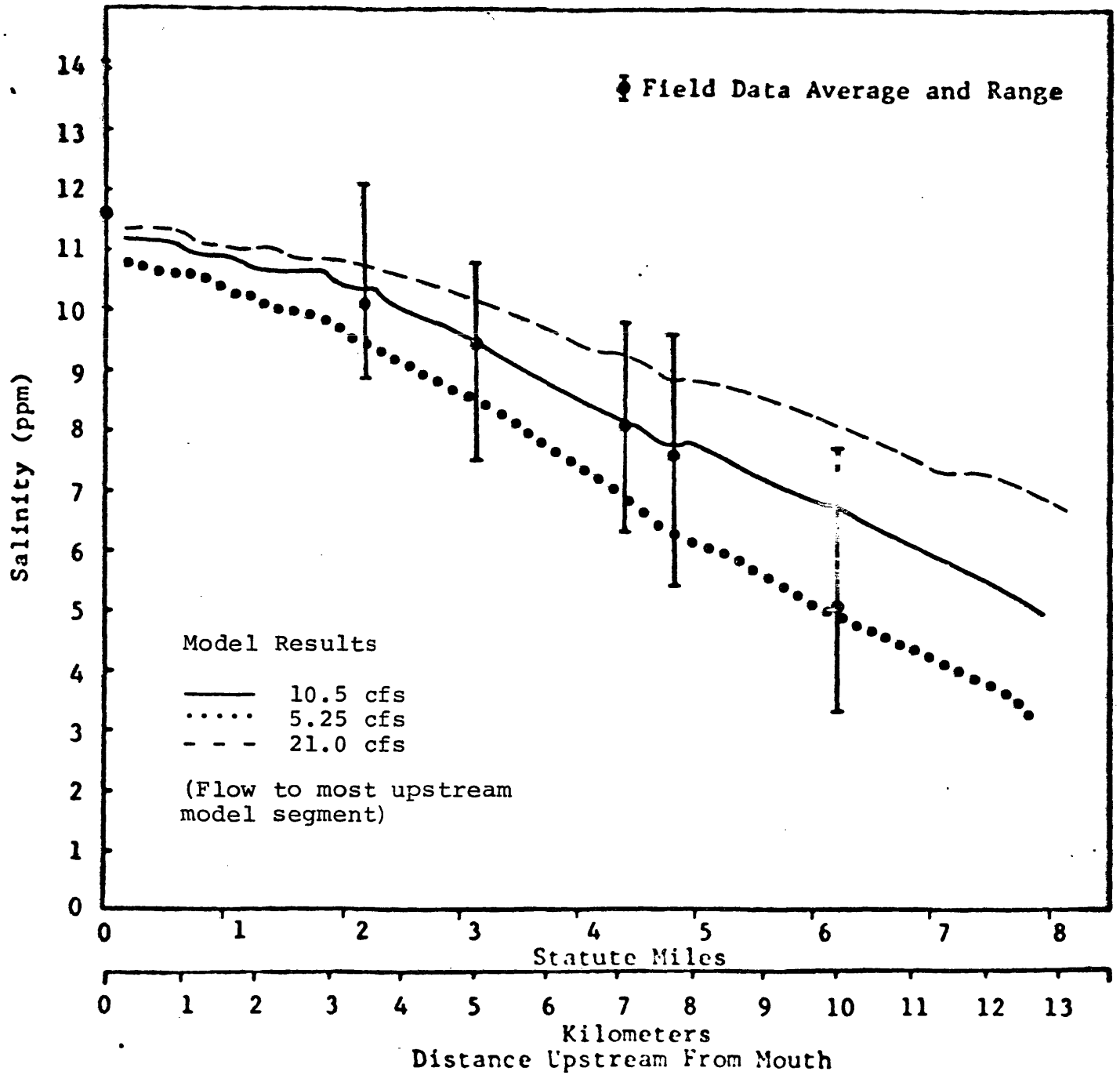

Figure 42. Effect of base freshwater discharge on salinity concentration.

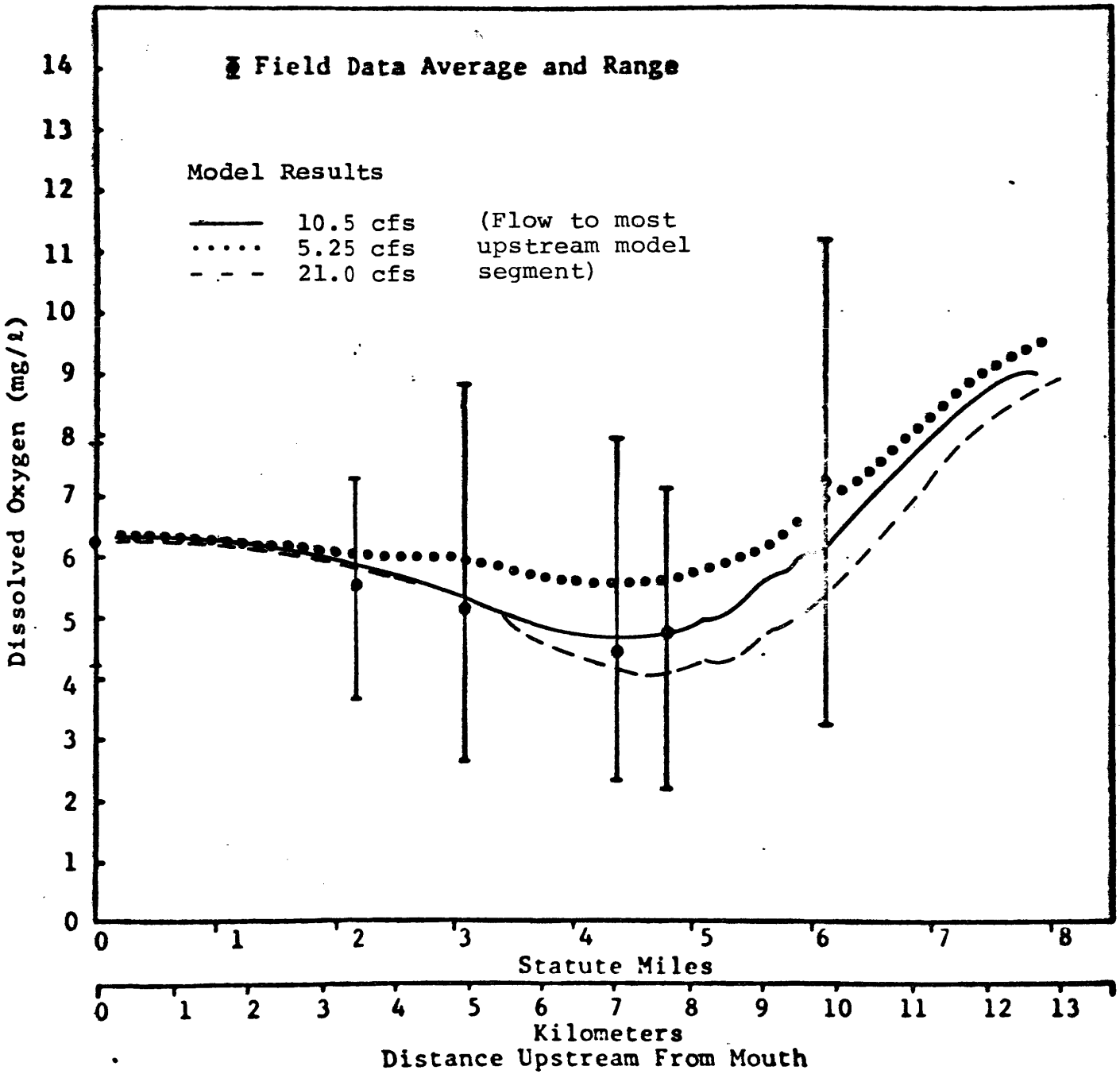

Figure 43. Effect of base freshwater discharge on DO concentration.

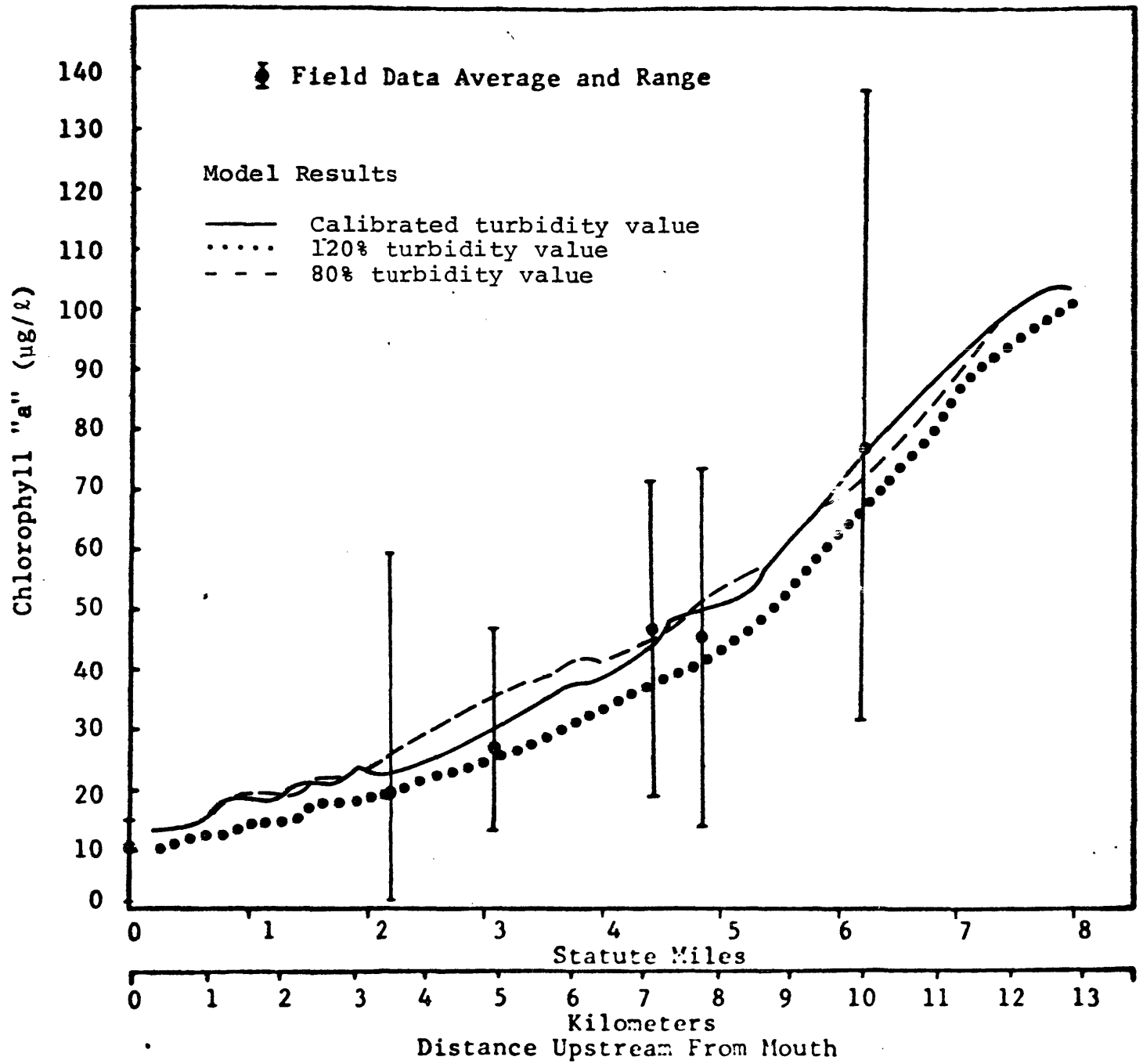

Figure 44. Effect of turbidity on chlorophyll "a" concentration.

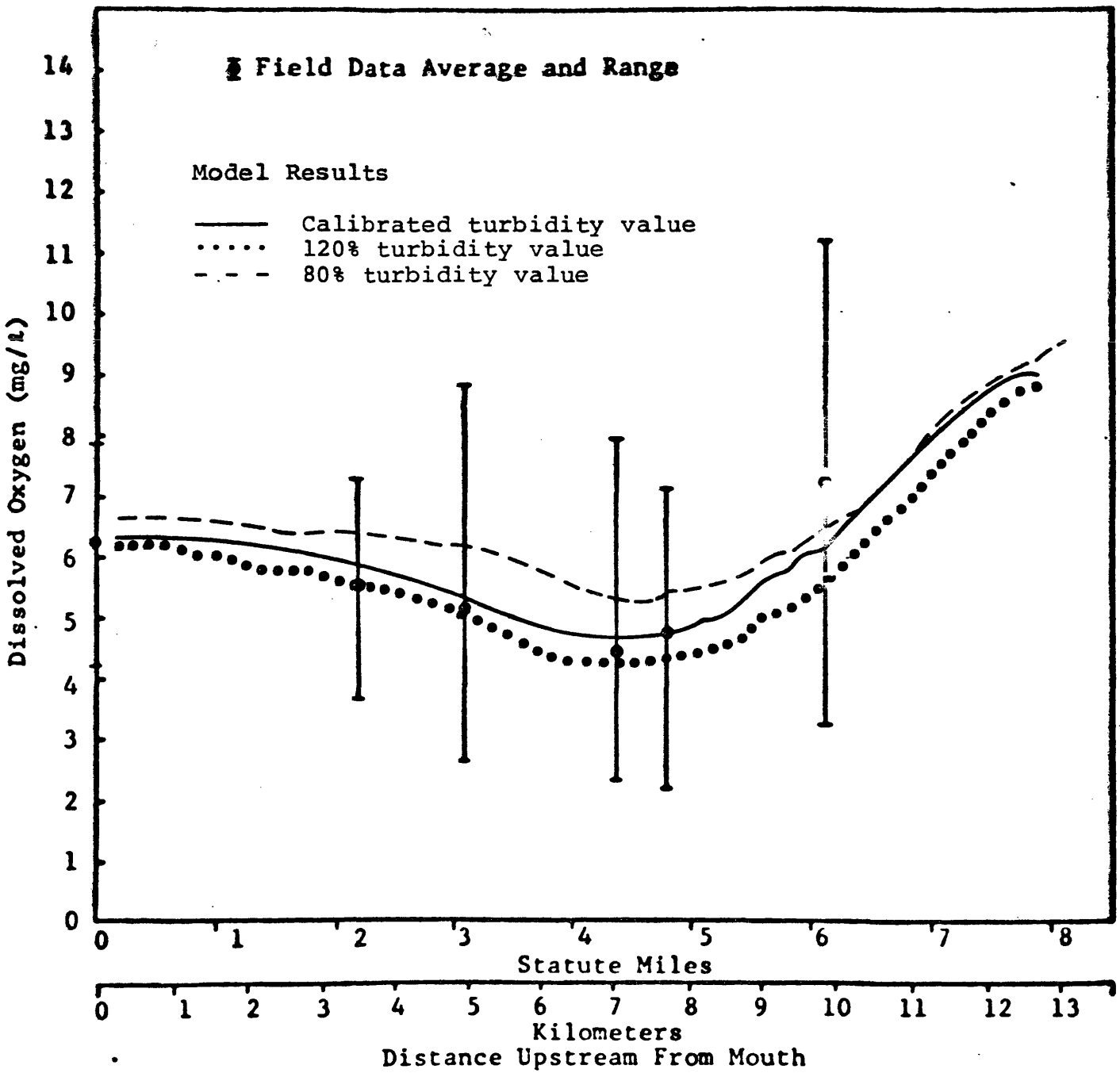

Figure 45. Effect of turbidity on DO concentration.

the benthal demand to the quality of the overlying waters.

When the base freshwater discharge was increased, salinity values decreased (see Figure 42). The increased flow results in greater downriver transport. Since the predominant source of salt is located at the mouth of the river, the salinity cannot intrude as far upriver when freshwater flow is increased. The model predictions agree with field observations for the Nansemond and similar estuaries.

The model also predicts that DO levels tend to increase if freshwater flow increases (Figure 43). This effect probably results from a variety of factors. The reduced salinity values, mentioned above, will result in increased saturation values for oxygen in water. Additionally, nutrient concentrations in the lateral inflow were high (see Table 5) and this could be causing higher plankton levels.

Since sunlight is the major energy source for phytoplankton productivity, increasing the turbidity will reduce the levels of the standing crop. A 20% increase in turbidity resulted in a reduction of about 5 µg of chlorophyll "a" per liter of water (Figure 44). This in turn resulted in a reduction in DO levels of less than 0.5 mg/l (Figure 45). These predictions demonstrate that oxygen inputs from phytosynthesis play an extremely important role in determining the dissolved oxygen levels. Turbidity often varies directly with discharge rate, but this relationship is not known quantitatively.

V. SUMMARY AND RECOMMENDATIONS

The only prior water quality math model study of the Pagan River is that done for the Cooperative State Agencies Program by VIMS (Kuo, Lewis and Fang, 1976). A one-dimensional, real time model was used and included salinity, dissolved oxygen, carbonaceous and nitrogenous BOD (biochemical oxygen demand). The two sets of field data have been compared in the water quality report on the Pagan River. Briefly, both data sets documented degraded conditions in the Pagan River, but the 208 field survey included additional measures of water quality so that the problems were illustrated in greater detail.

A so-called ecosystem model of water quality has been applied to the Pagan River for the 208 study. This model includes nutrient uptake by phytoplankton and fecal coliform die-off as well as those parameters inlcuded in the earlier model. Calibration of the model was made using the intensive survey data, while verification was achieved with the slack water data. Predictions for dissolved oxygen and chlorophyll "a", parameters that integrate the various processes at work, were extremely close to the field observations.

Both model studies showed that a dissolved oxygen sag occurred approximately 8 kilometers (5 miles) upstream from the mouth. Both indicated that benthic oxygen demand was an important factor for determining DO levels. The ecosystem model showed that phytoplankton also play a major role in determining water quality. Living phytoplankton produce oxygen during photosynthesis and can raise surface DO levels above

saturation values. However, bacterial decomposition of dead algal cells exerts an oxygen demand which may be felt downstream from the site where the plankton growth occurred.

Future studies in the Pagan River should include measurements of the freshwater inflow both quantity of base flow and the biochemical makeup of the water, and should inlcude detailed examinations of benthic oxygen demand. Point source loadings during 1976 were large and variable; these should be carefully monitored before and during future field studies. Predicted nonpoint loads are often quite large. These, too, should be monitored during the time of field measurement if that is possible. Ideally, in-stream sampling should occur prior to and following a storm event to document the impact of nonpoint loads.

LITERATURE CITED

APHA, AWWA, WPCF. 1971. Standard Methods for the Examination of Water and Wastewater, 13th Edition, New York.

Cronin, William B. 1971. Volumetric, Areal, and Tidal Statistics of the Chesapeake Bay and its Tributaries. Chesapeake Bay Institute, the Johns Hopkins University. Special Report No. 20. Reference 71-2.

Halmann, M. and M. Stiller. 1974. Turnover and Uptake of Dissolved Phosphate in Freshwater. A Study of Lake Kinneret. Limnology and Oceanography, Vol. 19, No. 5, pp. 774-783, September.

Kuo, A. Y., J. K. Lewis and C. S. Fang. 1976. Mathematical Model Studies of Water Quality in the Pagan Estuary. Spec. Rep. No. 107 in Appl. Mar. Sci. and Oc. Eng., VIMS.

McAllister, C. D., T. R. Parsons, K. Stephens and J. D. H. Strickland. 1961. Measurements of Primary Productivity using a Large-volume Plastic Sphere. Limnology and Oceanography, Vol. 6, pp. 237-258.

Parsons, T. R., K. Stephens, and J. D. H. Strickland. 1961. On the Chemical Composition of Eleven Species of Marine Phytoplankters. J. Fish. Res. Bd. Com. Vol. 18, No. 6, pp. 1001-1016. December.

Thomann, R. V., D. M. DiToro, and D. J. O'Connor. 1974. Preliminary Model of Potomac Estuary Phytoplankton. J. ASCE, Vol. 100, No. EE3, pp. 669-715, June.